SANDIA REPORT
SAND2004-8032
Unlimited Release
Printed February2004

A general methodology and applications for conduction-like flow-channel design

E. B. Cummings, G. J. Fiechtner

Prepared by
Sandia National Laboratories
Albuquerque, New Mexico 87185 and Livermore, California 94550

Sandia is a multiprogram laboratory operated by Sandia Corporation,
a Lockheed Martin Company, for the United States Department of Energy's
National Nuclear Security Administration under Contract DE-AC04-94AL85000.

Sandia National Laboratories

Issued by Sandia National Laboratories, operated for the United States Department of Energy by Sandia Corporation.

Available to DOE and DOE contractors from
U.S. Department of Energy
Office of Scientific and Technical Information
P.O. Box 62
Oak Ridge, TN 37831

Telephone: (865)576-8401
Facsimile: (865)576-5728
E-Mail: reports@adonis.osti.gov
Online ordering: http://www.osti.gov/bridge

Available to the public from
U.S. Department of Commerce
National Technical Information Service
5285 Port Royal Rd
Springfield, VA 22161

Telephone: (800)553-6847
Facsimile: (703)605-6900
E-Mail: orders@ntis.fedworld.gov
Online order: http://www.ntis.gov/help/ordermethods.asp?loc=7-4-0#online

SAND2004-8032
Unlimited Release
Printed February 2004

A general methodology and applications for conduction-like flow-channel design

LDRD Final Report

E. B. Cummings
G. J. Fiechtner

Microfluidics Dept.
Sandia National Laboratories
P.O. Box 969
Livermore, CA 94551-0969

Abstract

A novel design methodology is developed for creating conduction devices in which fields are piecewise uniform. This methodology allows the normally analytically intractable problem of Lagrangian transport to be solved using algebraic and trigonometric equations. Low-dispersion turns, manifolds, and expansions are developed. In this methodology, regions of piece-wise constant specific permeability (permeability per unit width) border each other with straight, generally tilted interfaces. The fields within each region are made uniform by satisfying a simple compatibility relation between the tilt angle and ratio of specific permeability of adjacent regions. This methodology has particular promise in the rational design of quasi-planar devices, in which the specific permeability is proportional to the depth of the channel. For such devices, the methodology can be implemented by connecting channel facets having two or more depths, fabricated, e.g., using a simple two-etch process.

This page intentionally contains only this sentence.

Contents

List of Figures

Acknowledgment

The authors gratefully acknowledge the CAD and fabrication assistance of Boyd Wiedenman. This work was funded by a Sandia Engineering Sciences LDRD. Sandia is a multiprogram laboratory operated by Sandia Corporation, a Lockheed-Martin company, for the United States Department of Energy under contract DE-AC04094AL85000.

Nomenclature

Symbols

σ specific permeability (permeability per unit width) of conduction channel [m]
$\mathbf{u}$ conduction velocity [$\mathrm{m \cdot s^{-1}}$]
$\mathbf{j}$ volumetric flow rate per unit width [$\mathrm{m^2 \cdot s^{-1}}$]
μ mobility [$\mathrm{m^2 \cdot V^{-1} \cdot s^{-1}}$]
$\mathbf{E}$ electric field [$\mathrm{V \cdot m^{-1}}$]
θ flow-velocity angle
ψ material-line angle

Subscripts

1 pertaining to the high-specific-permeability region
2 pertaining to the low-specific-permeability region
o observed in an alterative reference frame
c critical, e.g., critical angle
e even-numbered interface
o odd-numbered interface
s skew-compensating interface

This page intentionally contains only this sentence.

CHAPTER 1

Introduction

1.1 Ideal electrokinesis

Electrostatic transport mechanisms such as electrokinesis and dielectrophoresis are planned and being employed to manipulate fluids and particles in microchannels in and between a wide range of microfluidic devices. Recent attention has turned toward numerical and analytical modeling to support the design of such microfluidic systems. Unfortunately, directly solving the full mathematical problem of electrokinesis in practical microsystems is generally impractical given the vast range in length scales that are involved and the imprecise knowledge of real liquid and surface behavior. Moreover, general electrokinetic transport supports flow instabilities[1] that further complicate the modeling. Fortunately, the electroosmotic component of transport degenerates to a remarkably simple flow if a few conditions are approached[2, 6]:

1. The liquids are uniform throughout the region of interest,
2. The boundaries are uniform, impermeable, and insulating throughout the region of interest,
3. The Debye layer is negligibly thin compared to characteristic device dimensions, and
4. The entry and exit flows are compatible with the simple flow or are sufficiently far from the region of interest that their incompatibilities relax (e.g., typically 3 channel widths for a microchannel).

In this limit, the fluid velocity in the region of interest is described by the gradient of a scalar velocity potential field $\phi_V(\mathbf{r})$ that satisfies the Laplace equation, $\nabla^2\phi_V(\mathbf{r}) = 0$ for all $\mathbf{r}$ in the volume of the fluid, and $\nabla\phi_V(\mathbf{r}) \cdot \hat{\mathbf{n}}$ for all $\mathbf{r}$ on the boundaries of the liquid, where $\hat{\mathbf{n}}$ is the normal vector to the liquid boundary. This result is remarkable: this kind of flow is a "potential flow"—the canonical incompressible fluid motion, amenable to mathematical analysis using all the power of complex analysis. The electrostatic potential ϕ_E satisfies precisely the same equations; thus, the two potential fields differ by only a constant coefficient and a physically inconsequential constant. The gradients of these potentials, the velocity and the electric field are therefore everywhere proportional to each other by this constant

coefficient, μ_{EO}, which is called the electroosmotic mobility. This "similitude" between the fields leads to the useful intuition that the fluid flows exactly like the electrical current in the liquid.

In addition to these mathematical and conceptual simplifications, ideal electroosmotic flow is desirable in devices: in two-dimensional channel geometries it produces zero hydrodynamic dispersion in the third dimension of suspended or solvated particles. It is conjectured and very likely that ideal electroosmosis produces the minimum hydrodynamic dispersion in channels of arbitrary geometry. Ideal electroosmotic flow is stable: at low Reynolds numbers exhibited in practically all electroosmotic flows, local perturbations to the flow rapidly relax back to the ideal flow. Thus, the conditions listed above to approach a mathematically tractable limit become practical guidelines for designing and operating devices to achieve the best and most repeatable performance.

Observation of the similitude between the electrical current and fluid flow is useful because it leads to another ideal limit: "ideal electrokinesis." An isolated charged particle immersed in a liquid migrates under the applied electric field at a velocity that is everywhere proportional to the local electric field through either its ionic or electrophoretic mobility, μ_{EP}. (The distinction between these mobilities is, for microfluidic purposes, purely semantic, related to the complexity and size of the particle.) The net motion of a charged particle moving electrophoretically through a liquid that is undergoing electroosmosis is called electrokinesis. If immersed (suspended or solvated) particles in such a flow do not interact with each other or the flow boundaries, the motion of these particles is again everywhere proportional to the local electric field. The constant of proportionality is called the electrokinetic mobility, the difference between the electrophoretic mobility of the particle/liquid system and the electroosmotic mobility of the liquid/boundary system, $\mu_{EK} \equiv \mu_{EP} - \mu_{EO}$. In addition to the conditions listed above, the following conditions are sufficient for ideal electrokinesis:

1. The particles are much smaller than characteristic device dimensions, and
2. The particles are much smaller than the interparticle spacing.

The ideal electrokinetic limit has several interesting characteristics. One of the most important is that particle flow is "incompressible" or solenoidal—that is, the flow does not concentrate or rarefy particles that are uniformly distributed. Thus an ideal electrokinetic flow *cannot* be employed to make a particle concentrator. However particle concentrators, e.g., electrokinetic traps and sample-stacking devices, can be made by intentionally violating any of the conditions listed above.

1.2 Modeling assisted design

In spite of the considerable mathematical and conceptual simplifications of ideal electroosmosis and electrokinesis, it remains challenging to use mathematical modeling to optimize microfluidic devices. One reason is that while an Eulerian description of a flow field (the velocity field) may be simple, the Lagrangian description relevant to particle and solute transport is generally far more complicated, even for seemingly simple geometries. Since most optimizations of these devices are related to controlling solute transport, considerable

numerical (and often analytical) work is needed in spite of the simplicity of the Eulerian velocity field[5]. A brute-force optimization consists of

1. Hand selecting a parameterized geometry, requiring a reasonable guess at the shape of the optimal geometry,
2. Solving the Laplace equation in this geometry to obtain the Eulerian velocity,
3. Solving for the Lagrangian particle motion in this flow field,
4. Evaluating a fitness function based on the particle transport,
5. Adjusting parameters systematically,
6. Regenerating the geometry, and
7. Iterating from step 2.

The idealization assists only step 2 of this optimization.

In spite of this difficulty, ideal electroosmosis has successfully been employed in a handful of optimizations. One example is the solution for channel geometries that turn the flow direction by specific amounts (e.g., 45°, 90° and 180°) while producing acceptably small amounts of solute dispersion. Unfortunately, these solutions have taken specialists and mathematicians considerable effort and time measured in months. There are presently no two-dimensional optimal solutions for common engineering needs like expanding a flow with low dispersion, displacing a channel (e.g., to plumb it an offset downstream device), rotating a flow by an arbitrary angle, rotating a flow with expansion, making low-dispersion manifolds, etc. Clearly, ideal electrokinesis alone does not trivialize the real problems of engineering electrokinetic devices! More importantly, it does not prescribe a rational methodology for general electrokinetic design for controlled solute transport.

Fortunately, such a design methodology does exist and the following chapters detail a technique that allows engineers to design dispersion-controlled channels, turns, expanders, and manifolds using a slide rule (!) or calculator. For the curious reader, the remainder of this introduction describes the serendipitous observations that sparked the development of this methodology. The rest of the material in this chapter is not necessary for understanding how to use this design methodology.

1.3 Origins

To validate the concept of ideal electrokinesis, experimental studies were conducted[5] to measure electrokinetic velocity fields by observing the motion of particle tracers. The flow studies were conducted in the interior of uniform arrays of insulating posts, ensuring that the boundary conditions were accurately prescribed. When these experiments were completed, a second set of experiments was conducted in the same geometries in which the applied electric field was increased until dielectrophoresis of the particles, a nonlinear electrostatic effect, became appreciable and ultimately dominant. Unlike ideal electrokinesis,

dielectrophoresis is not solenoidal: it can rarefy and concentrate particles such that its effects were observable in the induced variation in particle concentration as visualized by the intensity of fluorescence of the particles. One experiment momentarily produced the fluorescence image in Fig. 1.1 when an inhomogeneous front of fluid induced an angle of attack of the flow with respect to the array. Without going into excessive detail, the particles, being repelled by the regions of low electric field between the posts, are observed to flow along the windward side of the columns of posts. The suspending liquid follows the applied electric field. The tilt angle between the array and the applied field causes particles to be concentrated and filtered continuously[3, 4, 5, 7, 8].

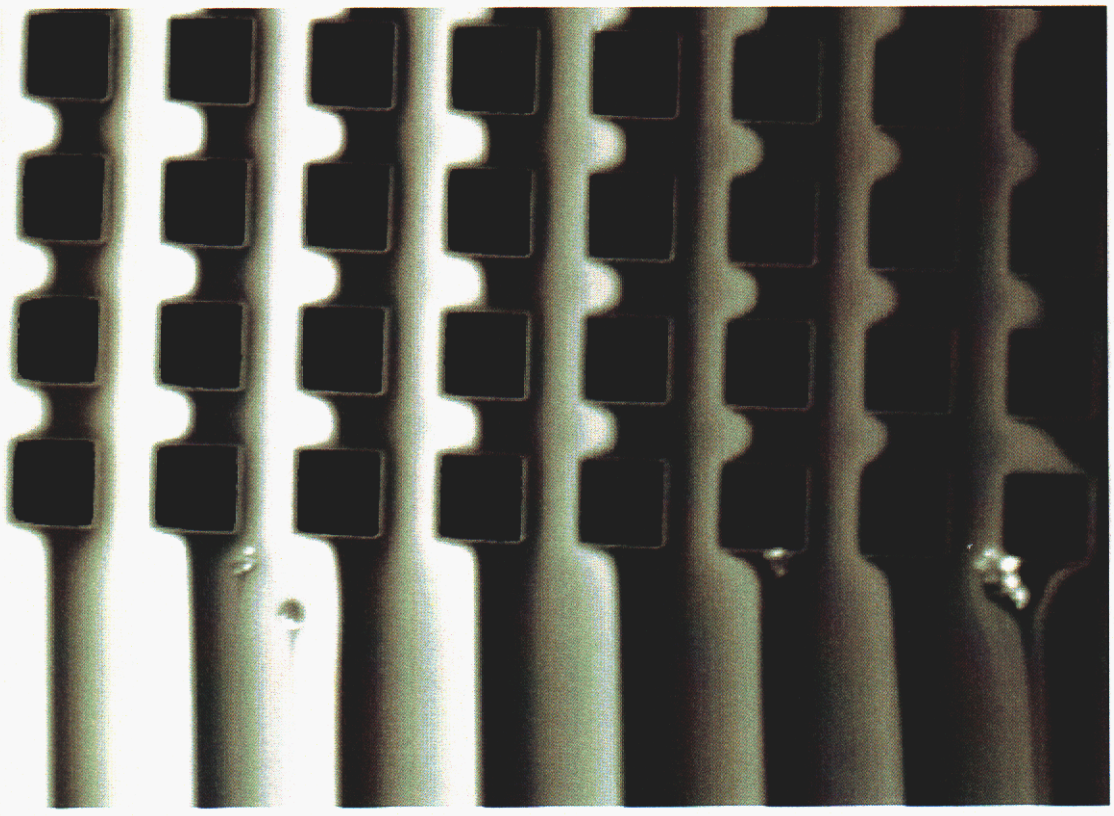

Figure 1.1: Particle-fluorescence image of combined electrokinesis and dielectrophoresis in an array of insulating posts. The mean liquid flow direction is from top to bottom. Excluded from the low-field regions between the posts, the particles flow along the windward (left) side of the columns of posts, being concentrated and filtered continuously. This observed phenomenon is the basis of a class of dielectrophoretic filter/concentrators.

This serendipitous experimental observation sparked the development of continuous-flow dielectrophoretic filter/concentrators based on this phenomenon. One of the issues in optimizing the design of such a system is ensuring that the flow and electric field are consistent for all posts in the array. This consistency can be designed trivially into arrays having symmetry normal to the flow direction, but is much more difficult for tilted arrays.

For example, the walls of the array are contoured to the shape of a particle streamline within an infinite tilted array. Figure 1.2 shows the numerical simulation of the speed field within such a tilted array[3]. The fringes are contours of constant speed. Per design, the speed field near the walls is nearly identical to that in the adjacent cells. However, a half-fringe shift in the absolute speed field is evident across the width of the array, corresponding to about a 10% variation from the left wall to the right wall. This result was the second serendipitous observation.

It was evident that the interface between the ends of the array required special attention. The issue is that the permeability of the open channel is significantly different from the permeability of the patterned array. A quick analysis (see Chapter 2) showed that the array must be tilted by a specific angle to obtain piecewise uniform electric fields within the device. Figure 1.3 shows the simulation of the design when the proper tilt angles are applied. As prescribed, the speed fields are uniform in each section of the design.

Perhaps serendipitously as well, Sandia's μChemLab chip design employs multiple-level isotropic glass etches for a variety of engineering reasons[14]. It was clear that the complexity of this additional fabrication step was not considered prohibitive. If two etching operations are already used for engineering convenience, perhaps the operations could also be used to support a new design methodology for creating channels having piece-wise uniform flow velocities. This practical observation motivated the development of the rational "facets" design methodology outlined in the following chapters.

This design methodology allows an engineer to create arbitrary turns, expansions, offsets, and manifolds, often using only a slide rule or simple calculator. More complicated designs can be constructed by a process of picking points off some of the plots included in the following chapters[10]. In addition to the mathematical advantages of this methodology, it also represents a solution for asymptotically *zero* hydrodynamic dispersion: the only essential hydrodynamic dispersion occurs at the interfaces and is proportional in extent to the channel depths. By using sufficiently shallow and wide channels, hydrodynamic dispersion can be made arbitrarily small. Interestingly, the quest for mathematical simplicity has again illuminated the path to optimal device performance.

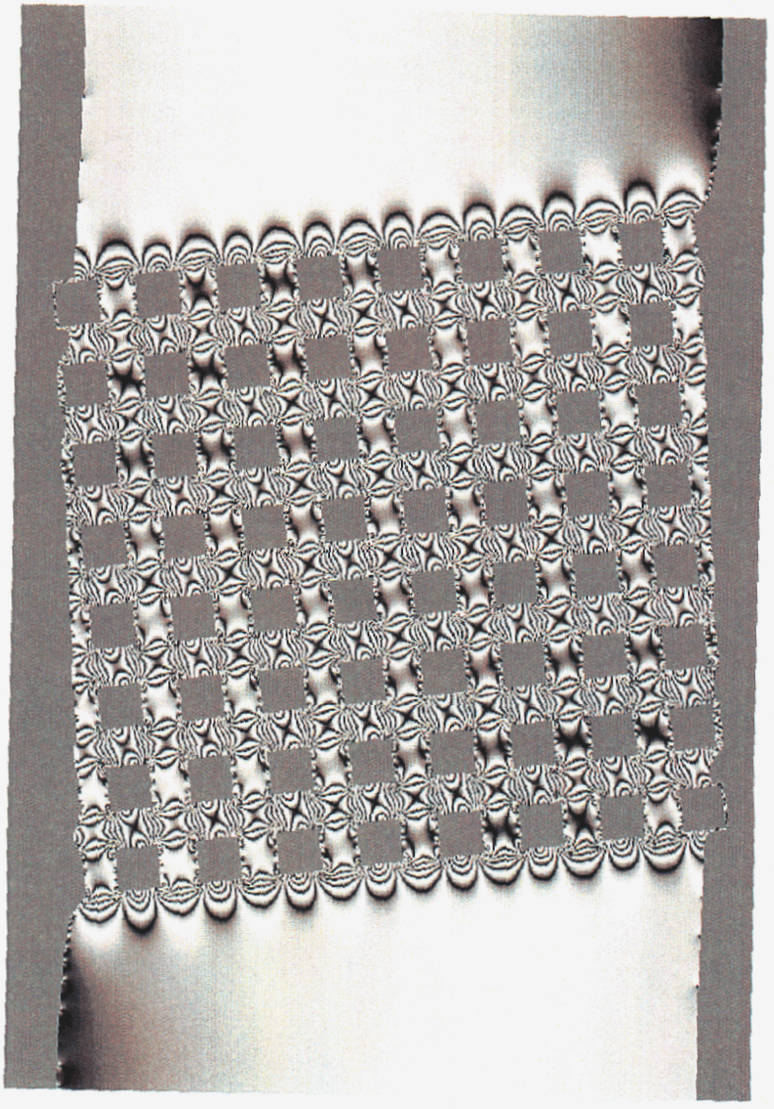

Figure 1.2: Simulated speed field of the tilted-array design. Fringes are contours of constant speed. The fringe across the inlet and exit channels and the fringe shift across the array shows that the electric field and velocity field varies by about 10% across the channel. This variation results from the tilted interface between the open and patterned channel sections.

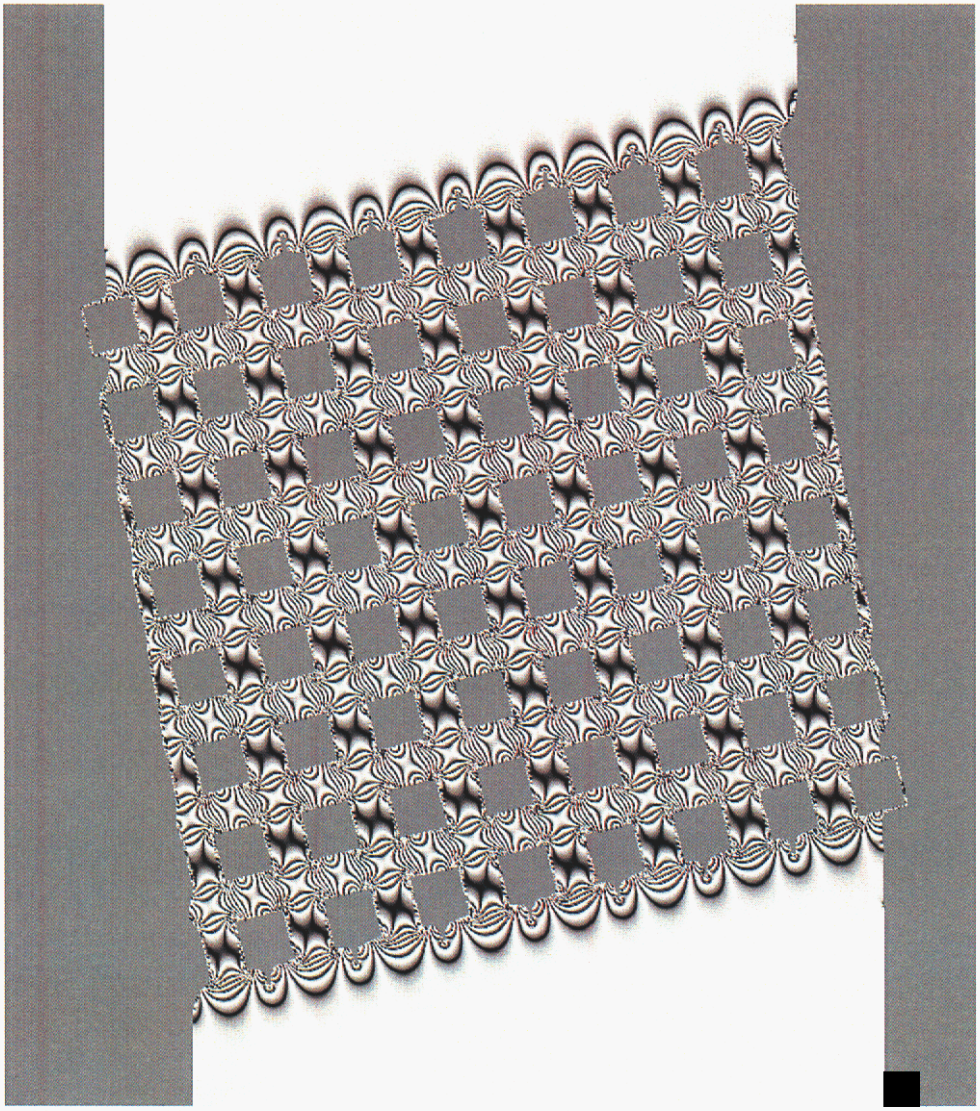

Figure 1.3: Simulated speed-field contours of the tilted-array design after rotation to the angle needed for piece-wise uniform electric/velocity fields.

This page intentionally contains only this sentence.

CHAPTER 2

One-dimensional conduction across an abrupt permeability change

2.1 Conduction across a normal interface

The mathematics of conduction, which appears in many physical contexts, is among the simplest and most thoroughly studied of any physical process. However, even an old equation can yield new tricks: this chapter introduces a new general method to design conduction channels algebraically.

For clarity, we define the mathematical relations and apply semantics that are relevant to ideal electrokinesis. This semantic bias does not exclude the use of the methodology for other conduction-like transport. The velocity $\mathbf{u}$ of the conduction fluid is everywhere proportional to the driving force $\mathbf{E}$,

$$\mathbf{u} = \mu \mathbf{E}, \tag{2.1}$$

where the coefficient μ is the mobility of the fluid. In this analysis the mobility and the fluid conductivity are constant everywhere.

The volumetric flow rate per unit width $\mathbf{j}$ is proportional to the conduction velocity by

$$\mathbf{j} = \sigma \mathbf{u}, \tag{2.2}$$

where σ is defined as the channel permeability, a property only of the channel geometry. This permeability is permitted to vary across a straight interface in this analysis. These semantics are physically correct for ideal electrokinesis and other forms of conduction in which the local flow velocity is independent of the permeability of the medium.

Permeation is usually treated as a continuous subscale phenomenon whose constitutive coefficient is the permeability. Normally a large separation in length scales is needed to support this subscale notion because fluctuations from the randomness of the permeable medium must average to insignificance over the larger scales. In contrast, the separation in length scales required to attach a meaningful permeability to an orderly medium such as a uniform patterned array is surprisingly small: roughly an order of magnitude. Figure 2.1 shows several examples of subscale designs that modify the specific permeability of a channel, that is, the permeability per unit channel width. In a quasi-planar microsystem, the

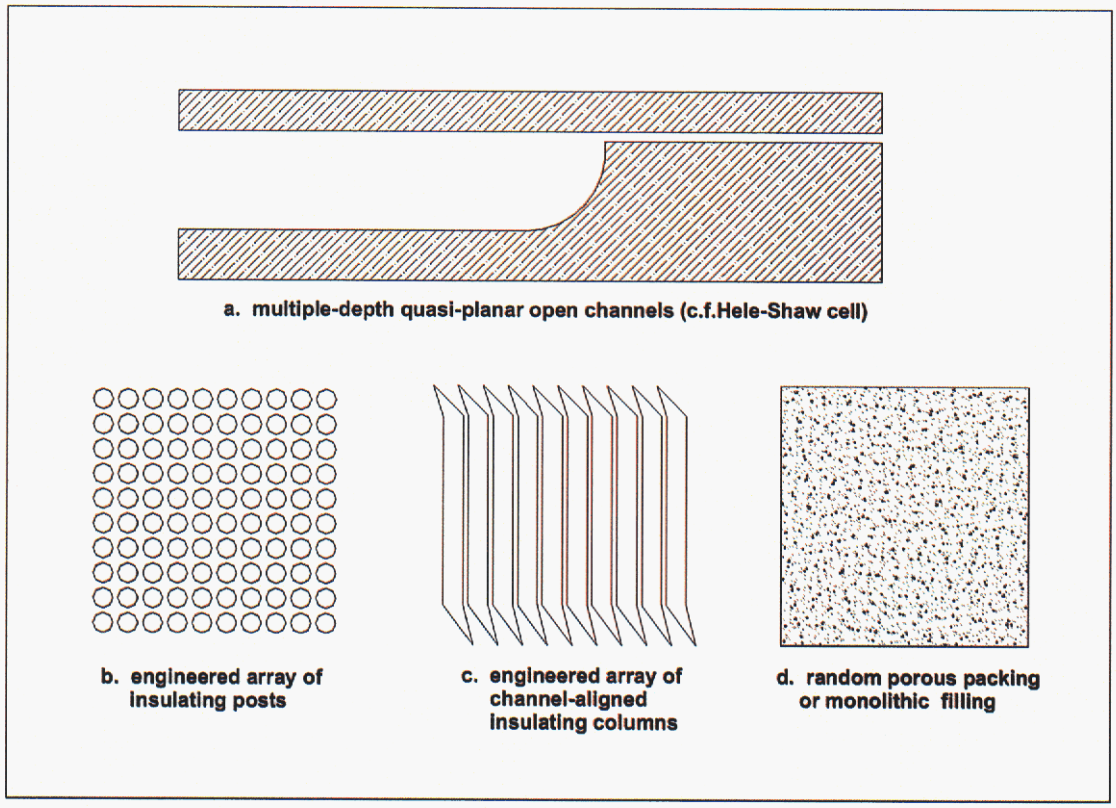

Figure 2.1: Methods of modifying the specific permeability of a conduction channel.

specific permeability of a channel is proportional to the channel depth. A two- or more-level etched microsystem, for example can be used to implement these designs as shown in Fig. 2.1.a. Alternatively, the effective specific permeability of a channel can be lowered with respect to an open channel by blocking part of the channel, for example by filling the channel with array of posts (b) or channel-aligned parallel columns (c). Another technique is to fill the channel with a packing or porous medium or generate pores in the substrate (d). These methods generate varying amounts of hydrodynamic dispersion at the interface and throughout the conduction channel and can be used separately or in combination.

To analyze steady fluid conduction past a permeability change, we first consider the infinite one-dimensional conduction channel sketched in Fig. 2.2, having a uniform specific permeability $\sigma = \sigma_1$ in region 1, left of a finite transition-region, and a uniform specific permeability $\sigma = \sigma_2$ in region 2, right of a transition region. Inside the transition region, the permeability variation is unspecified but bounded such that $0 < \sigma < \infty$ everywhere in the conduction channel.

Continuity requires a constant volumetric flow rate $\mathbf{j}$ throughout the channel, thus

$$\mathbf{j}_1 = \mathbf{j}_2 \rightarrow \sigma_1 \mathbf{u}_1 = \sigma_2 \mathbf{u}_2 \text{ or } \sigma_1 \mu \mathbf{E}_1 = \sigma_2 \mu \mathbf{E}_2. \tag{2.3}$$

This simple one-dimensional consequence of continuity will be used in the next section

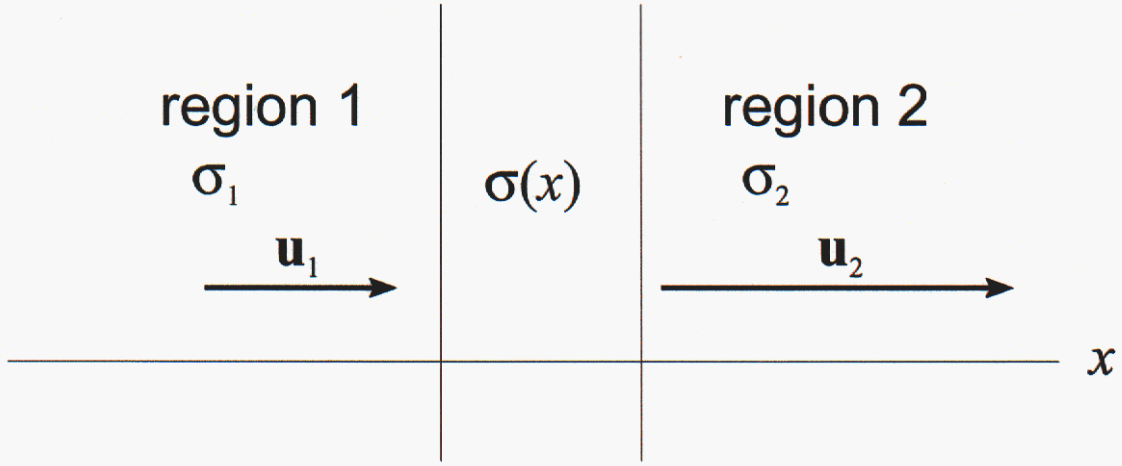

Figure 2.2: Sketch of the one-dimensional conduction channel. The specific permeability σ is constant in regions 1 and 2 and varies only in the flow direction in the transition region, $\nabla\sigma \times \mathbf{u} \equiv \mathbf{0}$.

to establish a compatibility relation for low-dispersion, quasi-two dimensional flow channel design.

2.2 A special case of two-dimensional conduction

Figure 2.3 shows the system of Fig. 2.2 from the standpoint of an observer moving at a steady velocity $\mathbf{u}_o$ along the interface, i.e., $\mathbf{u}_o \cdot \nabla\sigma = 0$. Because the position of the interface is steady in this moving frame, Eq. 2.1 holds and by extension

$$\sigma_1 \mathbf{u}_{1o} \cdot \hat{\mathbf{n}} = \sigma_2 \mathbf{u}_{2o} \cdot \hat{\mathbf{n}}, \text{ and} \tag{2.4}$$

$$\mathbf{u}_o = \mathbf{u}_{1o} - \mathbf{u}_{1o} \cdot \hat{\mathbf{n}} = \mathbf{u}_{2o} - \mathbf{u}_{2o} \cdot \hat{\mathbf{n}} \tag{2.5}$$

where $\hat{\mathbf{n}}$ is a unit vector normal to the interface, i.e.,

$$\hat{\mathbf{n}} \equiv \frac{\nabla\sigma}{||\nabla\sigma||} \tag{2.6}$$

everywhere $\nabla\sigma$ is finite.

In variables that are more suitable for design, these simultaneous equations can be rearranged to yield

$$\frac{\tan\theta_1}{\sigma_1} = \frac{\tan\theta_2}{\sigma_2}, \text{ and} \tag{2.7}$$

$$u_{1o} \sin\theta_1 = u_{2o} \sin\theta_2, \tag{2.8}$$

where $u \equiv ||\mathbf{u}||$ and θ_1 and θ_2 are the flow angles shown in Fig. 2.3. Equation 2.7 resembles Snell's law of refraction, except tangents of the propagation angles are matched instead of sines. Equation 2.8 describes how the speed varies across the interface.

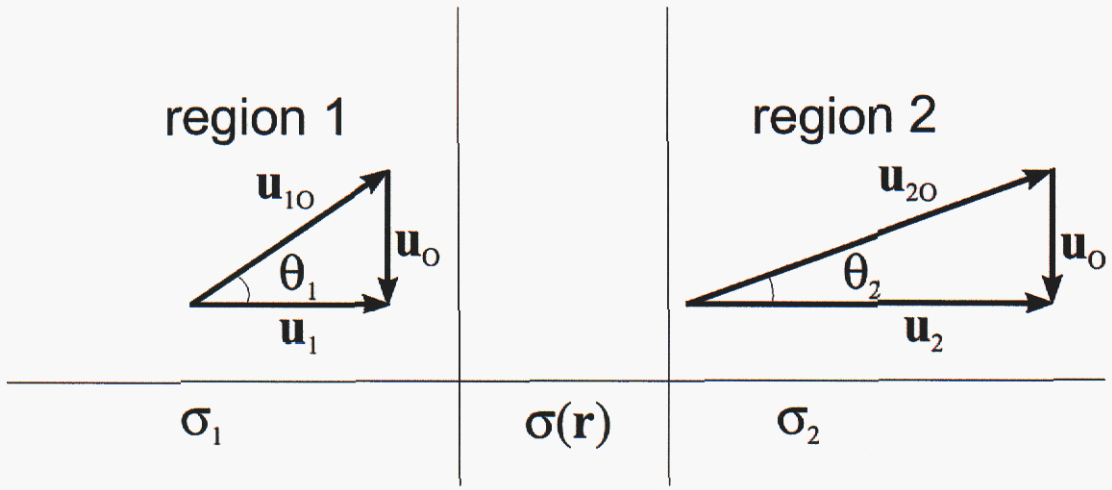

Figure 2.3: Sketch of the one-dimensional conduction channel from the standpoint of an observer moving with velocity $\mathbf{u}_o$ along the interface. The velocities $\mathbf{u}_{1o}$ and $\mathbf{u}_{2o}$ are observed in this frame.

Equations 2.7 or 2.8 can be considered "compatibility" conditions for locally one-dimensional flow in regions 1 and 2. In other words, if a conduction channel interface is designed to satisfy Eq. 2.7, then the flow everywhere in region 1 will have a uniform velocity $\mathbf{u}_{1o}$; region 2 will have a uniform velocity $\mathbf{u}_{2o}$. This case produces the minimum hydrodynamic dispersion within regions 1 and 2.

The motion of material lines through a conduction channel is often of interest. Material lines are distorted or rotated only at the interface. Fig. 2.4 shows an idealization of the system in which the interface is abrupt compared to the length of the initial material line (represented by the vector $\mathbf{r}_1$). This vector is drawn in Fig. 2.4 as one end reaches the interface. The other end reaches the interface after a time t having propagated through the vector $\mathbf{u}_{1o}t$. During this period, the other end propagates through region 2 by the vector $\mathbf{u}_{2o}t$. Consequently

$$\mathbf{r}_1 - \mathbf{u}_{1o}t = \mathbf{r}_2 - \mathbf{u}_{2o}t, \tag{2.9}$$

but

$$t = \frac{\mathbf{r}_1 \cdot \mathbf{u}_{1o}}{\mathbf{u}_{1o} \cdot \mathbf{u}_{1o}}, \tag{2.10}$$

such that

$$\mathbf{r}_2 = \mathbf{r}_1 + (\mathbf{u}_{2o} - \mathbf{u}_{1o})\frac{\mathbf{r}_1 \cdot \mathbf{u}_{1o}}{\mathbf{u}_{1o} \cdot \mathbf{u}_{1o}}. \tag{2.11}$$

Equation 2.2 is an explicit equation for the distorted material line represented by $\mathbf{r}_2$ in terms of the undistorted material line, $\mathbf{r}_1$, and the velocities on both sides of the interface, $\mathbf{u}_{1o}$ and $\mathbf{u}_{1o}$.

The simplest implementation of such a design is a flow channel having a single internal interface whose side-walls are oriented according to Eq. 2.7, as shown in Fig. 2.5. The widths w_1 and w_2 of the conduction channels in regions 1 and 2 shown in Fig. 2.5 obey the

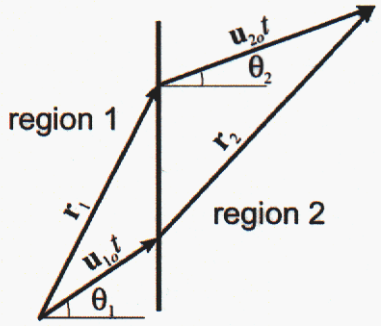

Figure 2.4: Diagram of a material line represented by $\mathbf{r}_1$ as it passes through the interface, being distorted into the material line represented by $\mathbf{r}_2$. An inclined interface satisfying the compatibility relation can rotate and stretch material lines but cannot curve lines.

relation

$$\frac{w_1}{\cos\theta_1} = \frac{w_2}{\cos\theta_2}. \tag{2.12}$$

2.3 Inclined-interface designs

The inclined interface between channels having dissimilar specific permeabilities can be viewed as a device primitive that

1. Rotates the conduction flow,
2. Changes the conduction velocity/time-of-flight,
3. Widens the conduction channel, and
4. Rotates and deforms material lines of the flow.

So far, issues of the entry and exit boundary conditions have been avoided by assuming an infinite domain. The domain can be truncated provided the entry- and exit-flow conditions are compatible with the uniform flow in the respective regions, i.e,

$$\mathbf{u}_i = \mathbf{u}_{io} \text{ and } \nabla\mathbf{u}_i = \mathbf{0} \tag{2.13}$$

on the entrance to region $i = 1$ or 2.

To illustrate the effect the compatibility condition Eq. 2.2, Fig. 2.6 shows numerical simulations of the speed field and flow streaklines within three instances of a system of two interfaces. The spectral color map depicts the speed field: blue and red are respectively the highest and lowest speeds. In case a., compatibility is not satisfied for either interface because the specific permeability ratio (SPR), σ_1/σ_2, is half that required by Eq. 2.2. Consequently, the speed field is not uniform within each region, streaklines are curved, and material lines are curved, as evidenced by the curved front of the streaklines. In case b., compatibility is satisfied. In case c., compatibility is not satisfied because the specific

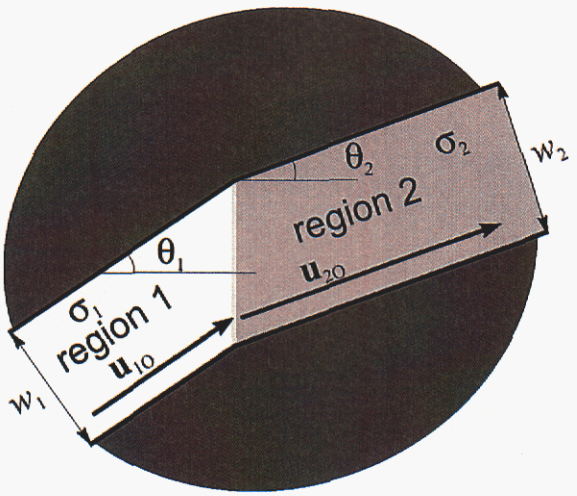

Figure 2.5: Sketch of a conduction channel having a single interface between regions of two specific permeabilities, σ_1 and σ_2. The side walls of the channel are designed to satisfy the compatibility relation Eq. 2.7 so that the velocity within each region is uniform and given by Eq. 2.8. Such a channel rotates the flow direction, changes the flow velocity, changes the flow width, and reorients material lines of the fluid. This simple channel is a primitive from which useful devices can be designed.

permeability ratio is twice that required by Eq. 2.2. Streamlines and material lines are curved in the opposite direction and the speed field variation is the opposite of those in case a. Designs satisfying the compatibility conditions navigate an algebraically tractable subset of general conduction.

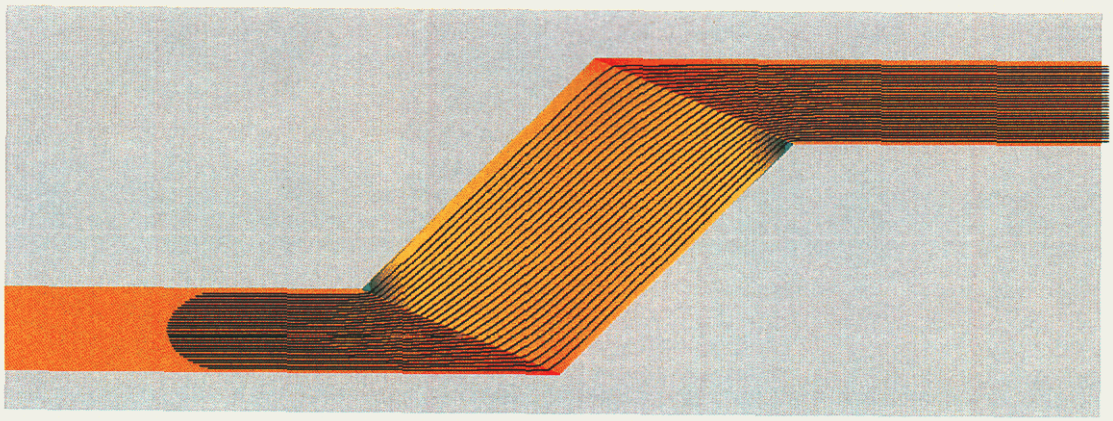

a. permeability ratio = one-half nominal

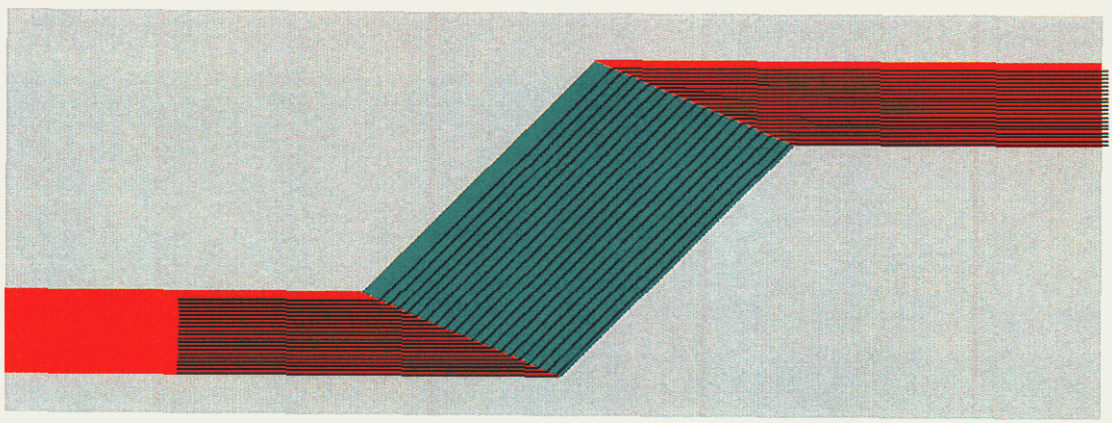

b. permeability ratio = nominal

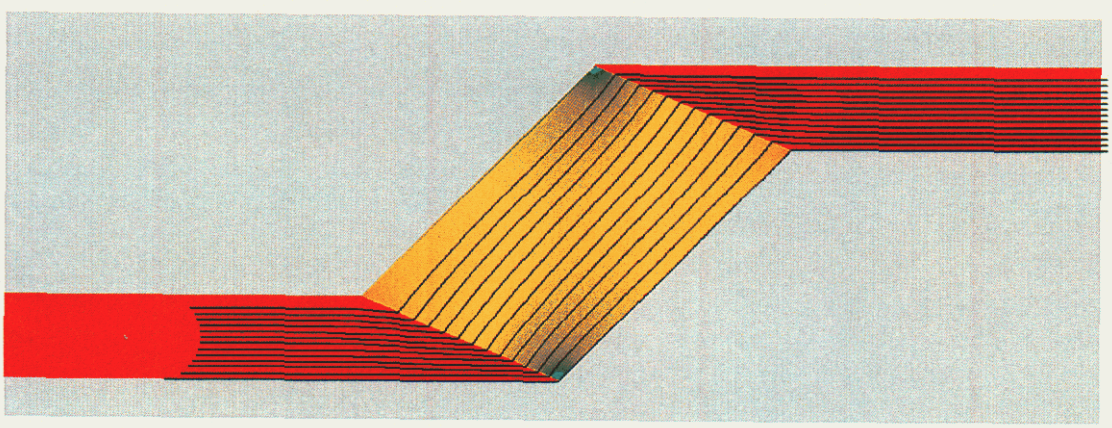

c. permeability ratio = twice nominal

Figure 2.6: Numerical simulation of flow past two symmetrical interfaces. The black lines are streaklines, the spectral color map depicts the speed field: blue and red are respectively the highest and lowest speeds. The three instances show the effects of violating (a. and c.) and satisfying (b.) the compatibility relation, Eq. 2.2. The solution of flows within designs that satisfy compatibility are algebraically tractable.

This page intentionally contains only this sentence.

CHAPTER 3

Critical-turning-angle interfaces

3.1 Maximum turning angle

Figure 3.1 shows the variation of the turning angleof a single interface, $\theta_1 - \theta_2$, with the incidence angle, θ_1, for a variety of specific permeability ratios (SPRs). The maximum turning angle of an interface, called the critical turning angle is

$$\theta_c \equiv \max(\theta_1 - \theta_2) = 2\tan^{-1}\left(\sqrt{\frac{\sigma_1}{\sigma_2}}\right) - \frac{\pi}{2}, \tag{3.1}$$

and occurs at the angles

$$\theta_1 = \tan^{-1}\left(\sqrt{\frac{\sigma_1}{\sigma_2}}\right) \text{ and } \theta_2 = \tan^{-1}\left(\sqrt{\frac{\sigma_2}{\sigma_1}}\right). \tag{3.2}$$

Figure 3.2 shows the variation of these angles with the SPR across the interface. The SPR at the critical turning angle, θ_c is from Eq. 3.1,

$$\left.\frac{\sigma_1}{\sigma_2}\right|_c = \tan^2\left(\frac{\pi}{4} + \frac{\theta_c}{2}\right). \tag{3.3}$$

For example, to achieve turning angles of 30, 45, and 60 degrees across a single interface, the specific permeability ratio σ_1/σ_2 must respectively be at least 3, ~5.828427, and ~13.92820. The maximum turning angle asymptotes to 90° as $\sigma_1/\sigma_2 \to \infty$. Figure 3.3.a shows a design and simulation of the flow at an inclined interface designed to produce a 45° turn in the flow-velocity angle at this maximum-turning-angle condition. A 90° turn can be constructed by a sequence of two such turns "back-to-back," as shown in Fig. 3.3.b, or a channel offset with no turning can be constructed by sequencing the turns in the alternate arrangement shown in Fig. 3.3.c.

3.2 Minimum sensitivity to flaws

The use of maximum-turning-angle interfaces is advantageous because the sensitivity of the interface operation to angular or SPR errors the required SPR are minimized. However,

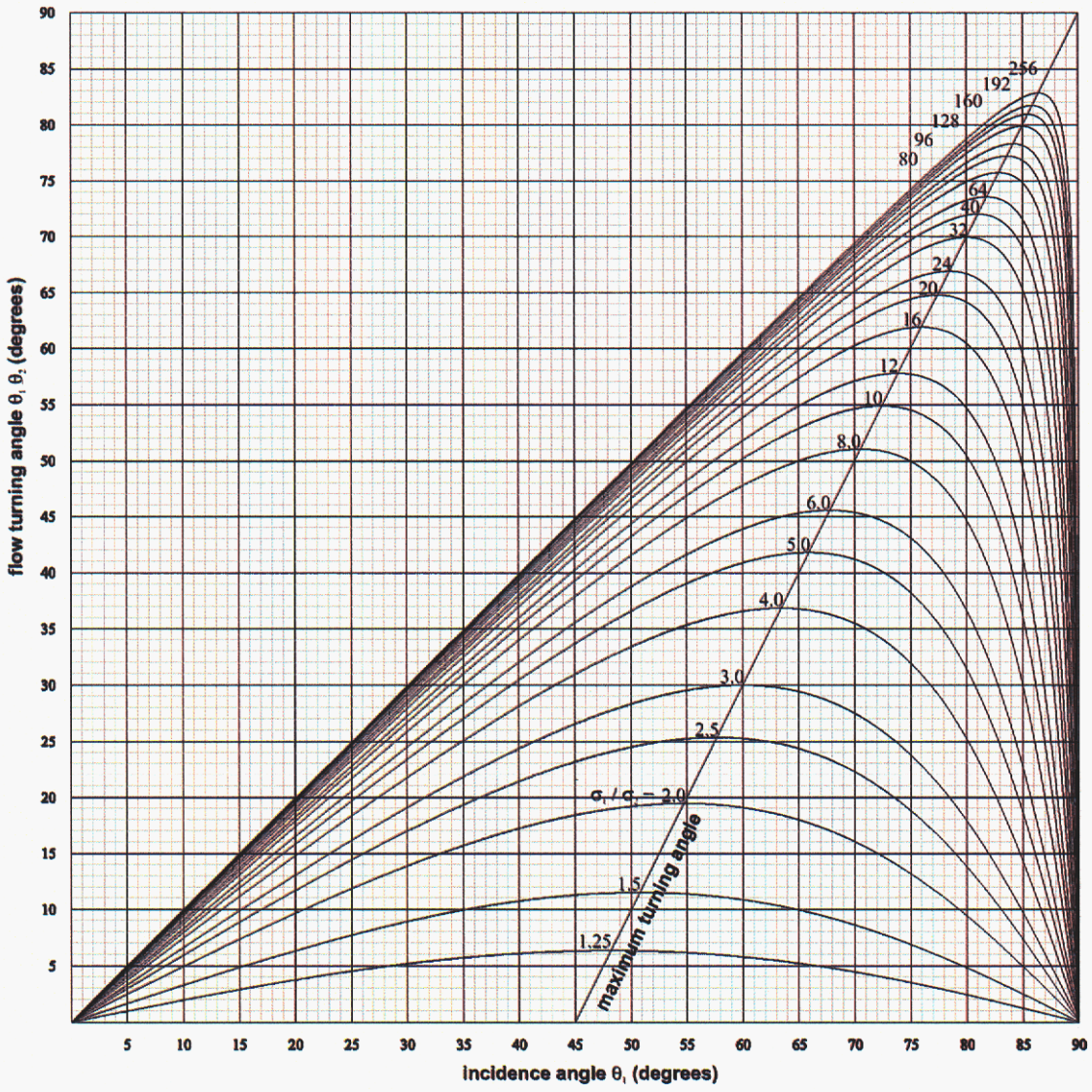

Figure 3.1: Variation of the flow-velocity turning angle, $\theta_1 - \theta_2$, with the incidence angle θ_1, at selected interface SPRs.

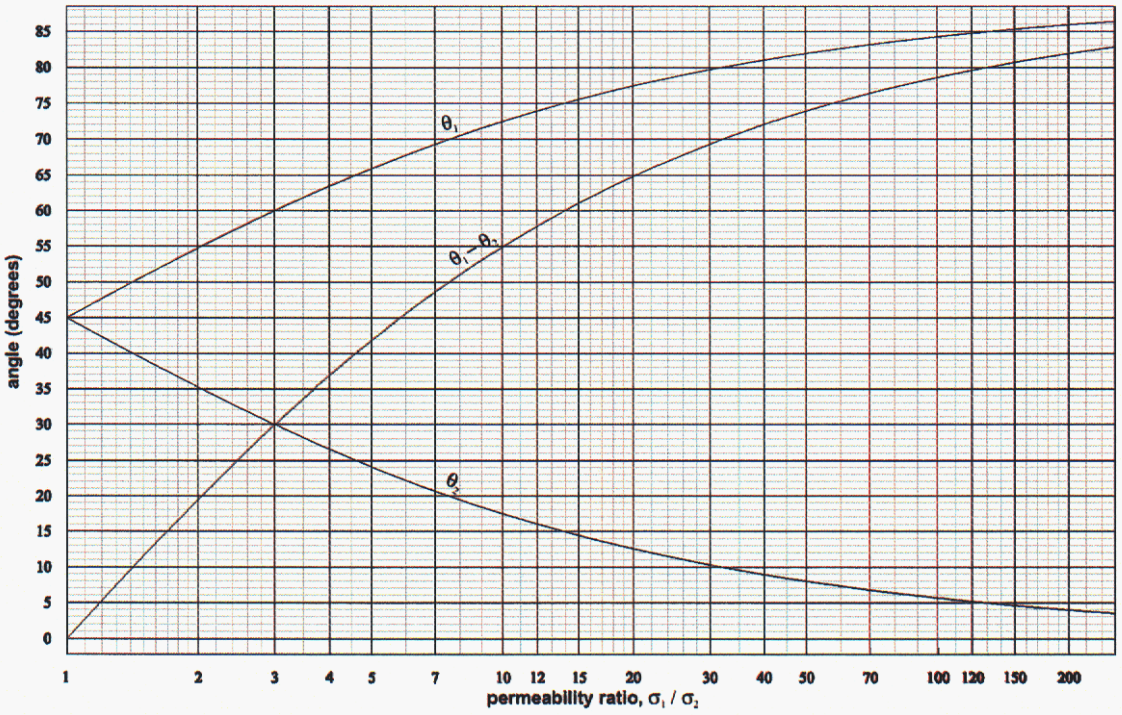

Figure 3.2: Variation with interface SPR of the incidence angle θ_1, exit angle, θ_2, and flow-velocity turning angle, $\theta_1 - \theta_2$, at the maximum turning angle.

sequences of interfaces designed at the maximum turning angle in a bi-specific-permeability system cannot change the channel width at either permeability and cannot generally compensate for rotation of material lines across the interface. Sub-critical turning interfaces provide the design flexibility lacked by the critical interfaces at the cost of additional sensitivity to fabrication errors.

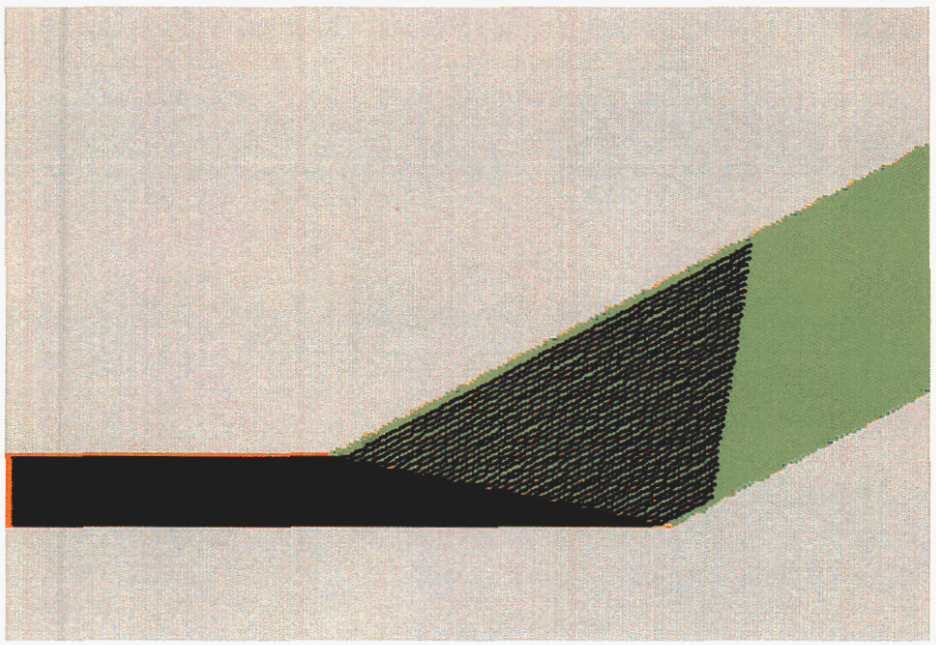

a. critical 45-degree interface

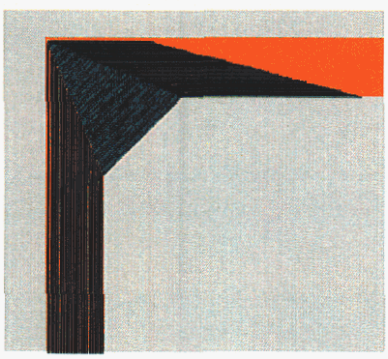

b. 90-degree turn

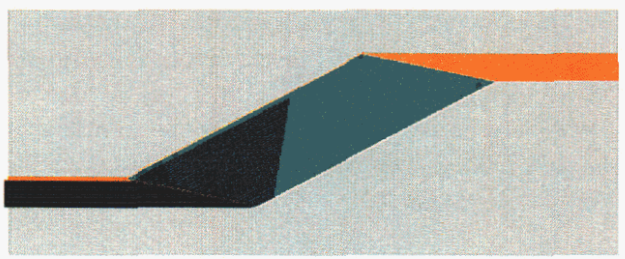

c. 45-degree offset

Figure 3.3: Numerical simulations of flow streaklines and speed fields within devices based upon critical flow-turning angle 45° turns. The speed field is a spectral color map: blue is the highest speed and red is the lowest speed. The superimposed streaklines show pronounced skew in the 90° turn (b.) with respect to the flow direction. The 45° offset (c.) nulls this skew at the second interface. Neither device b. nor c. can change the width of the exit port with respect to the entry port because of the criticality of the angle.

CHAPTER 4

Sub-critical turning angle interfaces

4.1 A degree of freedom

Any turning angle with a magnitude less than the maximum turning angle can be obtained at two different incidence angles. One may use this additional freedom to design interfaces to widen flow channels with or without rotation or to design interfaces that do not rotate material lines with respect to the flow. Figure 4.1 compares designs of two subcritical interfaces (b. and c.) that turn the flow by 10° to the critical design (a.) that turns the flow by 45°. The ratios of the channel widths at the interfaces are different for the two angles. Thus, one may construct a device to widen or narrow a channel without rotation by sequencing two such interfaces back to back, as shown in Fig 4.1 d. and e.

4.2 Expansions and turns

Figure 4.2 shows the variation in the width ratio at an interface, w_2/w_1, with the incidence angle, θ_1, at various SPRs. The width ratio is larger for the large-θ_1 interface than the small-θ_1 interface, especially at large SPR. The width ratio asymptotes to unity as $\theta_1 \to 0$ and to σ_1/σ_2 as $\theta_1 \to 90°$. The expansion or contraction ratio of a device having back-to-back interfaces is equal to the quotient of the width ratios at the larger and smaller incidence angles; thus, the expansion ratio for a bi-specific-permeability, two-interface device is bounded by the value of the SPR. Figure 4.3 shows a parametric plot of the turning angle versus the channel width ratio at various SPRs—an alternative view of the curves shown in Figs. 3.1 and 4.2 that is useful for device design. Multiple devices can be staged to produce any desired expansion ratio and/or turning angle.

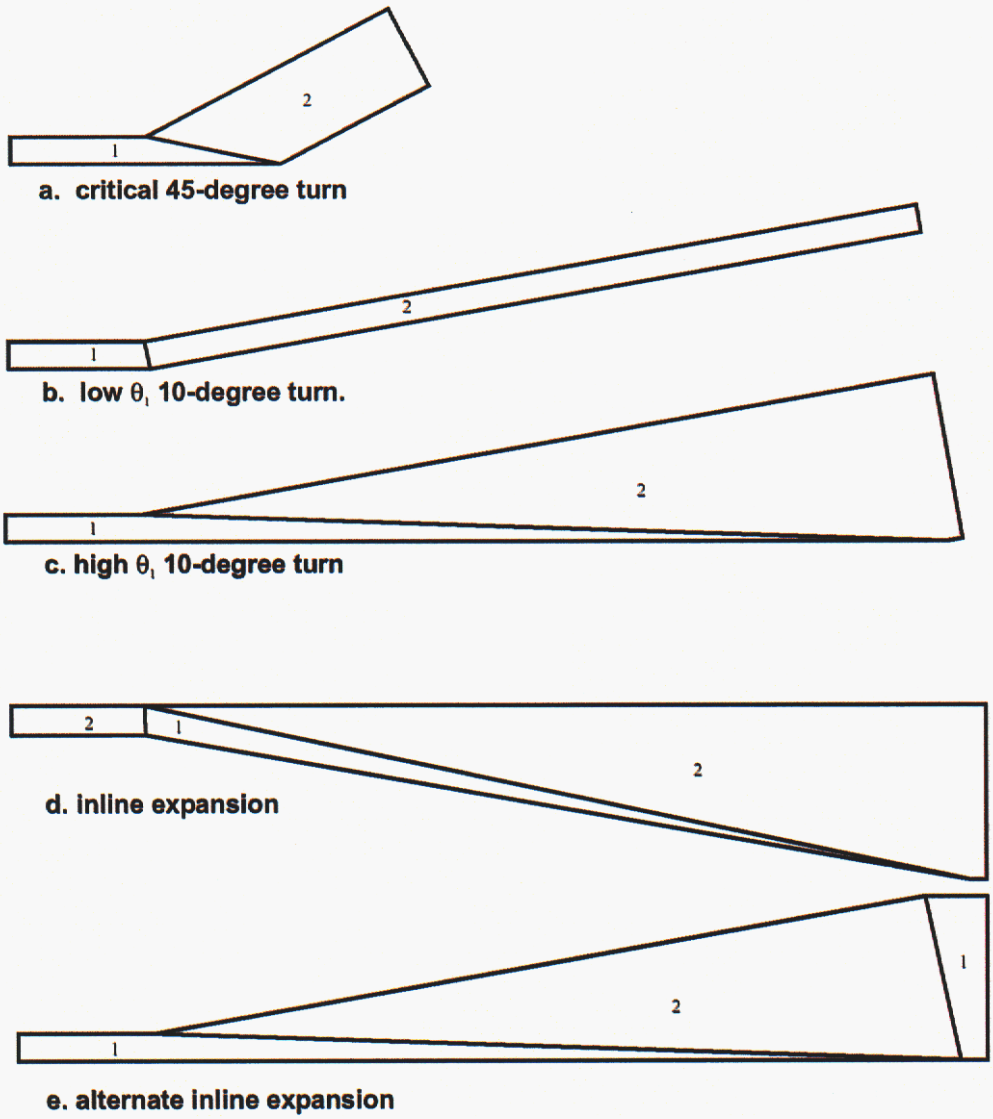

Figure 4.1: Sub-critical turning interfaces and their use in channel expansions. The numbers 1 and 2 identify the high and low specific-permeability regions, respectively. The interface in a. is at the critical turning angle of 45°. The interfaces in b. and c. both sub-critically turn the flow velocity by 10°. Rotation-free inline expansions, shown in d. and e. can be constructed by placing these interfaces back-to-back. Devices that both rotate and expand the channel (not shown) can be constructed similarly.

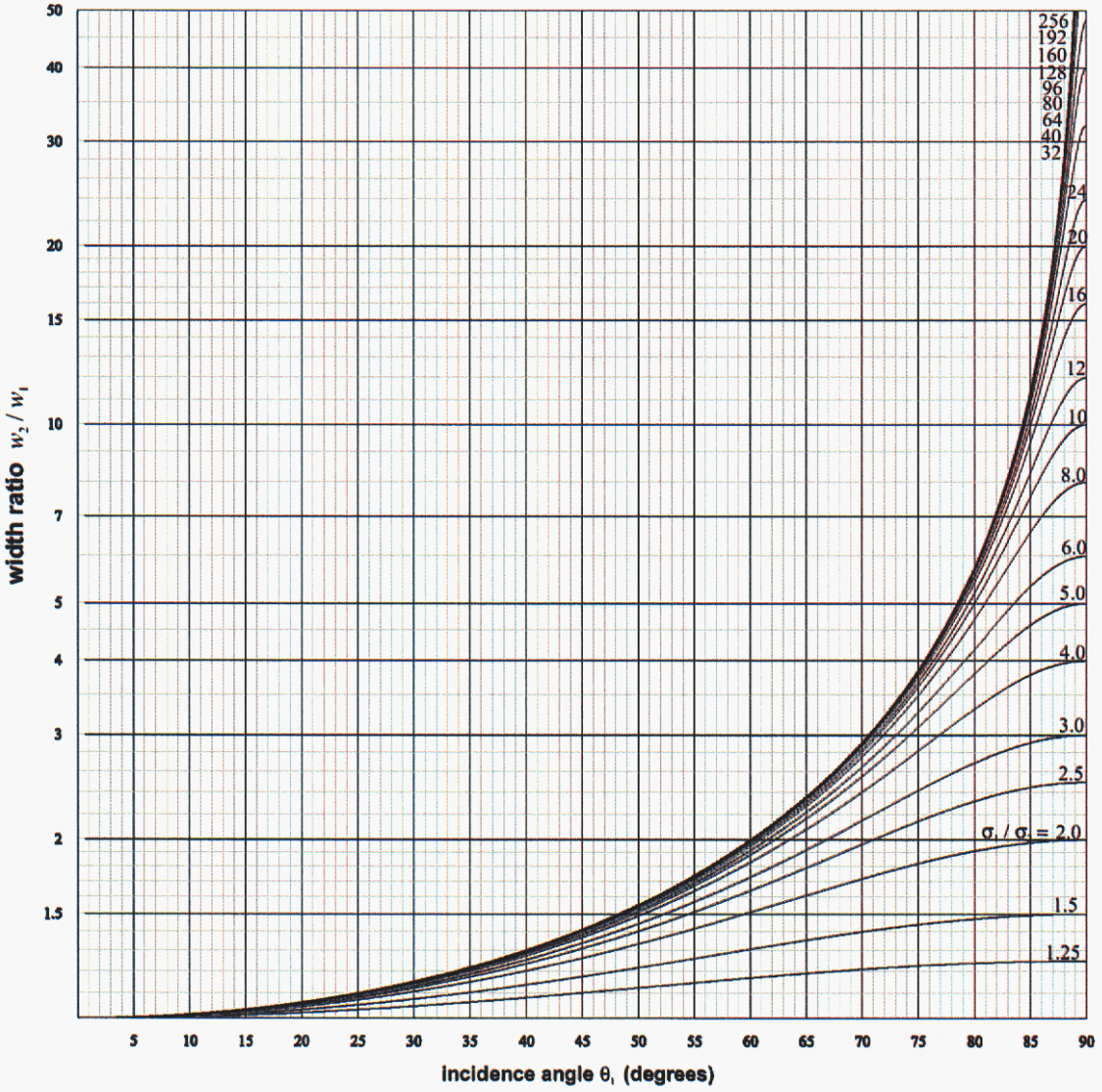

Figure 4.2: Variation of the ratio of channel widths with incidence angle across an interface having various SPRs. Because the high-incidence angles produce much larger width changes than the low-incidence angles, channel expanders or reducers can be constructed by sequencing high-incidence-angle and low-incidence-angle interfaces.

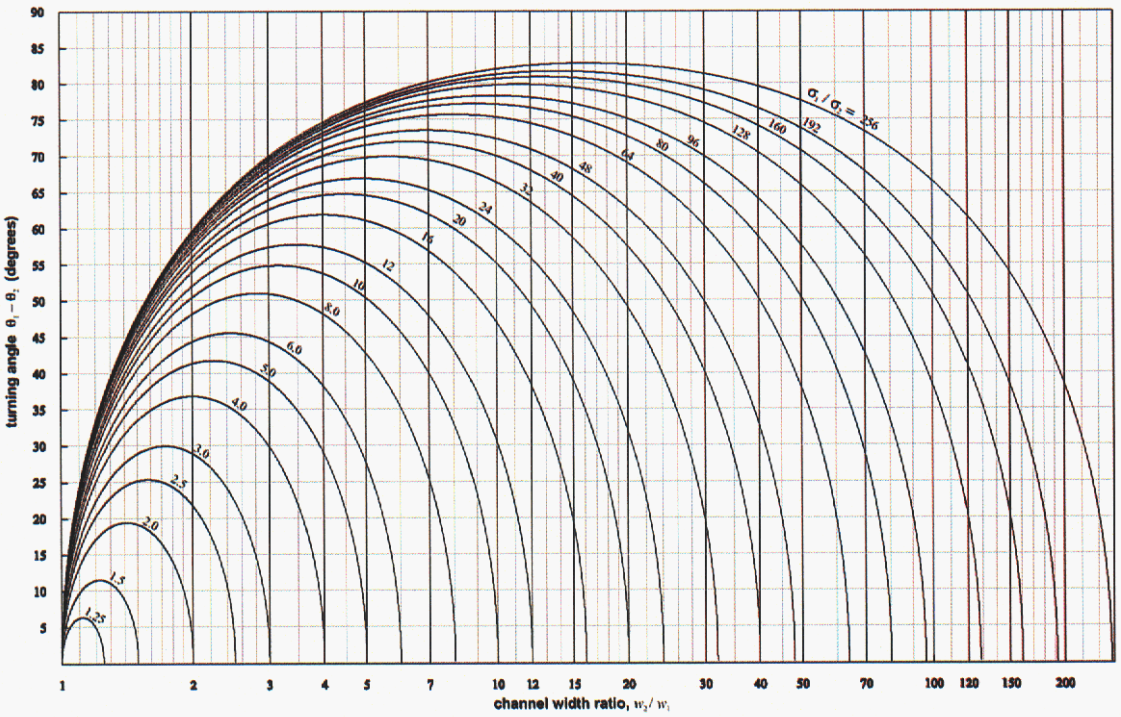

Figure 4.3: Variation of the turning angle with channel-width ratio across an interface having various SPRs.

CHAPTER 5

Skew-compensated interface pairs

5.1 Controlling skew

The use of sub-critical interfaces permits the design of interface sequences that rotate and stretch material lines by a prescribed amount. A common design goal is a device that produces no net rotation or skew of material lines with respect to the flow direction.

The angles ψ_1 and ψ_2 between the normal to a material line and the flow direction in the regions 1 and 2 (before and after an interface), respectively are related by

$$\tan\psi_2 \;=\; \frac{\sigma_1\cos^2\theta_1}{\sigma_2}\cdot\left[\tan\psi_1 \;+\; \tan\theta_1\,(1 \;-\; (\sigma_2/\sigma_1)^2(1 \;-\; \tan\psi_1\tan\theta_1))\right]. \quad (5.1)$$

If the material line is initially perpendicular to the flow direction, then $\psi_1 = 0$, and Eq. 5.1 simplifies to

$$\tan\psi_2|_{\psi_1=0} = \left(\frac{\sigma_1}{\sigma_2} - \frac{\sigma_2}{\sigma_1}\right)\frac{\sin 2\theta_1}{2}, \quad (5.2)$$

which is plotted in Fig. 5.1. Equation 5.2 and Fig. 5.1 indicate any single, non-trivial interface having a non-zero incidence angle skews material lines with respect to the flow. The critical incidence angle for rotating initially normal material lines is 45° regardless of the SPR. Expression 5.2 is symmetric about this critical angle, so back-to-back interfaces having incidence angles that sum to 90° can be used to compensate for interface-induced skew or rotation of material lines. The turning angle θ_T of such a skew-compensated turn is

$$\theta_T = \frac{\pi}{2} - 2\theta_1 - \tan^{-1}\left(\frac{\sigma_2}{\sigma_1\tan\theta_1}\right) + \tan^{-1}\left(\frac{\sigma_2\tan\theta_1}{\sigma_1}\right). \quad (5.3)$$

5.2 Critical skew compensation

Figure 5.2 plots Eq. 5.3, the turning angle versus incidence angle for skew-compensated interface pairs at various SPRs. The peak of these curves is the maximum, skew-compensated turning angle that is possible with two back-to-back interfaces. Again, designing for this

peak is desirable for minimizing sensitivity to fabrication problems and minimizing the SPR. The SPR to achieve a desired no-skew turn is twice that needed to achieve an uncompensated turn. Figure 5.3 shows the expansion factor for a skew-compensated interface pair.

5.3 Expanding and non-expanding turns

For example, Fig. 5.4 shows a simulation of a skew-compensated interface pair. The material front, as indicated by the black streaklines, again becomes perpendicular to the flow velocity after passing the second interface. This skew-compensated "prism" design expands or narrows the channel by a factor of ~4.6 as it turns the flow velocity by 45°. The SPR required for this prism is ~11.6, twice that for the critical interface shown in Fig. 3.3. Because this prism changes the width and direction of the flow, sequences of this prism design can be plumbed to make both skew-compensated turns, as shown in Figs. 5.5 and 5.6, expansions, as shown in Fig. 5.7, and expanding turns, as shown in Fig. 5.8.

Figure 5.5 shows a simulation of a device made by connecting the narrow channels from the prisms shown in Fig. 5.4. This device rotates the flow by 90° without changing the channel size. An alternate turn can be constructed by connecting the wide channels of the prisms. The straight section between the two prisms can be lengthened arbitrarily or shortened as shown in Fig. 5.6. This figure shows two simulations of this turn design, the left one having the correct SPR and the right one having a SPR that is off by 5%. The operation of the turn is relatively insensitive to such errors, but the small skew and curvature of the streakline front in the off-design simulation shows how such errors can limit the device performance. Additional prismatic elements can be added to the design to compensate for such effects and to minimize the sensitivity of the system to SPR errors.

Figure 5.7 depicts scaled copies of the same prism design arranged so the entry and exit channels are parallel and each prism expands the flow channel. The resulting expansion factor is ~ 21. Adding a third prism results in an expansion factor of ~ 99, and so on. Figure 5.8 shows the prism design arranged to rotate and expand the flow channel by a factor of ~ 21.

Figure 5.9 plots the incidence angles θ_1 that do not rotate material-line angles with respect to the flow, i.e., $\psi_1 - \psi_2 = 0$, for values of ψ_1 (and ψ_2) from 0 to 90°. Two such solutions exist at each material line angle,

$$\cos\theta_1 = \cos\psi_1 \left[\frac{1}{2}\left(1 + \frac{b}{a} \pm \sqrt{1 + \frac{2b}{a^2}}\right)\right]^{1/2}, \tag{5.4}$$

where

$$a \equiv 1 + \frac{\sigma_2}{\sigma_1} \text{ and } b \equiv 2\frac{\sigma_2}{\sigma_1}\tan^2\psi_1. \tag{5.5}$$

These curves can be useful for simplifying the design of interfaces within a multiple-interface system where skew is not internally compensated.

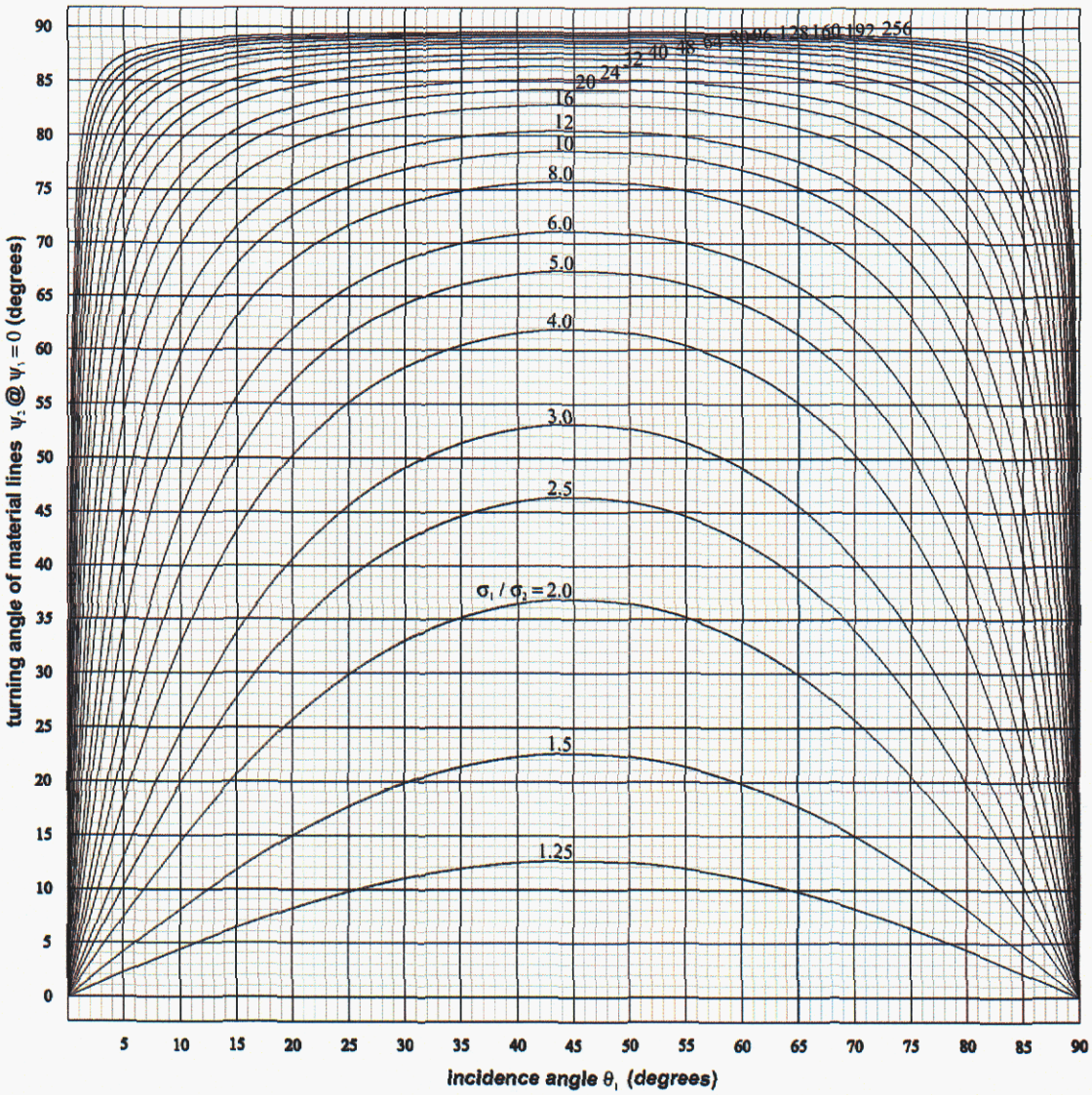

Figure 5.1: Variation with incidence angle and SPR of the skew angle introduced by an interface to a material line that is initially perpendicular to the flow direction. Since the skew is zero only at trivial points, a single interface cannot be designed to be skew-free. However, these curves are symmetric about 45° so two sequential interfaces having incidence angles that sum to 90° can compensate for skew.

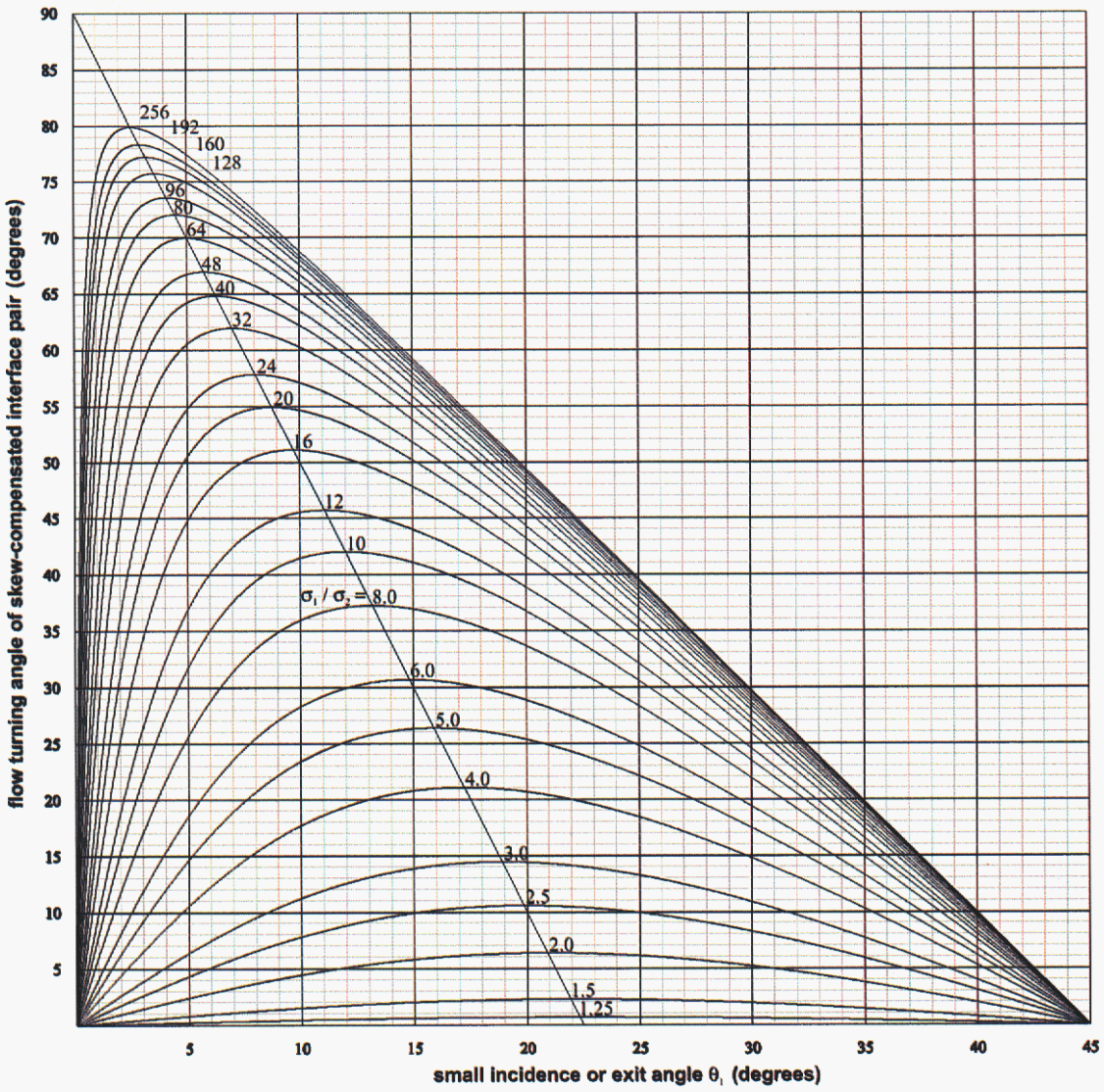

Figure 5.2: Variation of the flow-velocity turning angle of a skew-compensated interface pair with the smaller of the incidence or exit angles, θ_1, at various SPRs. The line indicates the loci of critical angles in which the required SPR to turn the flow and sensitivity to fabrication errors are minimized. This critical angle for skew-compensated interface pairs is not the same as the critical flow-turning angle shown in Figs. 3.2 and 3.1.

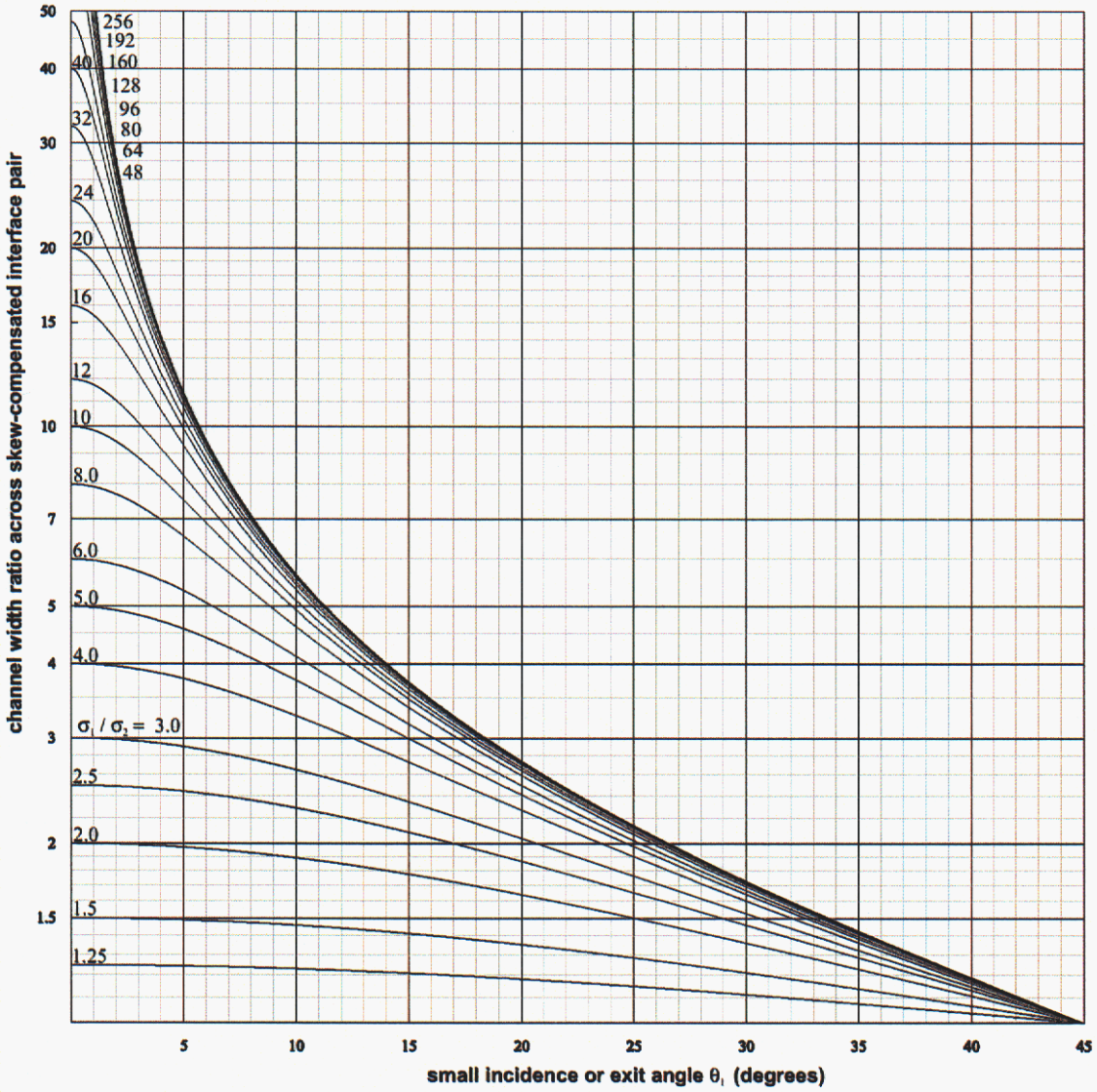

Figure 5.3: Variation of the channel expansion ratio of a skew-compensated interface pair with the smaller of the incidence or exit angles, θ_1, at various SPRs.

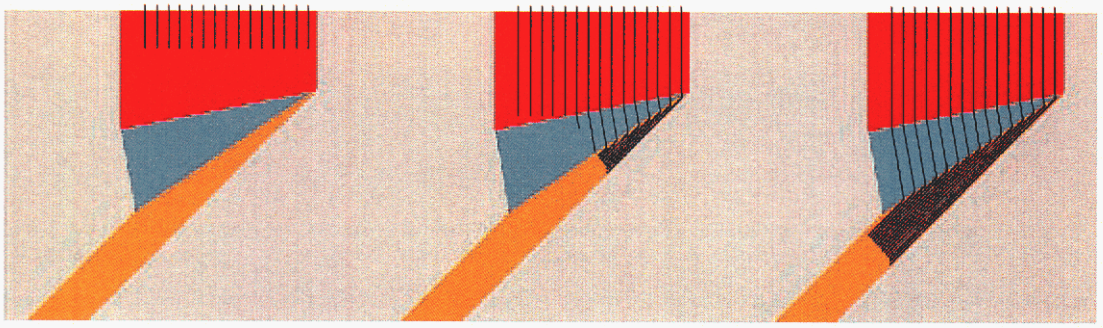

Figure 5.4: Flow simulation of a critical skew-compensated interface sequence that rotates the flow by 45° and narrows the channel by a factor of ~4.6. The spectral color map depicts the calculated speed field. Blue and red respectively represent the highest and lowest speeds. The black lines are streaklines showing the motion of material elements. The front remains straight and oriented perpendicular to the flow after passage through the interfaces. The slight deviation of the bottom streakline is a numerical artifact from its proximity to the channel boundary.

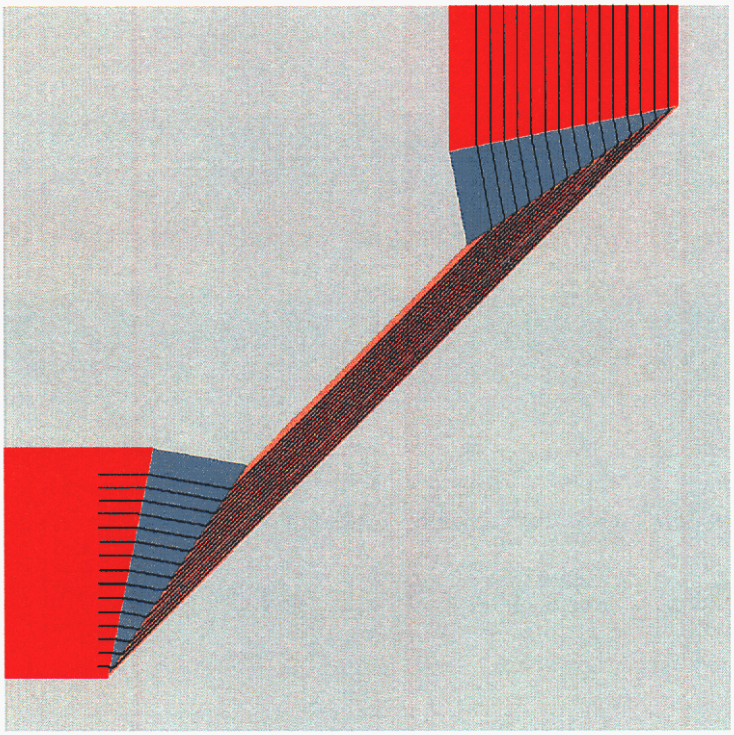

Figure 5.5: Flow simulation of a non-expanding 90° turn designed by connecting the narrow channels of two prisms like that in Fig. 5.4. The spectral color map depicts the calculated speed field. Blue and red respectively represent the highest and lowest speeds. The black lines are streaklines showing the motion of material elements. The front remains straight and oriented perpendicular to the flow after passage through the turn. An alternative turn could be designed by connecting the wide channels of the prisms. A simple, non-rotating offset could be designed by orienting the second prism to compensate for the rotation produced by the first.

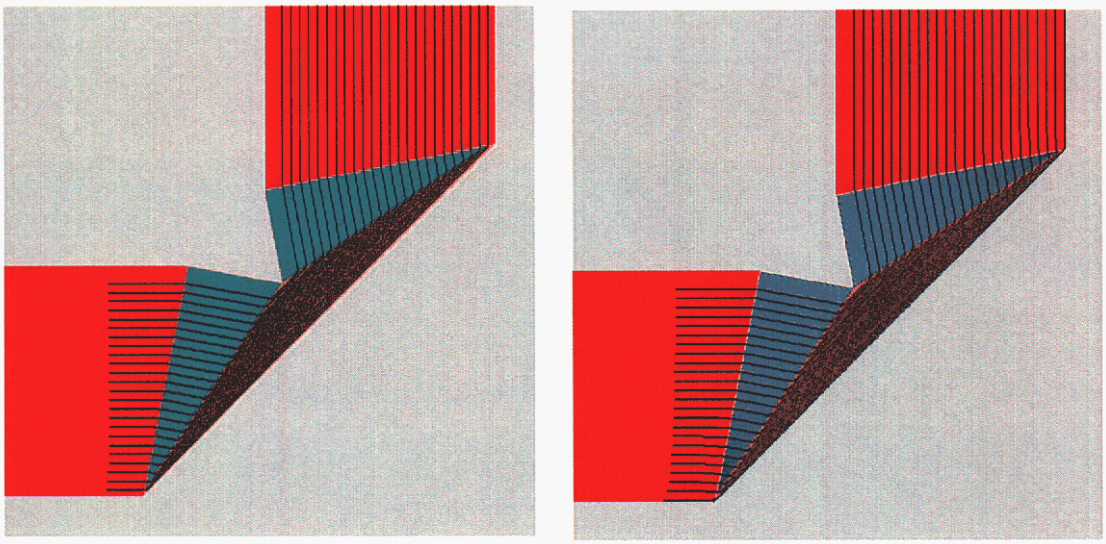

Figure 5.6: Flow simulation of an on-design (left) and off-design (right) non-expanding 90° turn. This design is the same as that in Fig. 5.5, but with the arbitrary length of the channel connecting the prisms shrunk to its minimum length. The SPR in the off-design turn is 5% off nominal. The impact on the operation is evidenced by a small skew of the streakline front. This impact is minimal because the prisms are designed at the critical angle in Fig. 5.2.

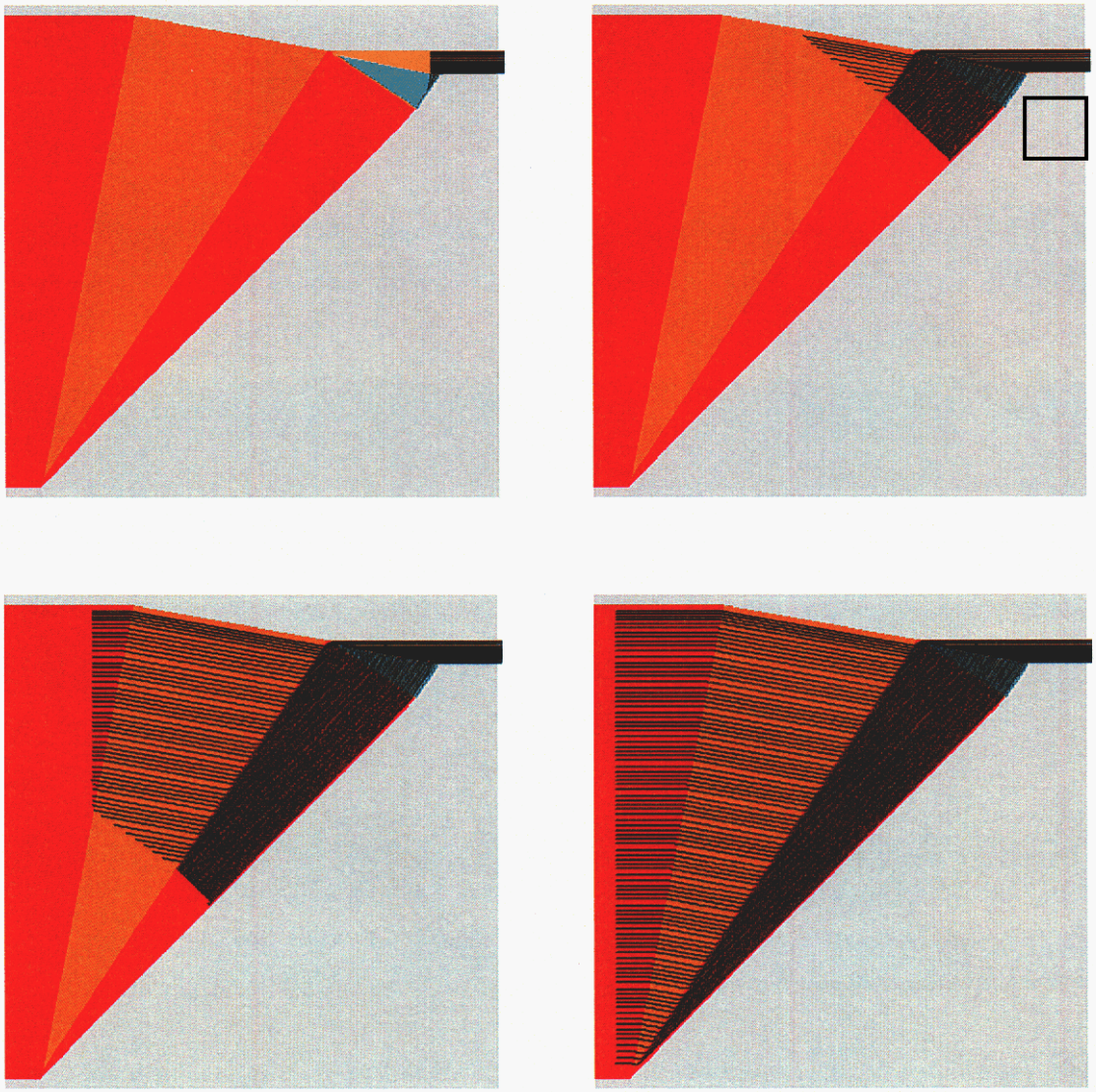

Figure 5.7: Flow simulation of an inline ~21-fold channel expander made from two prisms like that in Fig. 5.4 by connecting the wide port of one prism to the narrow port of the next.

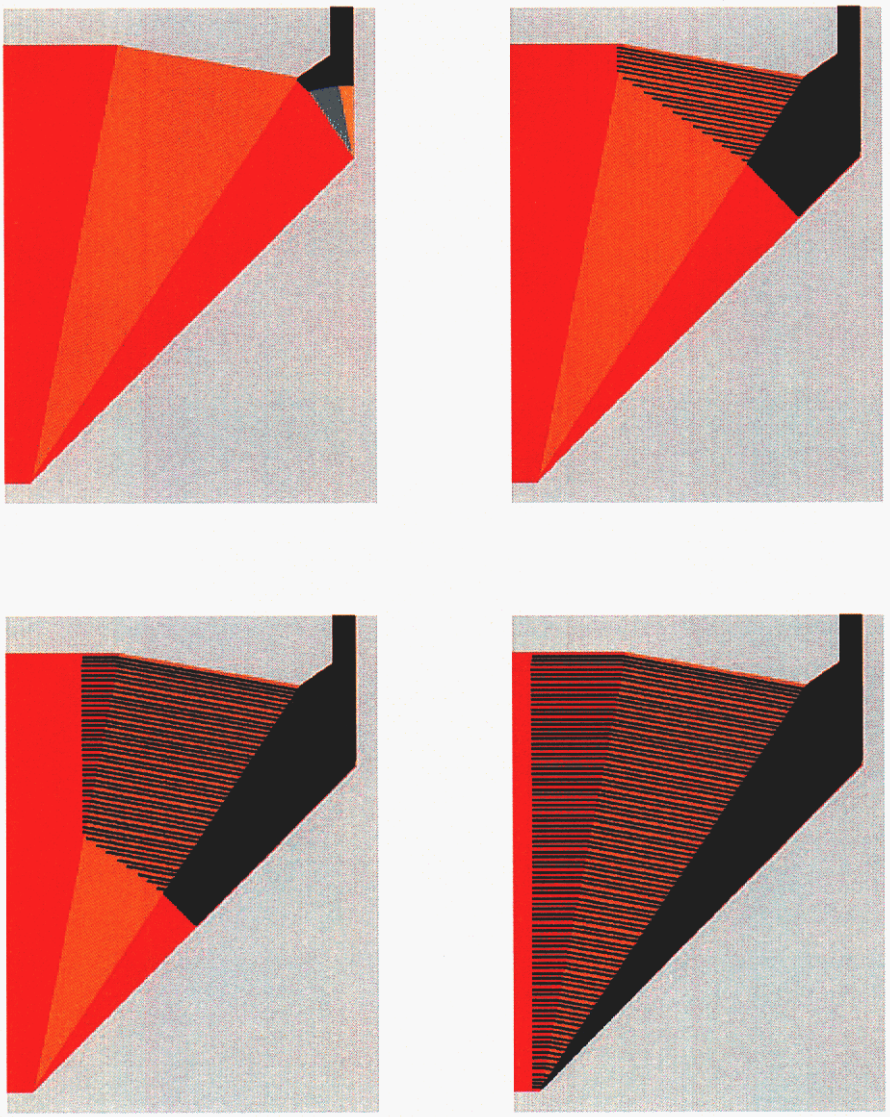

Figure 5.8: Flow simulation of a 90° ~21-fold channel expander made by connecting the wide port of one prism to the narrow port of the next in an alternative arrangement to that in Fig. 5.7.

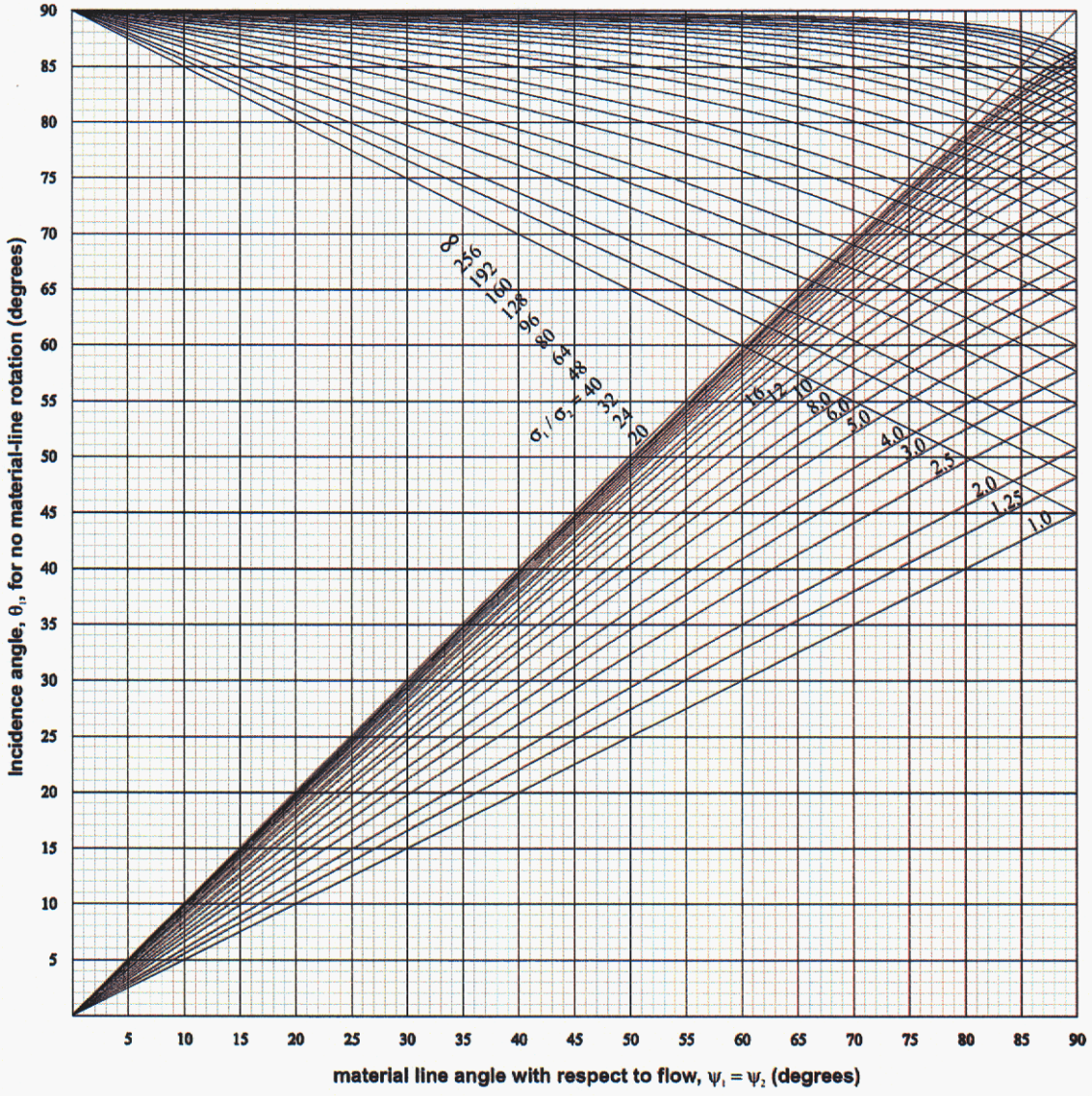

Figure 5.9: Plot of incidence angles that do not rotate material lines with respect to the flow, versus the orientation angle of the material lines at various SPRs.

This page intentionally contains only this sentence.

CHAPTER 6

Maximum-expansion skew-compensated three-interface systems

6.1 Three-interface systems

A single interface can expand a flow and change the specific permeability but cannot compensate skew. A two-specific-permeability system requires at least three-interfaces to compensate skew and change the specific permeability. The third interface adds one degree of freedom to the skew-compensation problem: given one interface, the two other interfaces can be adjusted in concert over a range of angles to compensate or control skew. This additional degree of freedom is useful, for example, to produce skew-controlled designs that produce a prescribed flow turning angle or the maximum expansion factor.

6.2 Maximum expansion factor with skew compensation

A system that expands a narrow, high-specific-permeability channel into a wide, low-specific-permeability channel is useful for open-channel electrochromatography. For this application, it is desirable to obtain a large channel expansion ratio. To achieve this expansion, a three-interface system will use large incidence angles for the first and third interfaces to expand the channel and the smallest possible incidence angle for the second interface to compensate skew while minimally contracting the channel. The largest allowable incidence angle ($|\theta_{1max}| < 90°$) depends on design constraints and fabrication limits. Assuming the allowable angle does not depend on channel width, an optimal three-interface system will set the first and third interface angles respectively to $+\theta_{1max}$ and $-\theta_{1max}$. The sign of the angle describes the relative orientation of the interfaces. This opposing orientation is chosen because it partly compensates skew.

Setting the incidence angles in this fashion removes the extra degree of freedom in the system, constraining the angle of the second interface to isolated solutions of a transcendental equation. Figures 6.1 and 6.2 show plots at various SPRs of the minimum skew-compensating incidence angle of the second interface obtained by solving this transcendental equation as a function of the magnitude of the first and third incidence angles.

The expanded plot in Fig. 6.2 shows the solutions for angles in the practically important range of 80–90°. The maximum expansion of the three-interface system occurs when the angle of the internal interface is zero, producing no contraction of the channel. The solutions for this angle approach zero as the magnitude of the first and third incidence angles approach 90°. However, the peak value of the internal angle also occurs near 90°, particularly at large SPRs. Practical systems may not benefit from this dip in the internal angle because of the extreme incidence angles required.

Figure 6.3 shows the resulting expansion ratio of the skew-compensating three-interface system. As the magnitudes of the first and third incidence angles approach 90°, the expansion ratio approaches the theoretical maximum of σ_1^2/σ_2^2. The expansion ratio drops precipitously away from 90°, therefore, much lower ratios are likely to be realized in practice. Figure 6.4 shows the ratio of the expansion factor of the three-interface system to that of the first (or third) interface. In the evident plateau region (at a ratio ~1.7) for larger SPRs, the contraction across the second interface largely overcomes the additional expansion from the third (or first) interface; consequently the overall expansion is less than a factor of two higher than that of a single-interface expansion.

Figure 6.5 plots the turning angle of the skew-compensating, three-interface system. The first and third angles are arranged oppositely; hence their turning angles cancel each other. Therefore, flow turning is produced by the second interface.

6.3 Comparison with maximum uncompensated expansion

Figure 6.6 shows numerical simulations of flow in a skew-compensated and an uncompensated system. Each system consists of a symmetrical pair of three-interface expansions. Both interfaces have a SPR of 10 and a maximum incidence angle of 85°. Channels are extended slightly more than necessary past each interface to highlight how the system works. The expansion factors for the compensated and uncompensated systems are respectively $\sim$ 14.32 ($\sim$ 1.9× the single-interface expansion factor) and $\sim$ 57.08 (the square of the single-interface expansion factor) at second-interface incidence angles (θ_2) of 22.82° and 0°. The arrows indicate the width of the channels following the expansion. In a separation column, the widened channel would typically extend a comparatively long distance to allow samples to separate before detection or collection.

The expanded channel can be contracted back to the width of the initial channel by the symmetrically placed interface systems shown in Fig 6.6. Since this symmetrical arrangement is always skew compensating, the resulting six-interface system produces no net skew. The skew of the uncompensated, three-interface system produces a net effect because of diffusion. The material-line angle along the expanded channel is $\psi \simeq 40.18°$. The material line is longer by $1/\cos\psi \simeq 1.31\times$ than an un-skewed line. The stretching of the line also sharpens gradients normal to the material line. Consequently, a skewed material line diffuses $1/\cos^2\psi \simeq 1.71\times$ faster than an un-skewed line. This degradation in performance may be offset by other factors or design considerations that favor an uncompensated or partly compensated three-interface system.

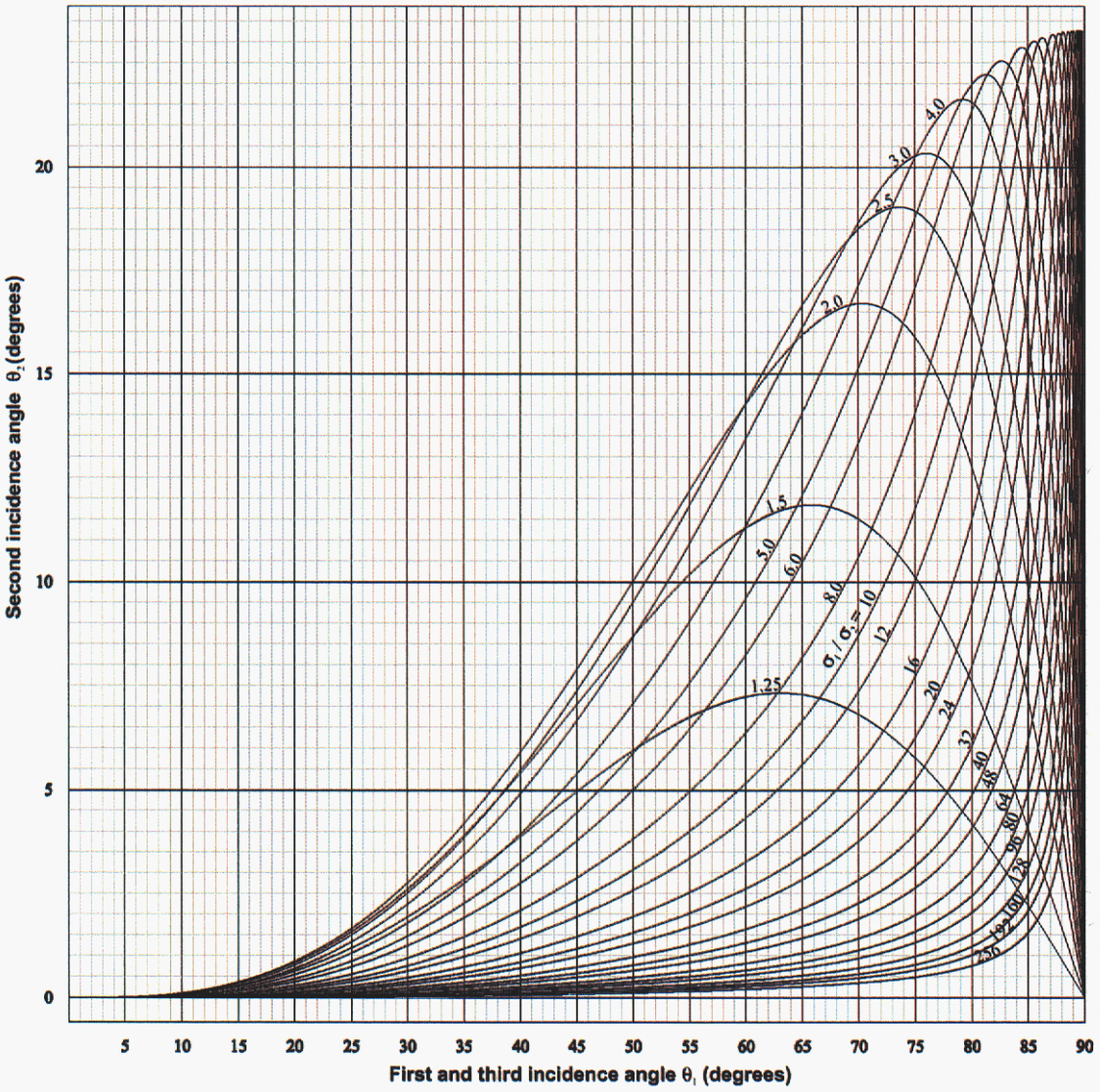

Figure 6.1: Plot of solutions for the second-interface incidence angle that compensates skew in a three-interface system vs. the magnitude of the first- and third-interface incidence angle at various SPRs.

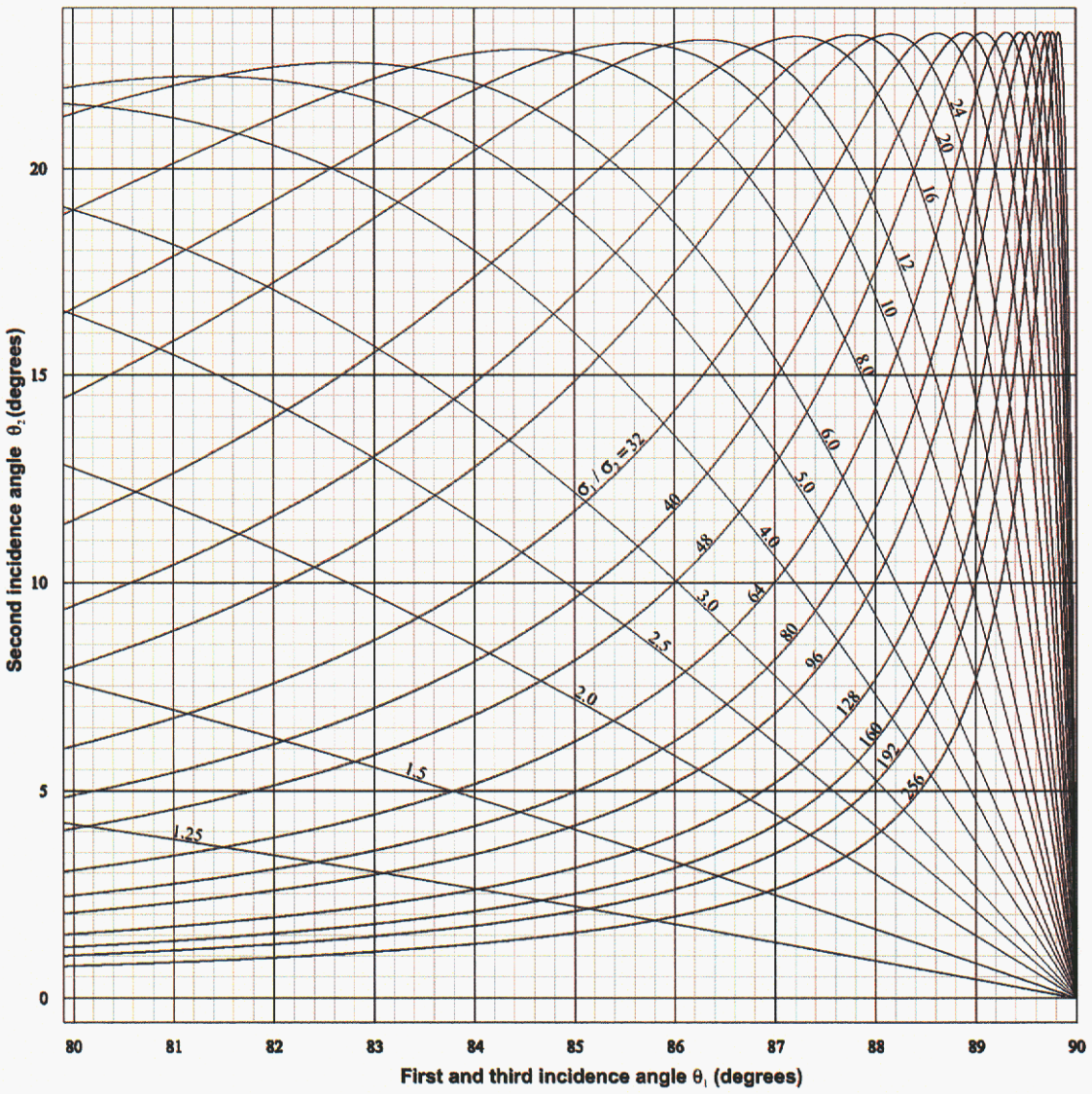

Figure 6.2: Expanded plot of solutions for the second-interface incidence angle that compensates skew in a three-interface system versus the magnitude of the first- and third-interface incidence angle at various SPRs.

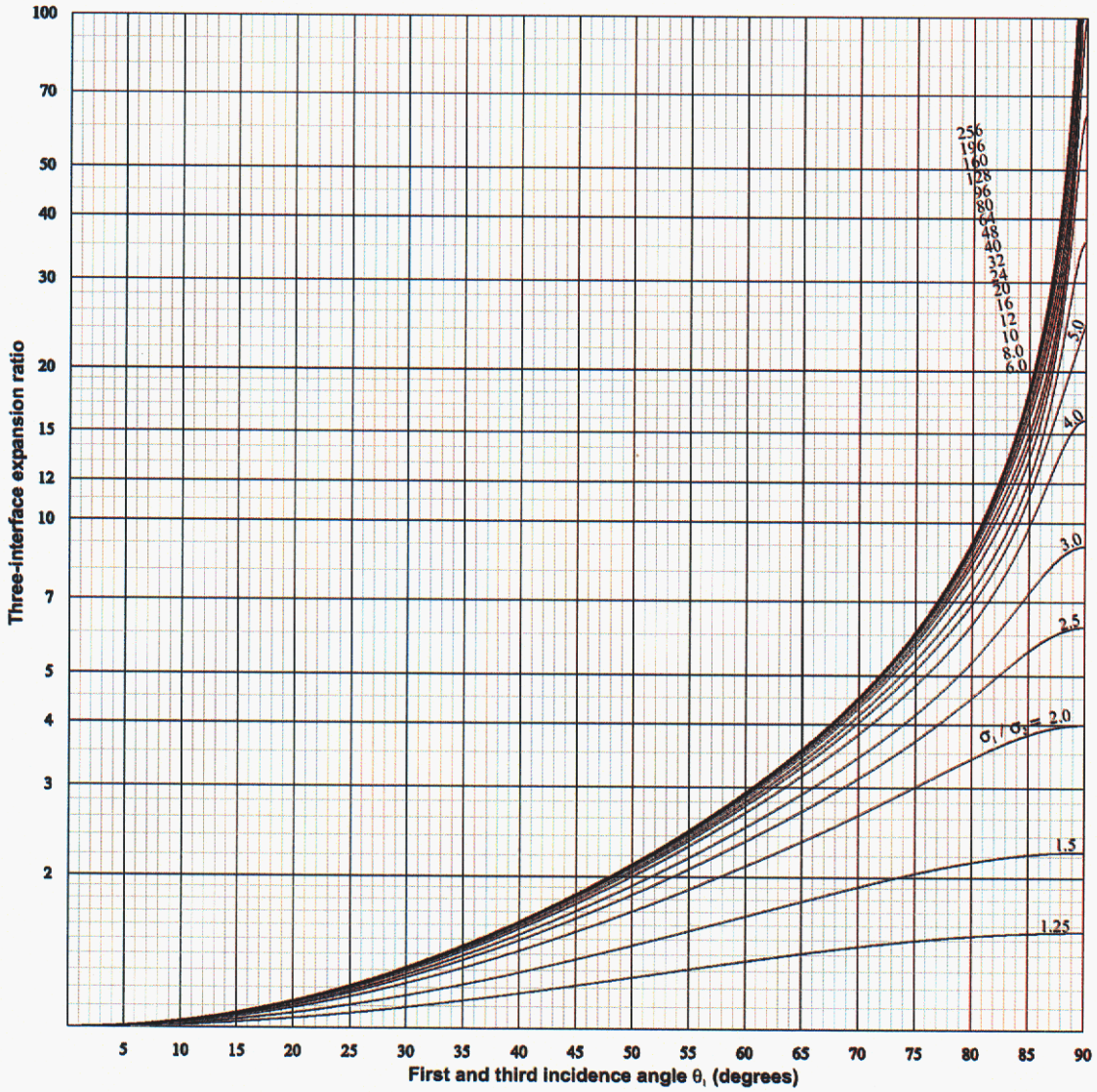

Figure 6.3: Plot of the expansion ratio of the three-interface, skew-compensated expander versus the magnitude of the first and third interface incidence angles at various SPRs.

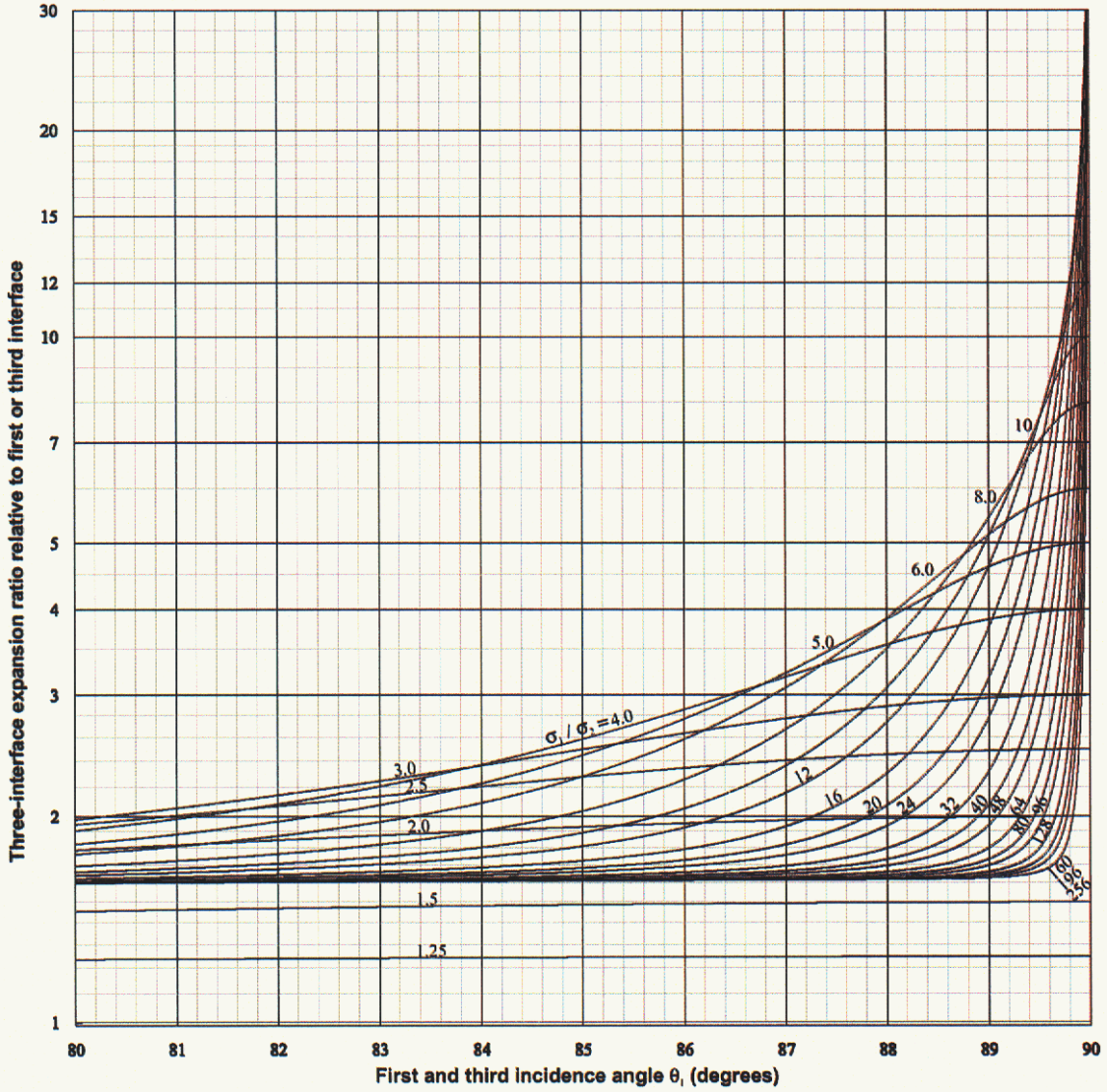

Figure 6.4: Plot of the ratio of expansion factor of the three-interface, skew-compensated expander to that of a single interface having the same initial incidence angle for various SPRs.

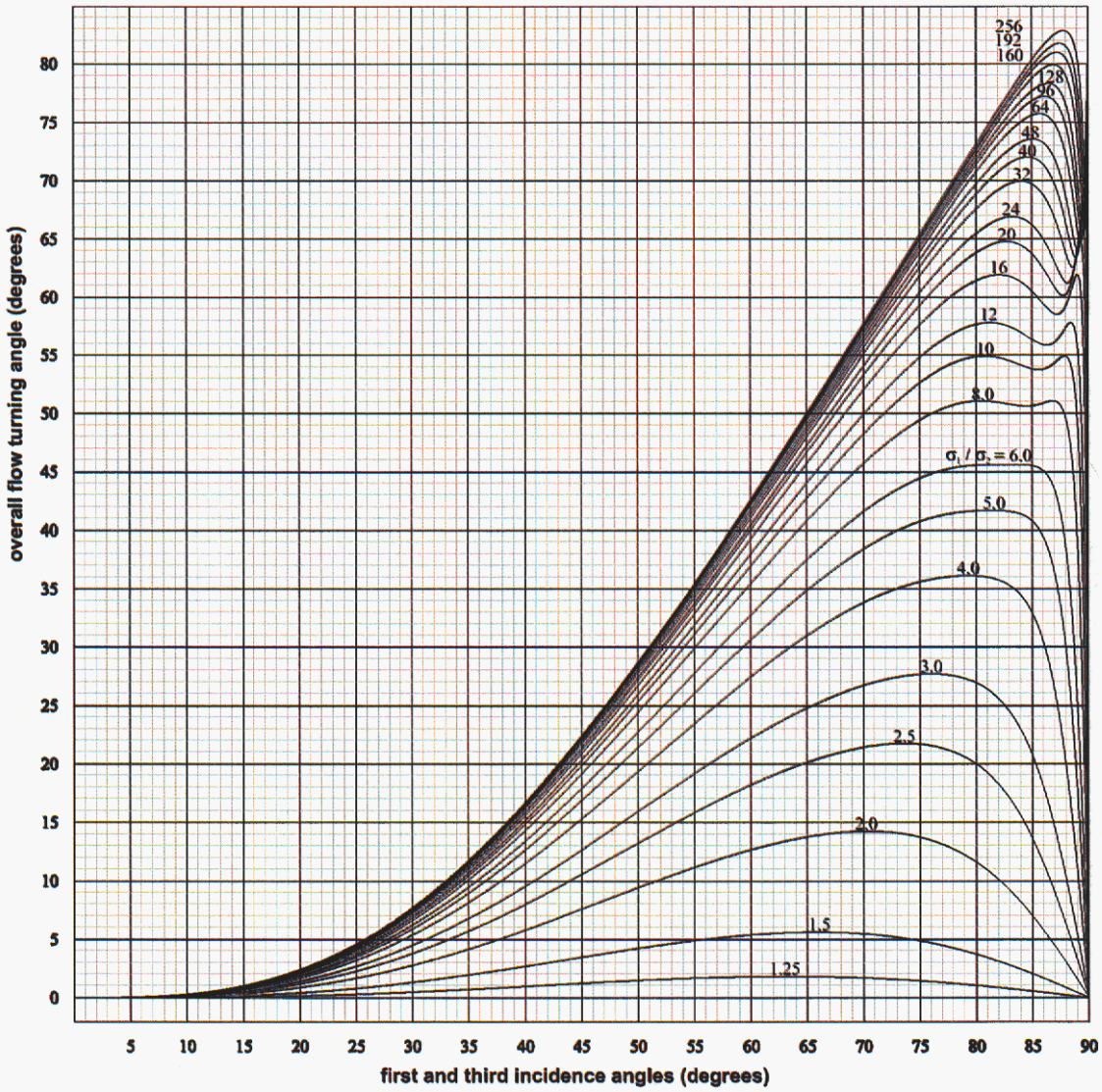

Figure 6.5: Plot of the turning angle of the three-interface skew-compensated expander versus the first and third incidence angles for various SPRs.

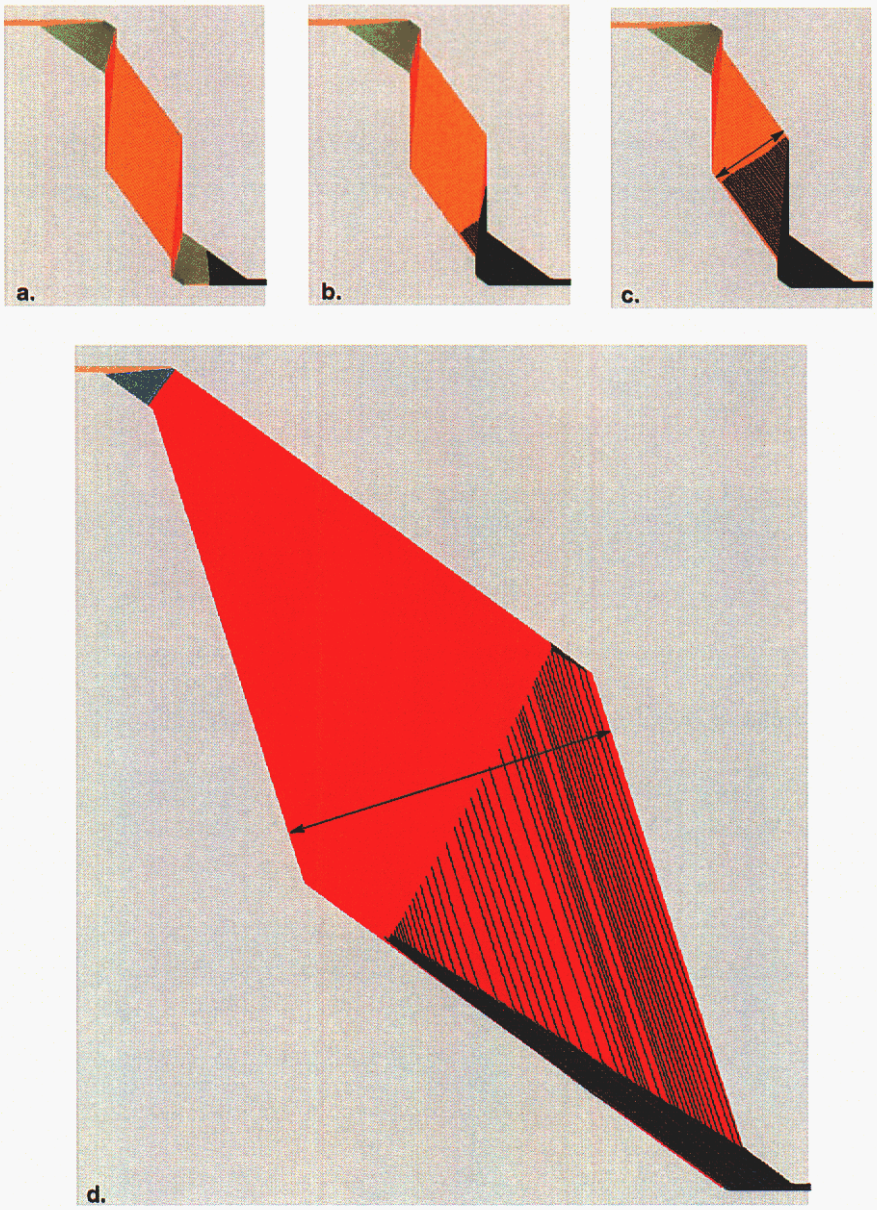

Figure 6.6: Flow simulation of transport in two systems of symmetrically placed three-interface expanders having a SPR of 10 and an incidence angle of 85°. The images a–c and d respectively show skew compensated and uncompensated systems. The background color depicts the magnitude of the speed field (red is the lowest speed). The black lines are calculated streak lines of particles that show the effect of compensation. The arrows show the relative magnitude of the expansion factor.

CHAPTER 7

Many-interface systems

7.1 More degrees of freedom and lower SPRs

Increasing the number of interfaces in a system decreases the incidence angles and SPRs needed to attain a given turning angle or expansion factor. The number of degrees of freedom increase with the interface count and many different interface arrangements can produce a prescribed turning angle, expansion factor, and skew.

7.2 Maximum skew-compensated expansion

Two arrangements of interfaces are explored to make a high-expansion, many-interface system. The following discussion applies to bi-permeability systems in which the inlet and exit channels have the larger specific permeability. The incidence angle on the upstream side of the i-th interface is θ_{i1}; the incidence angle on the downstream side (exit angle) is θ_{i2}. In the first arrangement, all incidence angles at interfaces that reduce the specific-permeability (odd interfaces) are set to a single prescribed angle, i.e.,

$$\theta_{i1} = \theta_o \text{ for odd } i \leq N, \tag{7.1}$$

where N is the (odd) number of interfaces in the expansion. The final interface ($i = N$) is oriented opposite to the other interfaces. All incidence angles at interfaces that increase the specific permeability (even interfaces) are constrained to the same angle, θ_e, i.e.,

$$\theta_{i1} = \theta_e \text{ for even } i < N. \tag{7.2}$$

These constraints along with the requirement for skew compensation remove all degrees of freedom allowing the solution for the magnitude of the even-interface angle.

Figures 7.1–7.4 plot solutions for the even-interface incidence angle for such five- and seven-interface systems. The resulting expansion factors are plotted in Figs. 7.5 and 7.6. For a given incidence angle or SPR, these expansion factors increase with interface count but are significantly smaller than is attainable without skew compensation, except as the odd incidence angles approach 90°.

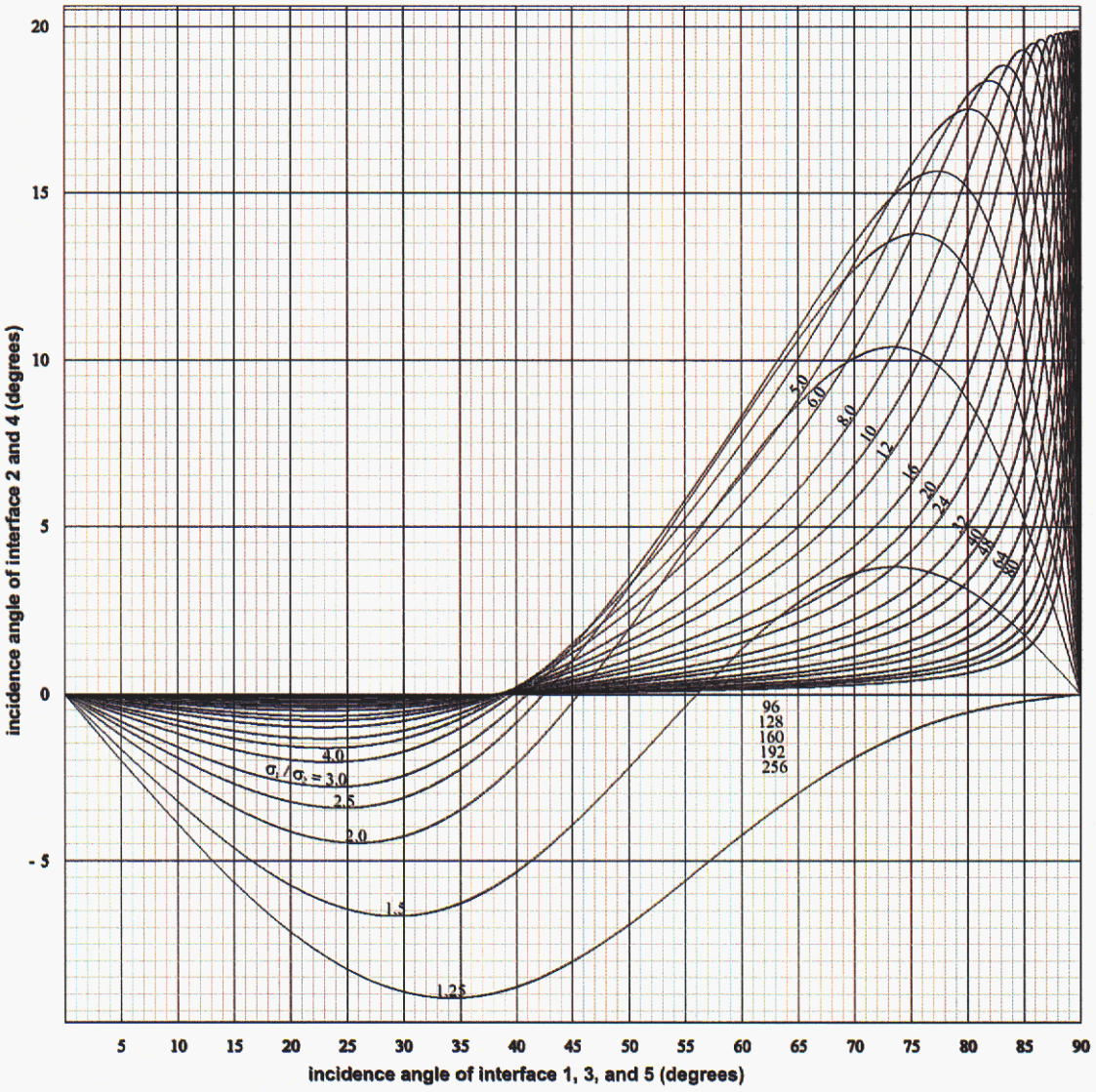

Figure 7.1: Plot of solutions for the even-interface incidence angle, θ_e, that compensates skew in a five-interface system vs. the magnitude of the incidence angle of the odd interfaces, θ_o, at various SPRs.

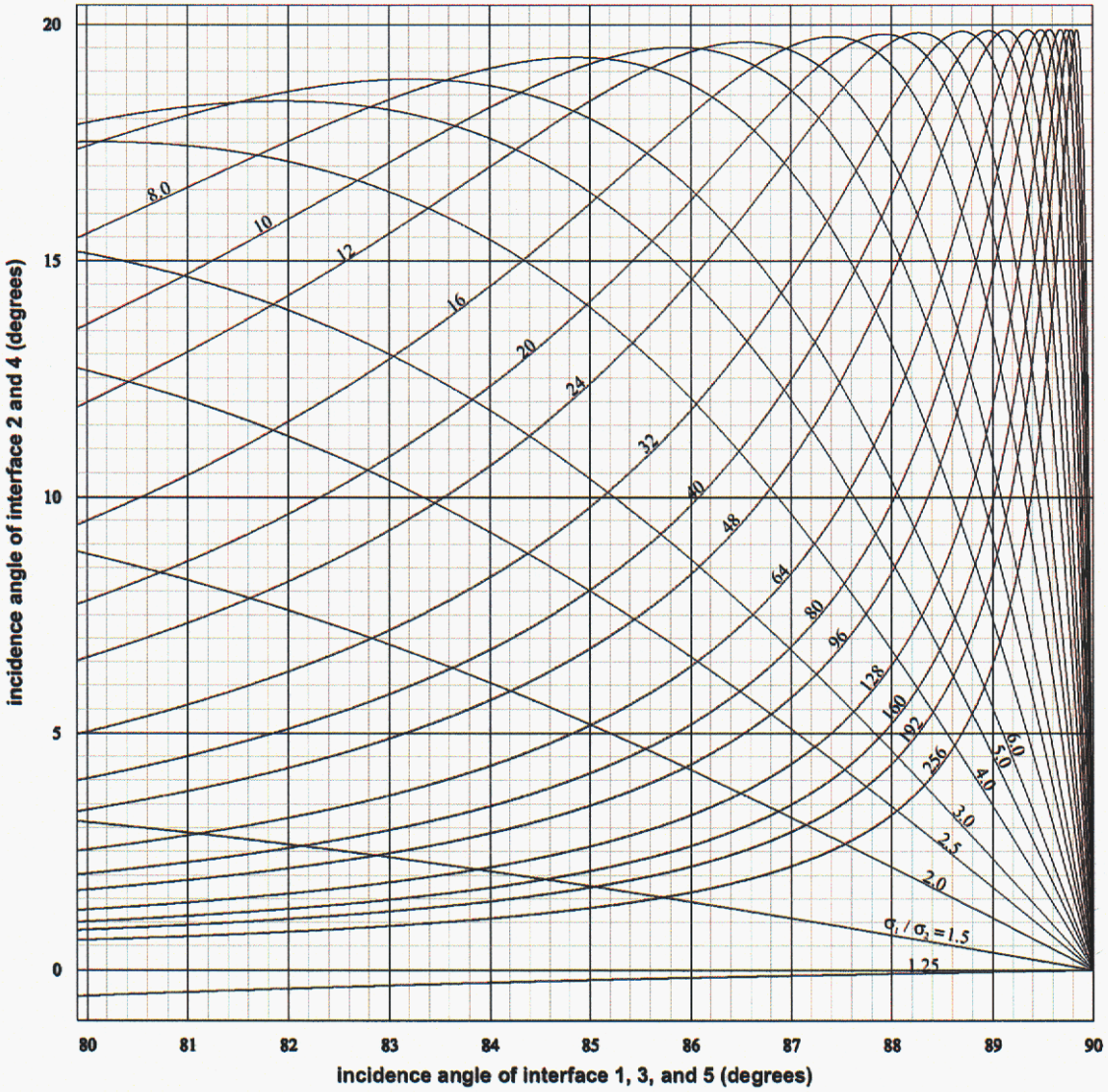

Figure 7.2: Expanded plot of solutions for the even-interface incidence angle, θ_e, that compensates skew in a five-interface system vs. the magnitude of the incidence angle of the odd interfaces, θ_o, at various SPRs.

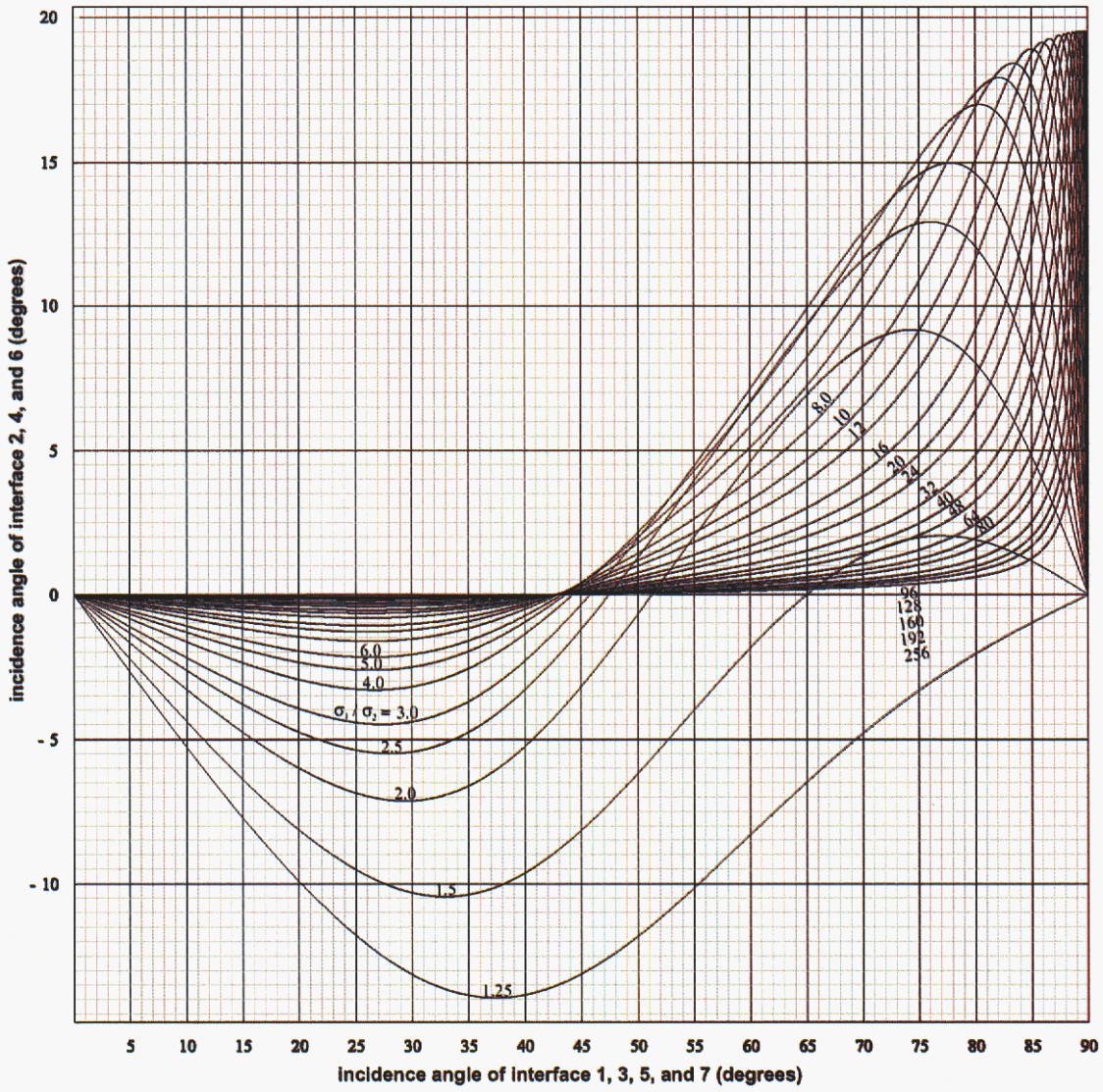

Figure 7.3: Plot of solutions for the even-interface incidence angle, θ_e, that compensates skew in a seven-interface system vs. the magnitude of the incidence angle of the odd interfaces, θ_o, at various SPRs.

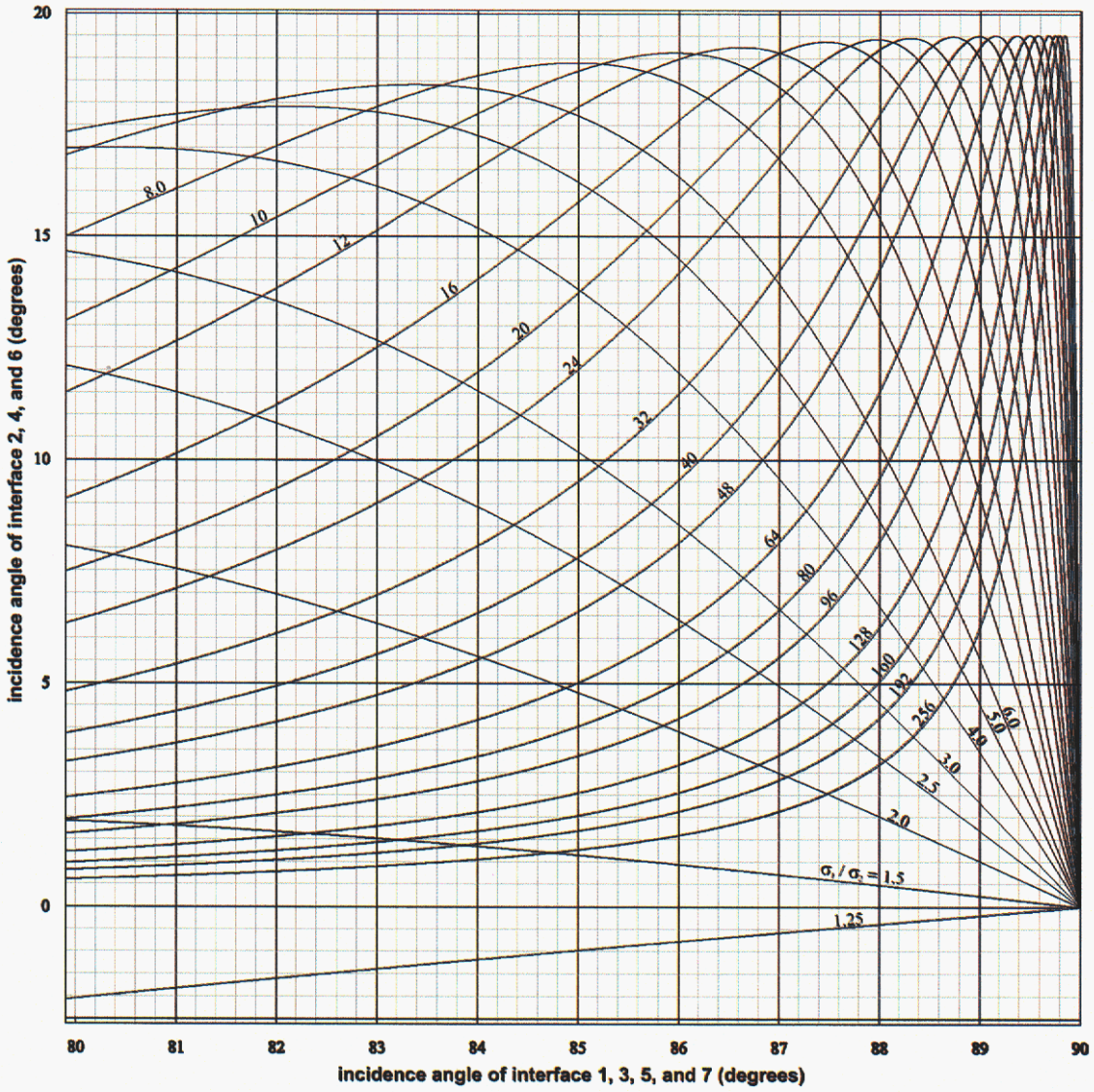

Figure 7.4: Expanded plot of solutions for the even-interface incidence angle, θ_e, that compensates skew in a seven-interface system vs. the magnitude of the incidence angle of the odd interfaces, θ_o, at various SPRs.

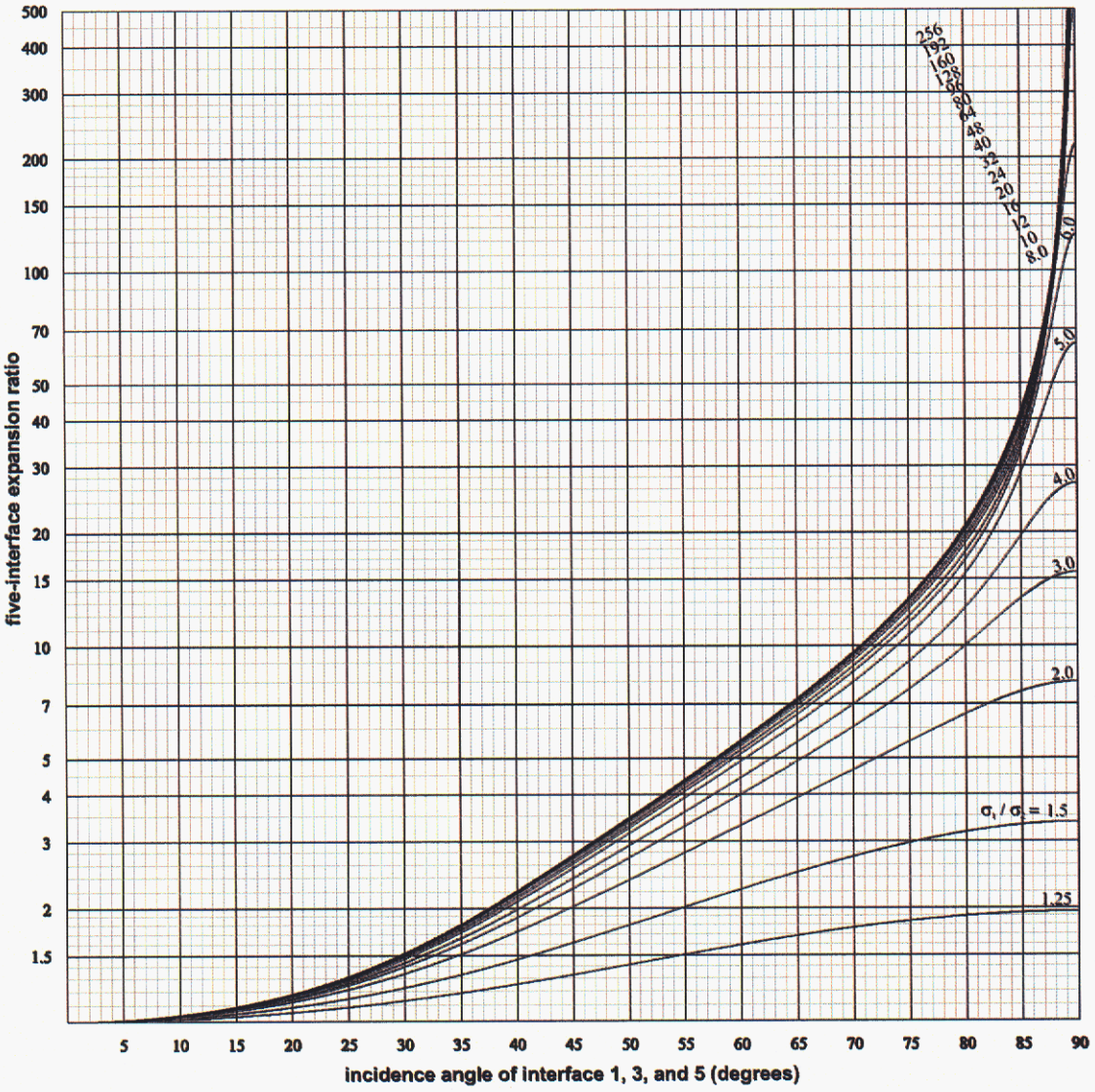

Figure 7.5: Plot of the expansion ratio of a five-interface, skew-compensated expander versus the magnitude of the odd-interface incidence angles, θ_o, at various SPRs. All even interfaces have the same incidence angle, θ_e.

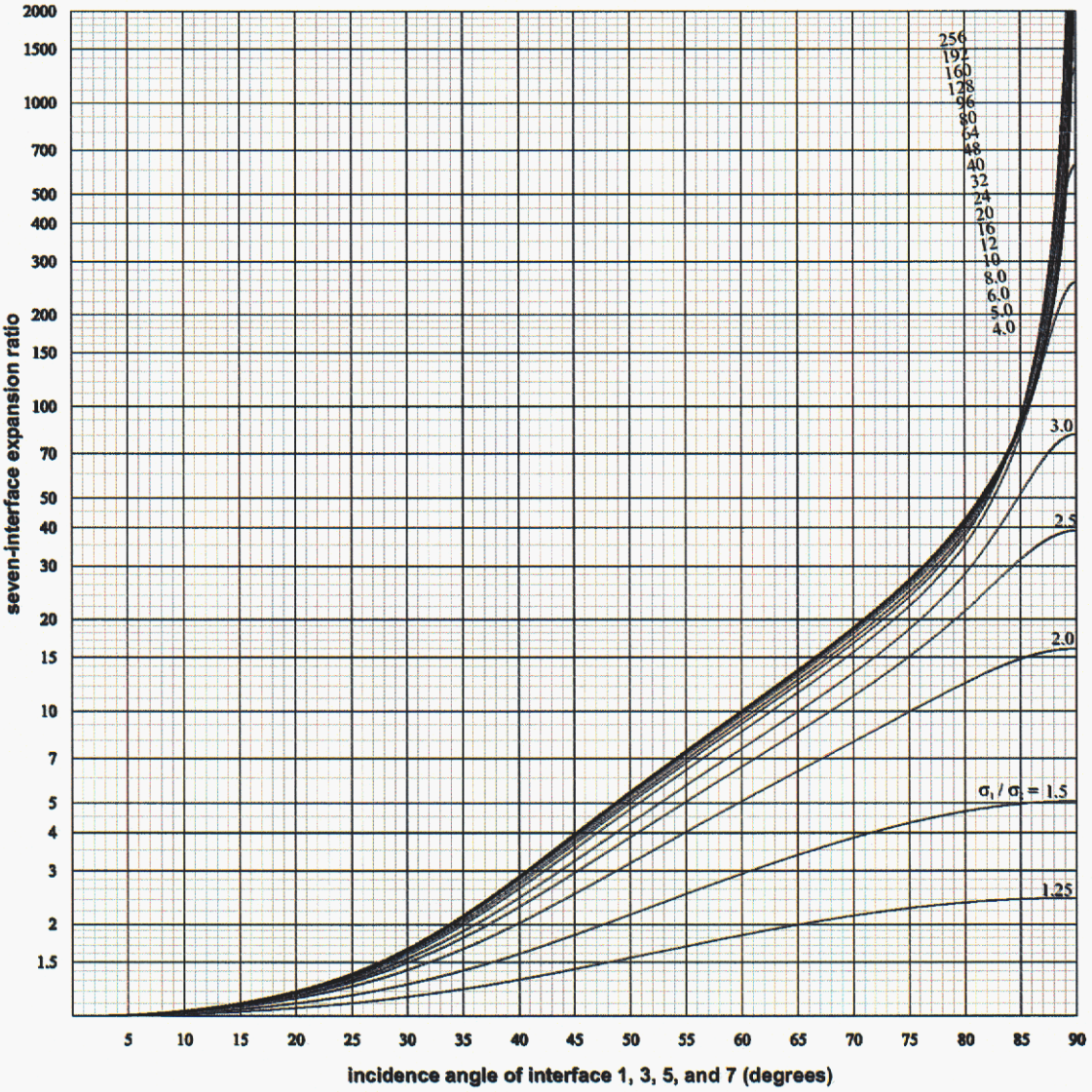

Figure 7.6: Plot of the expansion ratio of a seven-interface, skew-compensated expander versus the magnitude of the odd-interface incidence angles, θ_o, at various SPRs. All even interfaces have the same incidence angle, θ_e.

Figures 7.7 and 7.8 show the turning angles that result for such systems. It is noteworthy that these angles can exceed 360°, thus the interface system looks like an outwardly expanding spiral, an arrangement that may complicate interconnectivity. Because of the large expansion factors, the skew produced by the first few interfaces is negligible as is the ability of these interfaces to compensate the overall skew. However, the contraction in the even interfaces directly affects the expansion factor.

A more effective arrangement of interfaces for expanding a channel with skew compensation is to compensate skew only in the last interface. All even interfaces are oriented at 0° incidence, i.e.,

$$\theta_{i1} = 0 \text{ for even } i < N, \tag{7.3}$$

and therefore produce no contraction. Then, all odd interfaces except the final one are oriented with alternating orientations at the prescribed incidence angle and the final interface is tilted by an angle θ_s to compensate skew, i.e.,

$$\theta_{i1} = (-1)^{(i-1)/2}\theta_o \text{ for odd } i < N; \;\; \theta_{N1} = \theta_s. \tag{7.4}$$

This arrangement is amenable to analysis.

The solution for the final interface incidence angle, θ_s for such a five-interface system is

$$\theta_s = \cos^{-1}\sqrt{\frac{1 - 2\gamma^3\xi^2/\rho^2 + \left[1 - (2\gamma\xi/\rho)^2\right]^{1/2}}{2(1+\gamma^4\xi^2)}}, \tag{7.5}$$

where

$$\rho \equiv \frac{\sigma_1}{\sigma_2}, \tag{7.6}$$

$$\gamma \equiv 1 - \rho^{-2}, \text{ and} \tag{7.7}$$

$$\xi \equiv \sin^3\theta_o \cos\theta_o. \tag{7.8}$$

Figure 7.9 plots θ_s Eq. 7.2. This expression simplifies for large values of the SPR, ρ, to

$$\theta_s \sim \cos^{-1}\sqrt{\frac{1}{1+\xi^2}} \text{ as } \rho \to \infty, \tag{7.9}$$

which deviates from the exact solution by a maximum of 0.25° (~1%) at a SPR of 8.

Figures 7.10 and 7.11 plot the respective expansion factors that result from the five- and seven-interface expanders whose skew is compensated at the last interface. These expansion factors are significantly larger than those plotted in Figs.7.5 and 7.6 at angles less than 90°.

The turning angle for the five-interface system is equal to the turning angle of the final interface, since the even interfaces do not turn the flow, and the flow rotation from the other odd interfaces cancel. Figure 7.12 plots the turning angle. Unlike the other five-interface design, the turning angles are modest and the variation with the first and third interface incidence angle is gradual for large interface angles.

Using the arrangement in Eqs. 7.3 and 7.4, a high-expansion, low-turning-angle system can be generally constructed from N-interfaces, where N is odd and sufficiently large. For

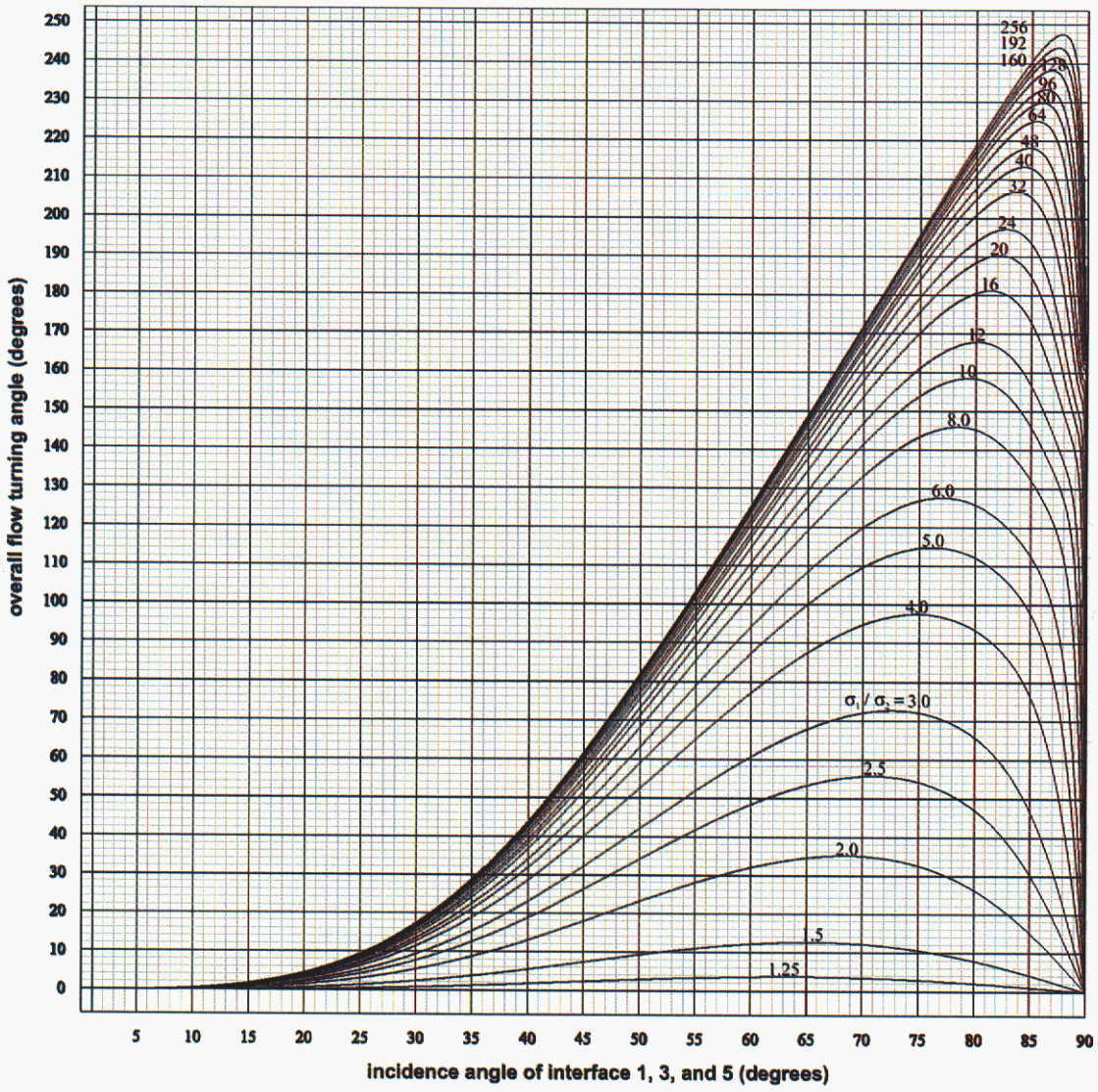

Figure 7.7: Plot of the flow-turning angle of a five-interface, skew-compensated expander versus the magnitude of the odd-interface incidence angles, θ_o, at various SPRs. All even interfaces have the same incidence angle, θ_e.

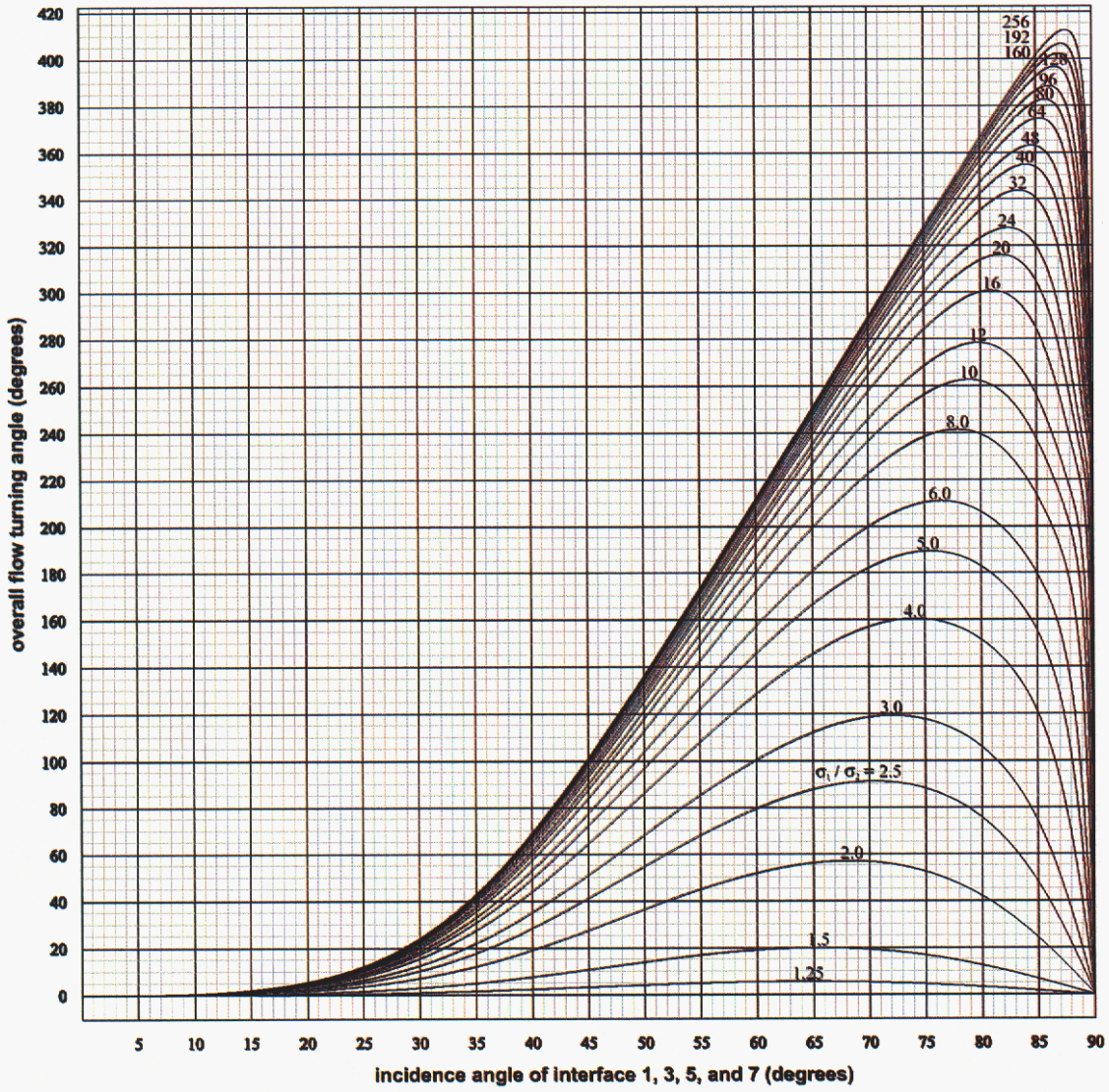

Figure 7.8: Plot of the flow-turning angle of a seven-interface, skew-compensated expander versus the magnitude of the odd-interface incidence angles, θ_o, at various SPRs. All even interfaces have the same incidence angle, θ_e. Flow turning angles greater than 360° represent an outward spiral.

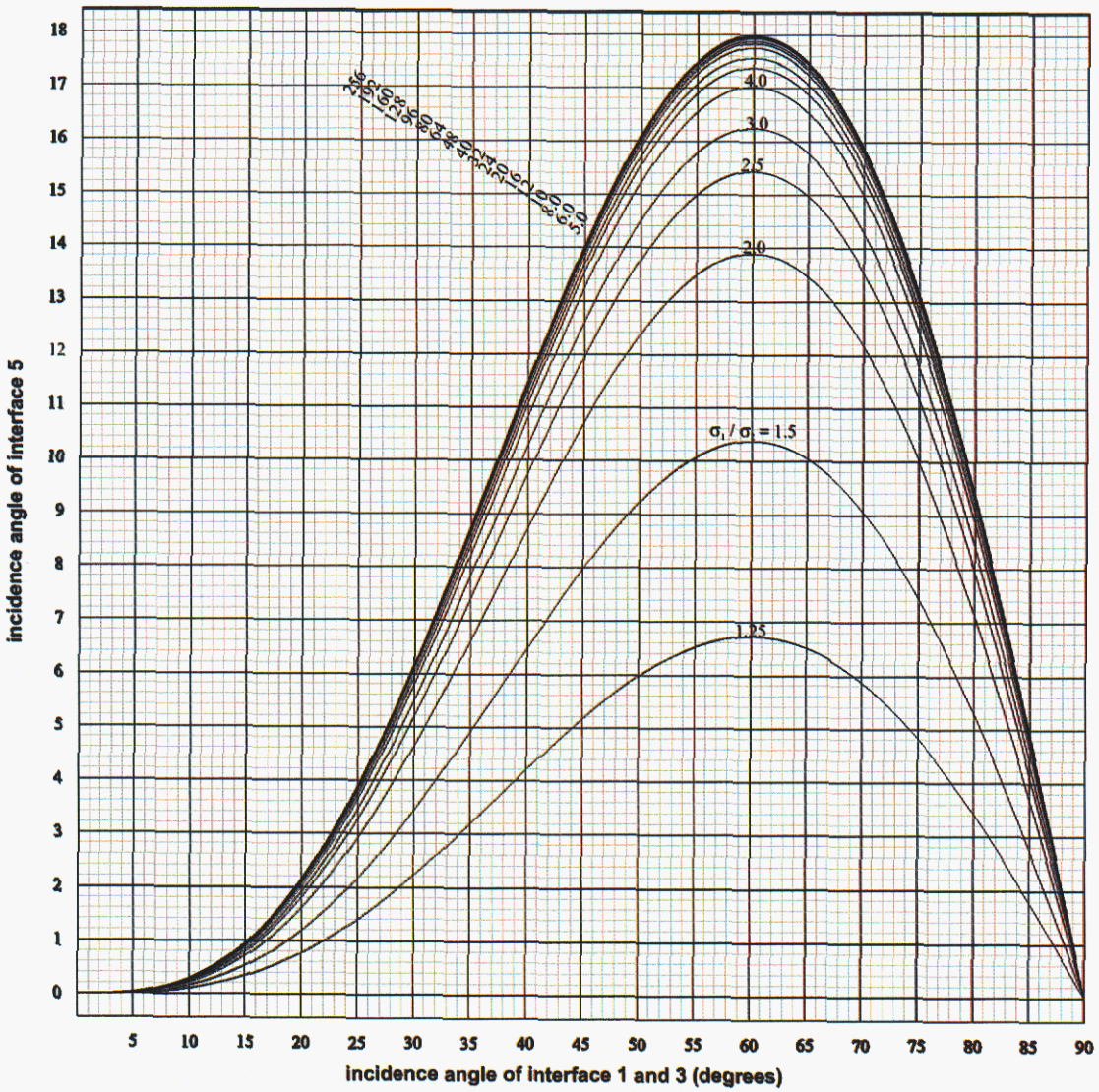

Figure 7.9: Plot of the incidence angle, θ_s of the last interface in a five-interface expander versus the magnitude of the first- and third-interface incidence angles, θ_o at various SPRs. All even interfaces are at normal incidence.

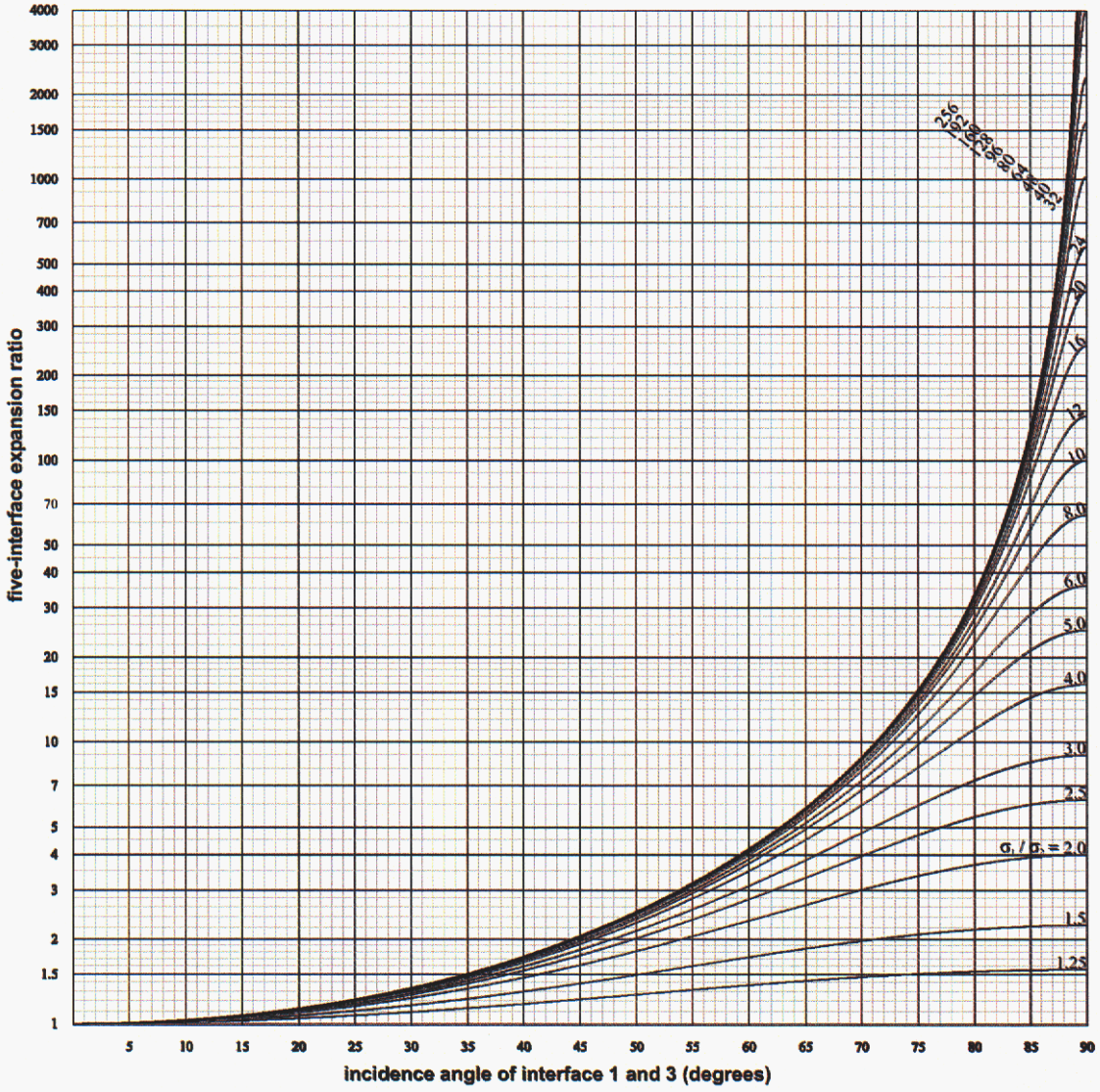

Figure 7.10: Plot of the expansion ratio of a five-interface expander whose skew is compensated only on the last interface versus the magnitude of the first- and third-interface incidence angles, θ_o at various SPRs. All even interfaces have zero incidence angle.

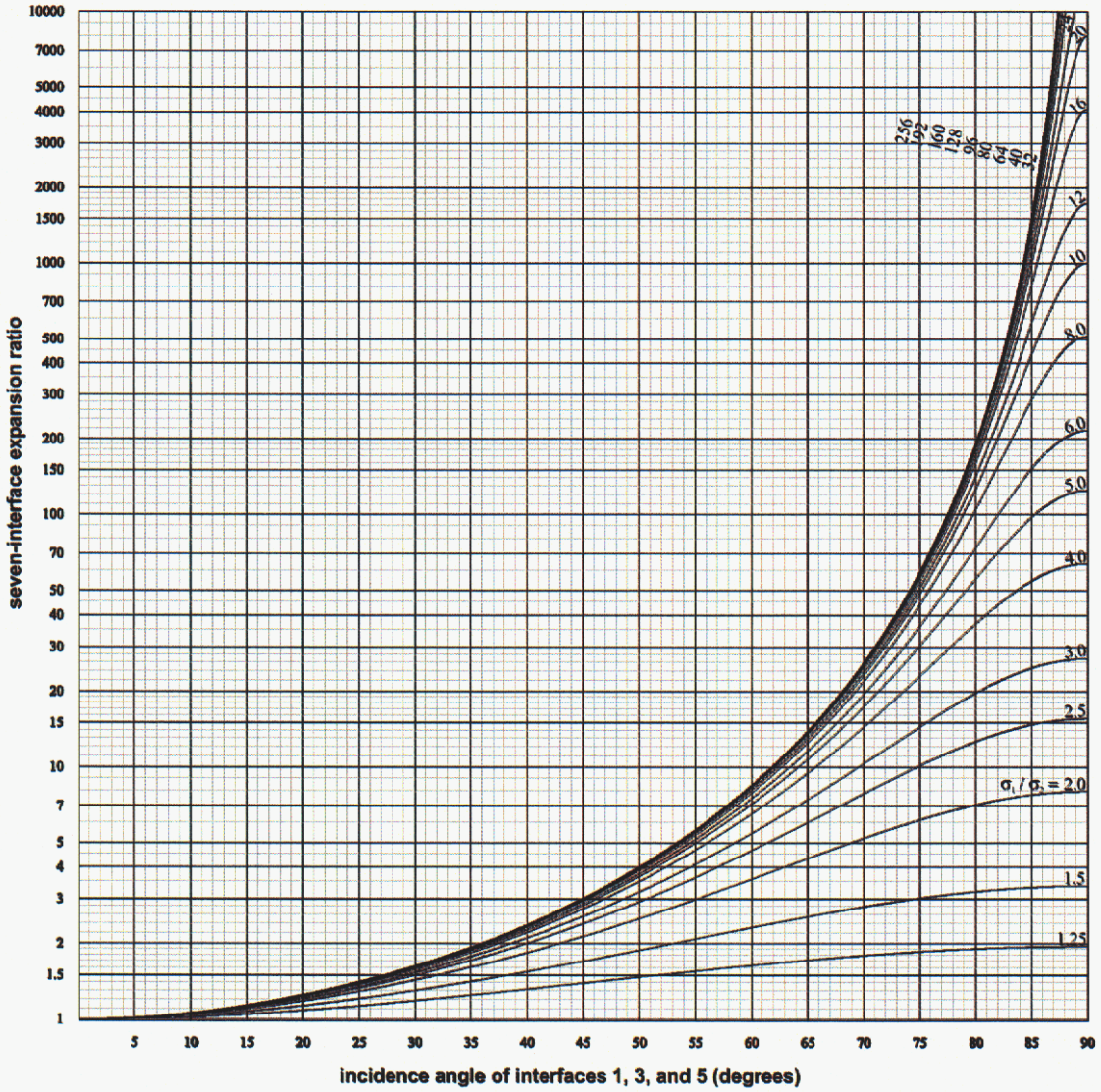

Figure 7.11: Plot of the expansion ratio of a seven-interface expander whose skew is compensated only on the last interface versus the magnitude of the first-, third-, and fifth-interface incidence angles, θ_o, at various SPRs. All even interfaces have zero incidence angle.

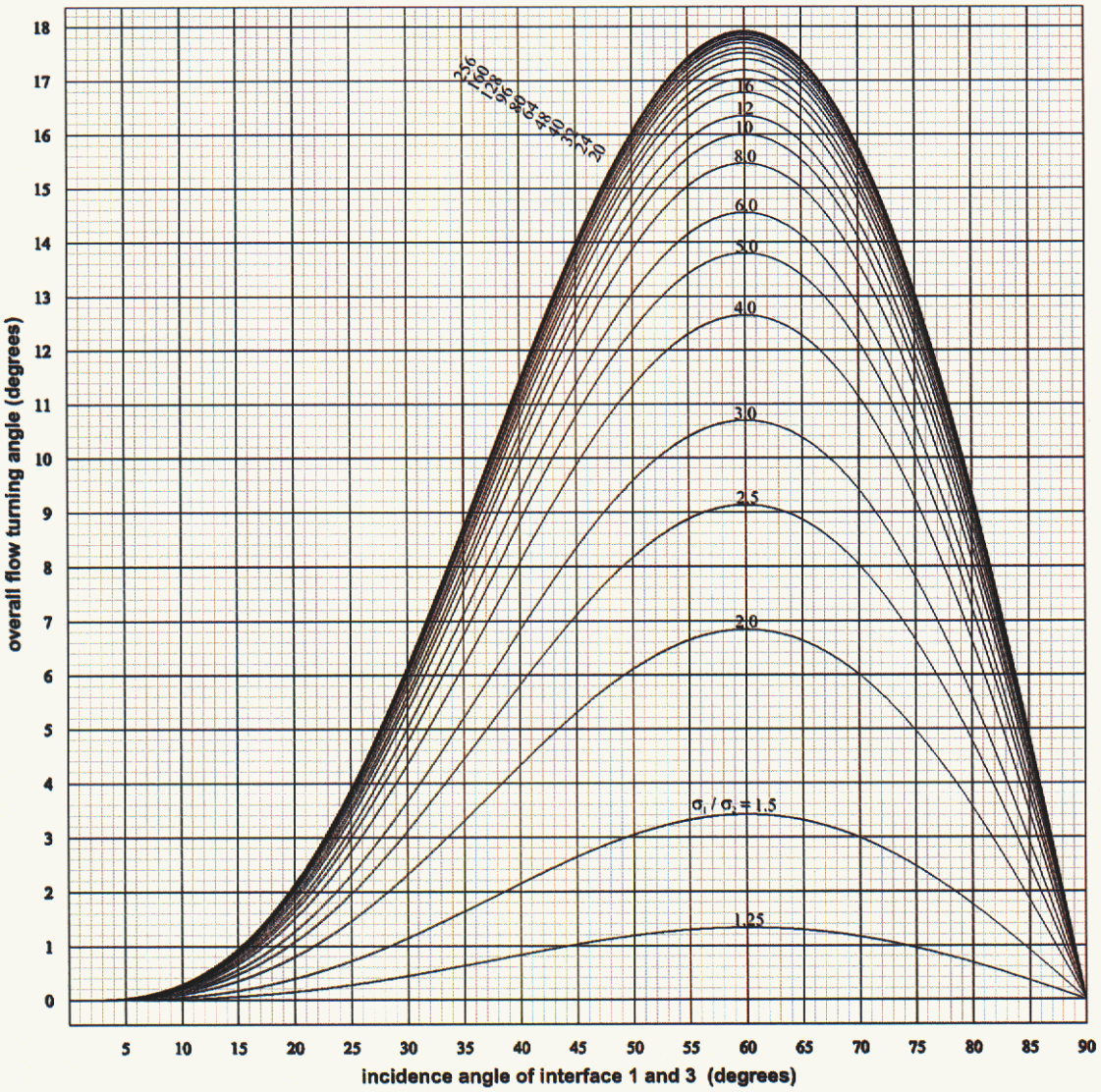

Figure 7.12: Plot of the flow-turning angle of a five-interface, skew-compensated expander versus the magnitude of the first- and third-interface incidence angles, θ_o, at various SPRs. All even interfaces are at normal incidence.

large, odd N, the solution for the the incidence angle, θ_s, of the skew-compensating interface approaches

$$\theta_s \sim \tan^{-1} \frac{(-1)^n \cos\theta_o \sin\theta_o [1 - (-\cos^2\theta_o)^n]}{1 + \cos^2\theta_o}, \tag{7.10}$$

where $n \equiv (N-1)/2$.

For large σ_1/σ_2, the expansion factors asymptotically approach

$$\frac{w_N}{w_1} \sim \frac{1}{\cos^n\theta_o} \left[1 + \left(\frac{\cos\theta_o \sin\theta_o [1 - (-\cos^2\theta_o)^n]}{1 + \cos^2\theta_o} \right)^2 \right]^{1/2}. \tag{7.11}$$

The second term inside the large square brackets accounts for the additional expansion from the finite angle of the final interface and is always $\leq 1/8$.

This page intentionally contains only this sentence.

CHAPTER 8

Practical applications

8.1 A plumber's delight

This general design methodology supports a wide variety of practical applications. It is a methodology that allows a designer to plumb together complicated microsystems with turns, expansions, and offsets. It allows a designer to skew and stretch material lines as needed. Several specific applications of these capabilities arise immediately.

8.2 Low-dispersion turns

Turns and displacers in conduction channels can introduce large amounts of dispersion, as illustrated by the 90° turn shown in Fig. 8.1(a). The skew-compensated turns and channel expanders described earlier can be used directly as low-dispersion turns. An example of a skew-compensated 90° turn is shown in Fig. 8.1(b). The methodology has been developed to create low-dispersion turns of any angle having arbitrary expansion. Figure 8.2a and b show the two arrangements of the two 45° turns that produce the low-dispersion 90° turn. Option 'b' may be preferred by a designer because it avoids the necking of the channel found in conventional low-dispersion turns.

8.3 Low-dispersion displacers

Another common microchannel plumbing need is to offset a channel to line up ports of separate devices. Figure 8.3 shows a comparison of streaklines in (a) a poorly designed conventional displacer and (b) a faceted displacer. The symmetrical facet arrangement of Fig. 8.3 produces no skew of material lines regardless of the incidence angles of the design. The use of critical-turning-angle interfaces in displacers limits the length of the displacer and minimizes sensitivity to SPR errors. The limitation of these devices is the dispersion associated with the interfaces or propagation through the channel having low-specific permeability. The importance of the interface dispersion diminishes for channels that are much wider than deep.

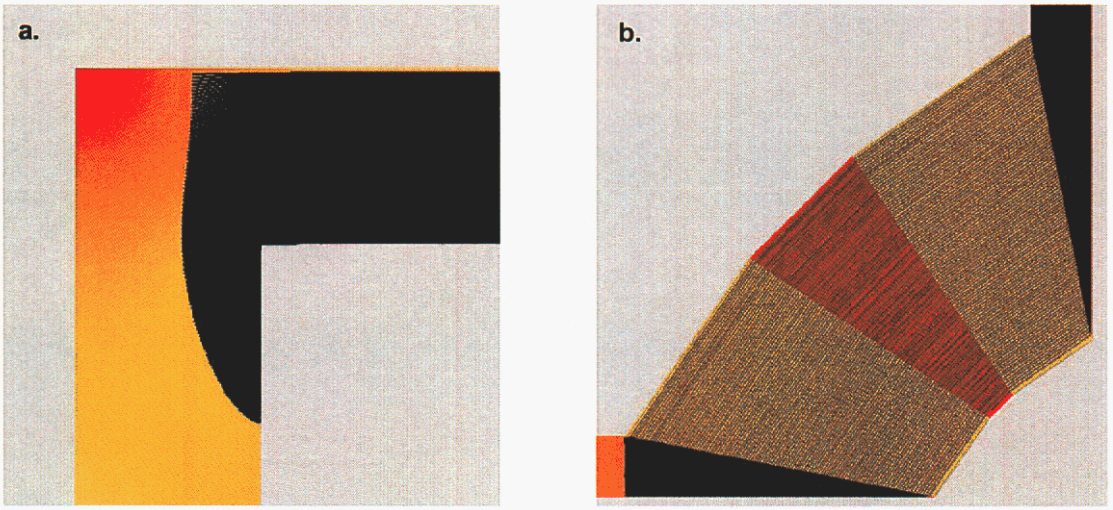

Figure 8.1: Streakline images in a 90° turn (a) in a uniform-depth channel and (b) in a skew-compensated, faceted turn.

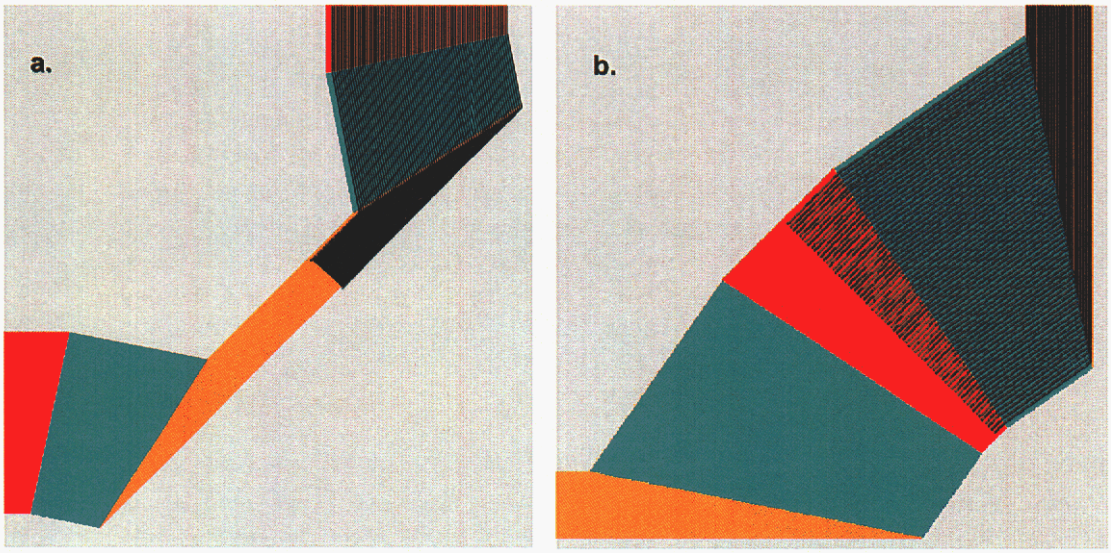

Figure 8.2: Streaklines superimposed over the velocity fields of two 90° skew-compensated turns. The design on the left shrinks the flow after an initial 45° turn, expanding the flow to its initial width during a second 45° turn. The design on the right expands the flow during the initial 45° turn, shrinking the width to its input value during the second 45° turn.

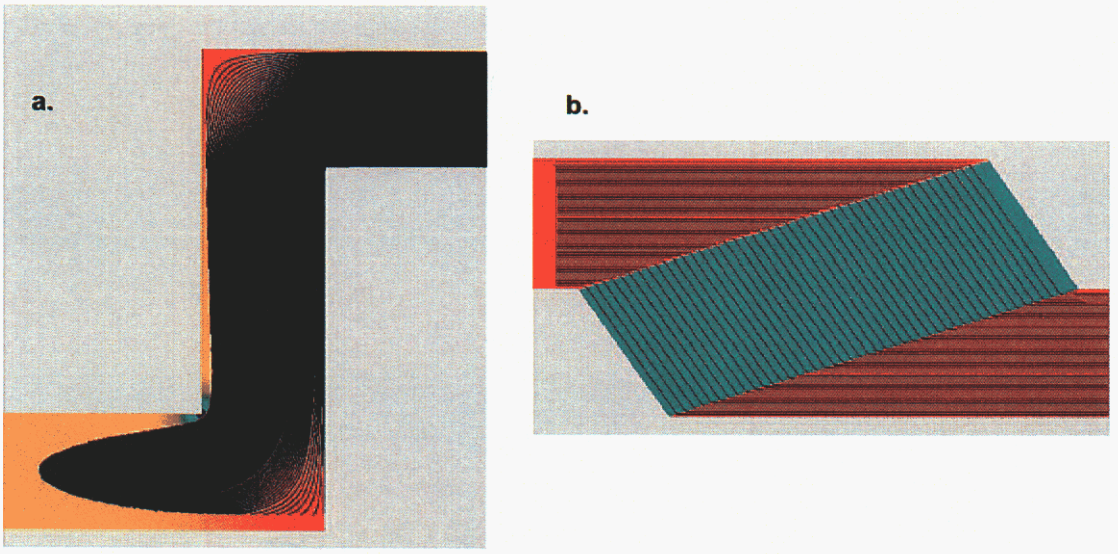

Figure 8.3: Streakline images in (a) a uniform-depth flow displacer and (b) a faceted flow displacer.

8.4 Low-dispersion splitters and manifolds

It is also possible to divide flow into multiple conduction channels with full skew compensation. This is beneficial for dividing a sample and sending it to numerous separation channels (e.g., for some "two-dimensional separation" techniques). A channel of single etch depth can be used to split flow, but this generally results in considerable dispersion, as demonstrated in Fig. 8.4. Fortunately, combinations of low-dispersion turns and displacers can be used to construct simple flow splitters and manifolds. This is done by noting that a streamline can be replaced by a channel wall and vice versa. By placing a flow displacer against its mirror image at the location of a streamline, a flow divider is formed, such as the splitter of Fig. 8.4(b), which was constructed using the displacer of Fig. 8.3(b). Further details about the design of such splitters is detailed in Chapter 9.

The entrance- and exit-channel flows remain parallel for Fig. 8.4. In contrast, constructing a flow splitter from two 29.0283° two-interface turns yields the divider of Figure 8.5, demonstrating that the exit flows can be split to travel in a wide range of directions with respect to the incident conduction channel. By splitting the flow in this manner, any number of exit channels can be obtained from a single inlet channel.

Splitters having 3 and 5 exit channels are shown in Figs. 8.6 and 8.7, respectively. A drafting method to design these splitters is detailed in Chapter 9. The central exit channels are wider than the edge channels.

A more compact design with four exit channels of equal widths is shown in Fig. 8.8, which is constructed using adjacent displacers having 25° and 45° incidence angles.

An alternative design is obtained in Fig. 8.9 using a central step at 0° incidence flanked by two displacers at 5° incidence. This design supports large numbers of exit channels, as

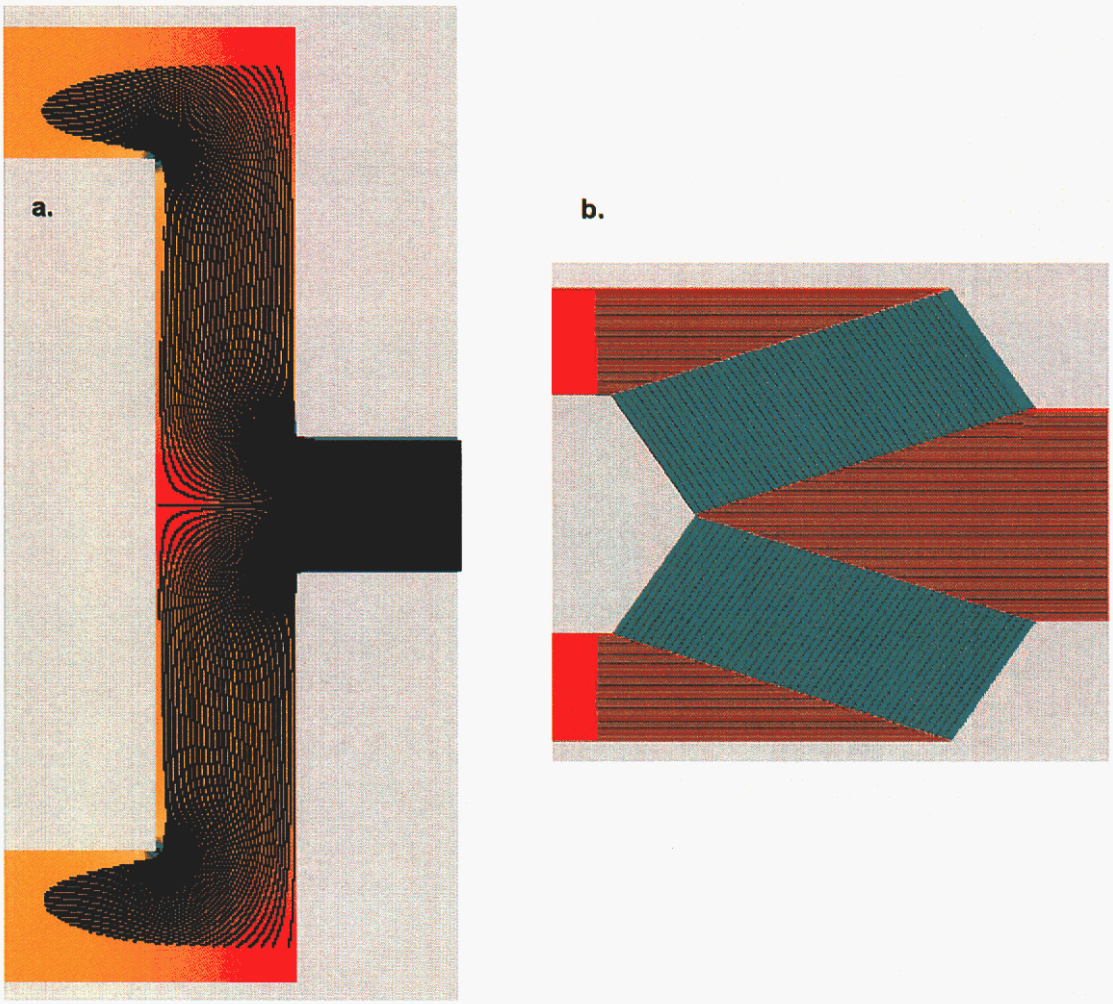

Figure 8.4: Streakline images in a simple flow splitter (a) for a uniform-depth system and (b) for a faceted system with full skew compensation.

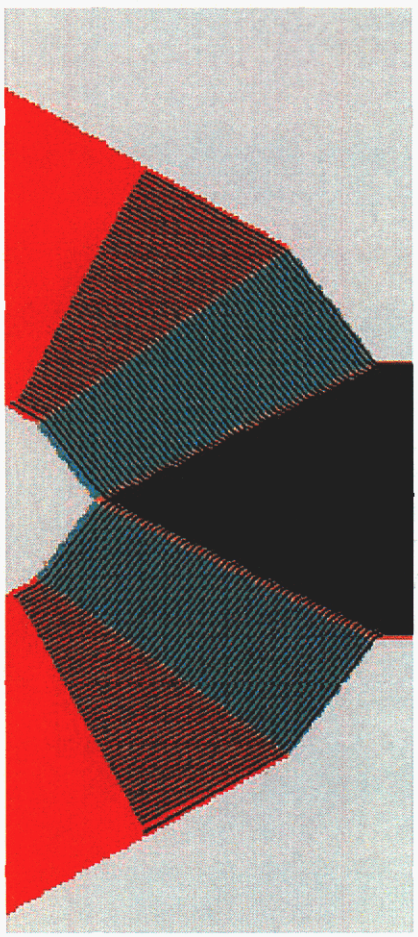

Figure 8.5: Streakline images in a skew-compensated, four-way flow splitter. The inner two splitter arms are constructed from mirrored 25° flow displacers; the outer splitter arms are constructed from mirrored critical 45° flow displacers.

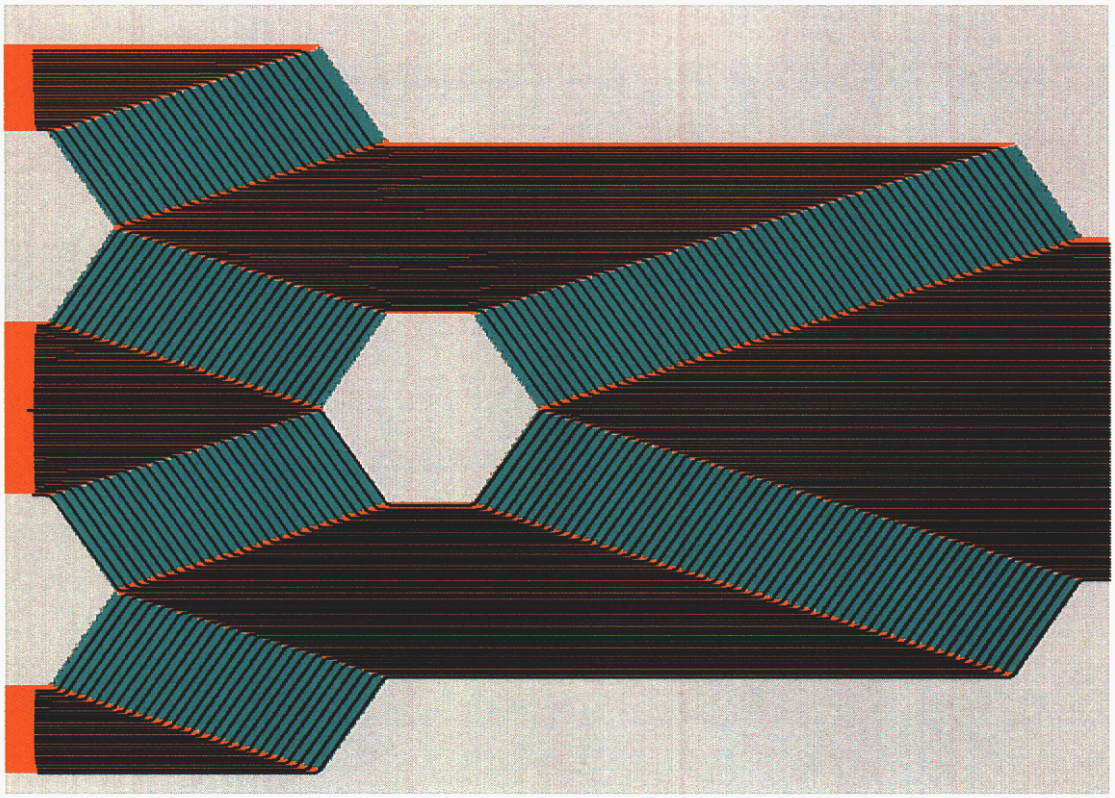

Figure 8.6: Streakline image superimposed over the velocity field of a skew-compensated, three-way flow splitter. The splitter is designed using three skew-compensated two-way flow splitters identical to that shown in Fig 8.4(b). Further design details are given in Chapter 9.

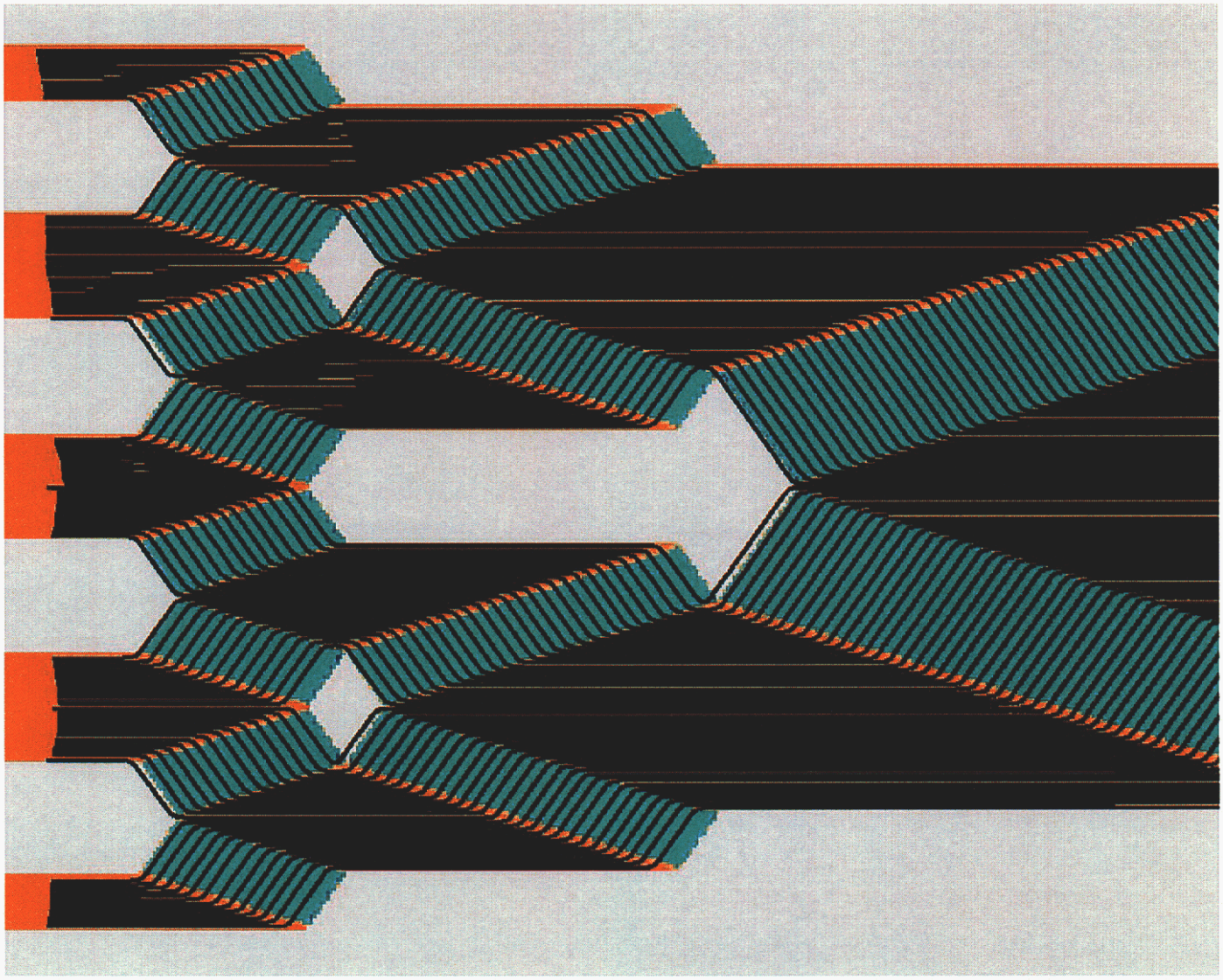

Figure 8.7: Streakline images in a skew-compensated, five-way flow splitter constructed by stacking two copies of the design in Fig. 8.6.

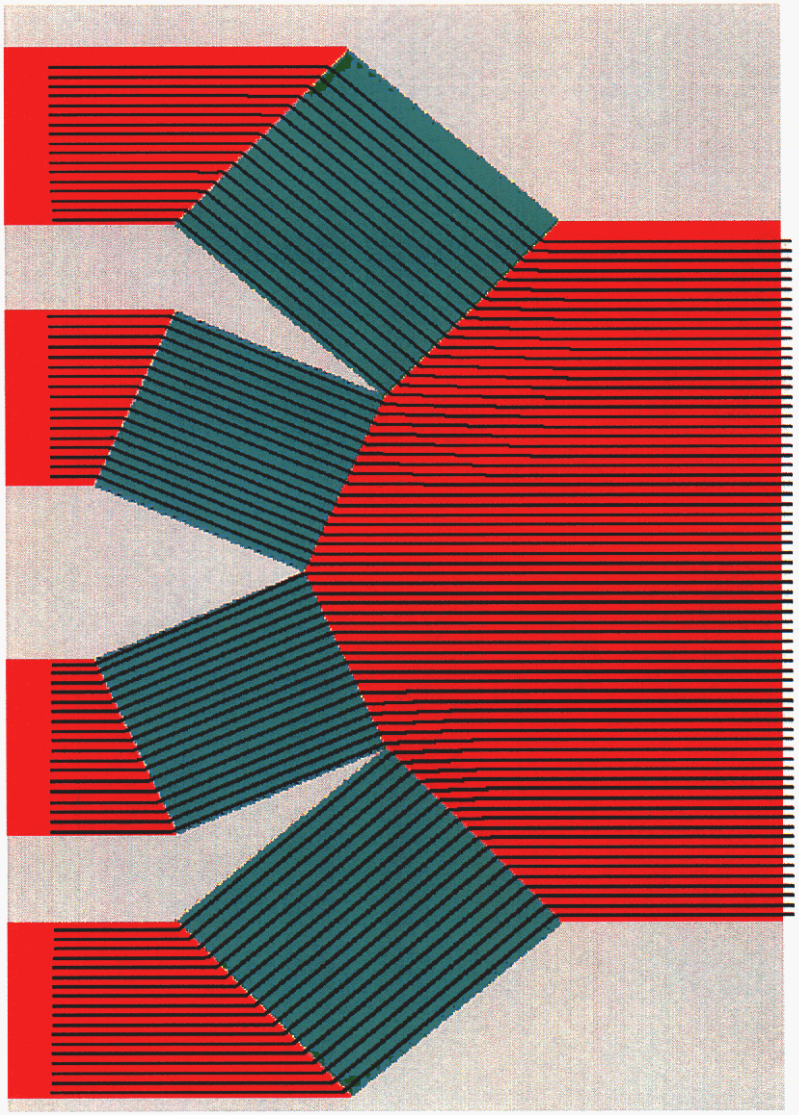

Figure 8.8: Streakline images in a skew-compensated, four-way flow splitter. The inner two splitter arms are constructed from mirrored 25° flow displacers; the outer splitter arms are constructed from mirrored critical 45° flow displacers.

demonstrated by the five-way splitter of Fig. 8.10, where two additional displacers, that are constructed using 10° incidence angles, are added to the sides of the design of Fig. 8.9.

The flow splitters of Figs.8.6–8.10 use exit channels of widths that are integer fractions of the input-channel width. It is possible to obtain exit conduction channels with nearly any width with expeditious choice of expansion ratio, as illustrated by the splitter shown in Fig. 8.11, which is obtained using a 4-interface displacer with expansion ratio of 4.

8.5 Low-dispersion medians

When operated in reverse, flow splitters and manifolds become low-dispersion flow combiners. Therefore, by placing splitters back-to-back, the narrow inlet can be split into multiple channels and then recombined into a narrow outlet, as shown in Fig. 8.12. Here, the medians are constructed using back-to-back five-way splitters identical to that of Fig. 8.10. More importantly, the multiple channels formed by the splitter form medians that do not perturb the flow field. Moreover, these medians can be extended to any length by extending the length of the manifold channels. Such medians may be used to provide structural support for wide, shallow channels, e.g., >1,000-μm wide by 1-μm deep, in which warping of the structural material could otherwise introduce significant errors in channel depth. The number of medians is one fewer than the number of manifold channels.

For the median design of Fig. 8.12 in a two-etch-level design, the inlet and exit channels are deep. Therefore it is necessary to place normal interfaces in both the first and last sections for insertion in a shallow, two-level-etched channel. Alternatively, it is possible to design medians using shallow entrance and exit channels, as shown in Fig.8.13, where manifolds are constructed using incident angles of 0°, ±1°, and ±2°. This design can be placed directly within a wide, shallow channel for structural support. Note that Figs. 8.12 and 8.13 have a convex and concave appearance, respectively.

Skew-compensated medians can be designed using back-to-back flow splitters that expand the flow, as demonstrated in Fig. 8.14. Here, a single median is formed by the channel walls, separating two channels that are each twice as wide as the incident flow channel.

By placing a copy of the system of Fig. 8.14 adjacently and connecting the two with an additional copy of Fig.8.14, and then repeating the process on the resulting expanded triple-median system, the eight channel, seven median design of Fig. 8.15 results. The overall expansion ratio of 64× is distributed between eight internal channels that are 8× wider than the inlet and exit conduction channels. Indeed, tremendous amounts of conduction-channel expansion are possible using this design methodology. Further construction details are given in Chapter 9.

It is also possible to place medians for structural support within a wide, shallow channel with little design effort provided their width is comparatively small. For example, consider the 30× non-skew-compensated expander of Fig. 8.16. As demonstrated in Fig.8.17, the addition of narrow medians to the central expanded channel results in no appreciable change to the streaklines and velocity distribution.

Alternatively, medians can be added to change the specific permeability of the channel deliberately. This is demonstrated in Fig. 8.18b, where permeability-modifying medians have been added to the shallow channel of a two-level etch having a depth ratio of 10:1.

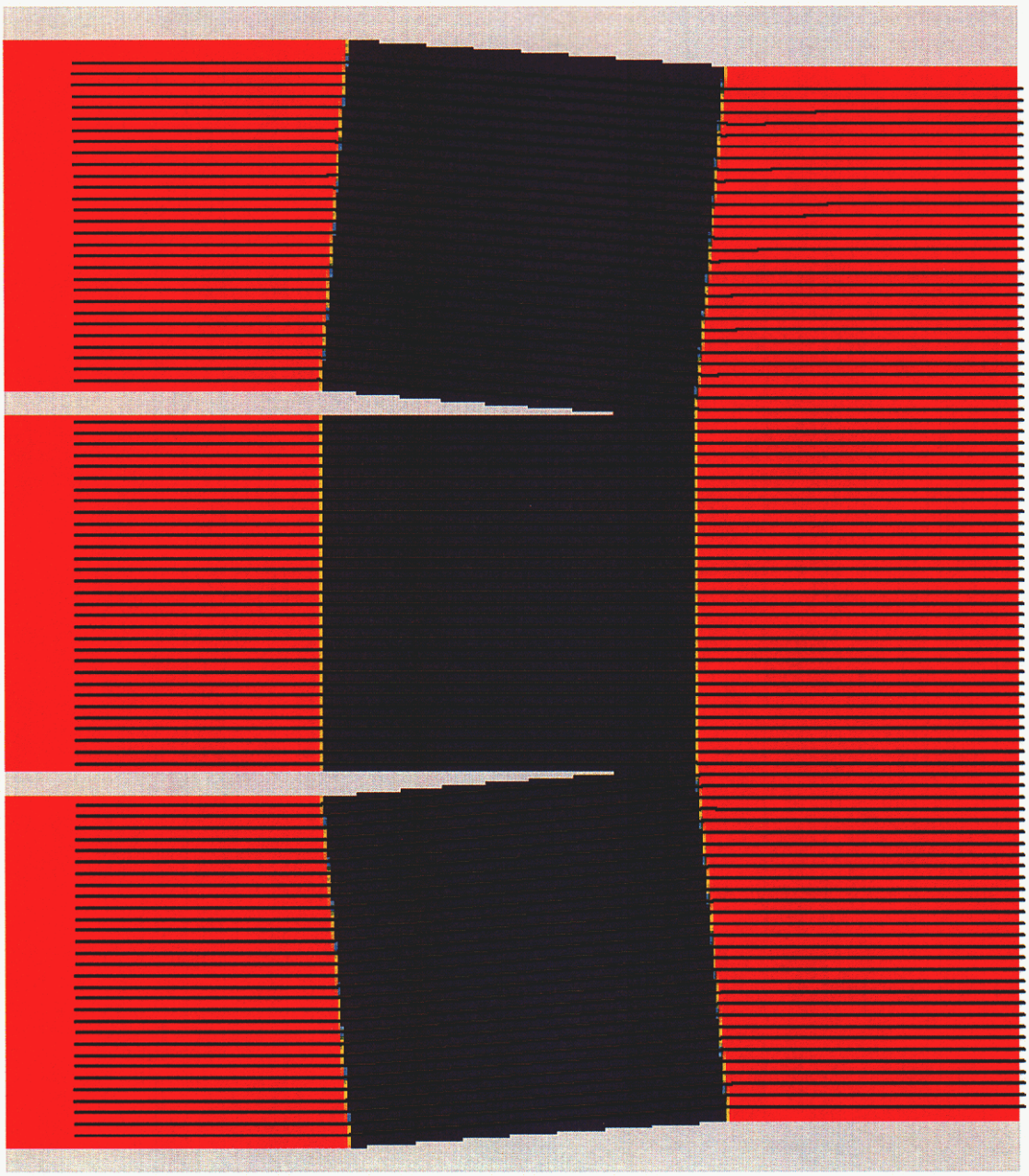

Figure 8.9: Streakline images in a skew-compensated, three-way flow splitter. Here, the middle arm of the splitter is a 0° step; the outer arms are mirrored 5° displacers.

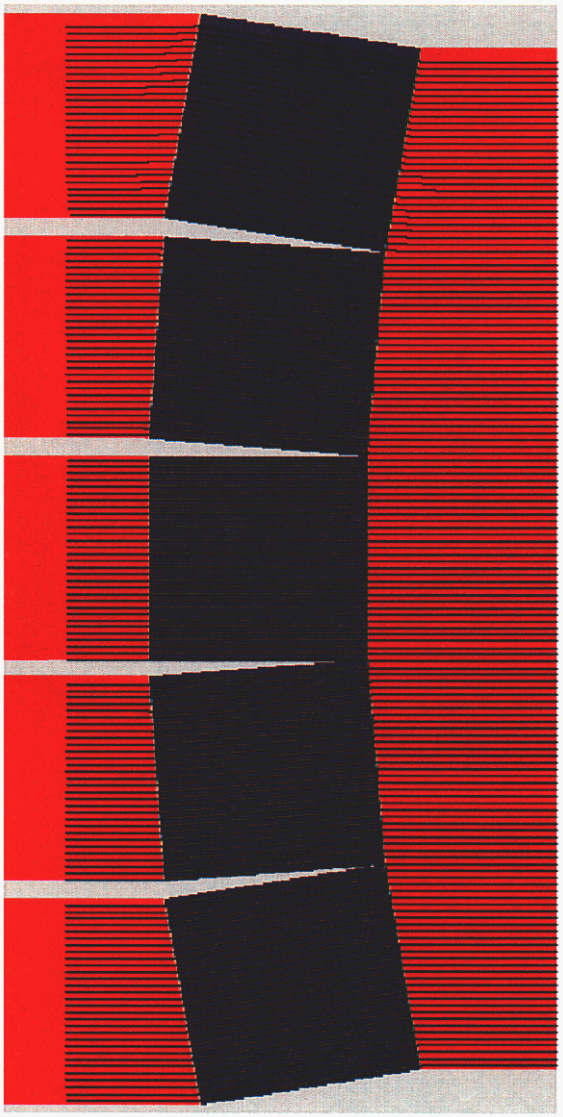

Figure 8.10: Streakline images in a skew-compensated, five-way flow splitter, constructed by adding mirrored 10° displacers to the three-way splitter of Fig 8.9.

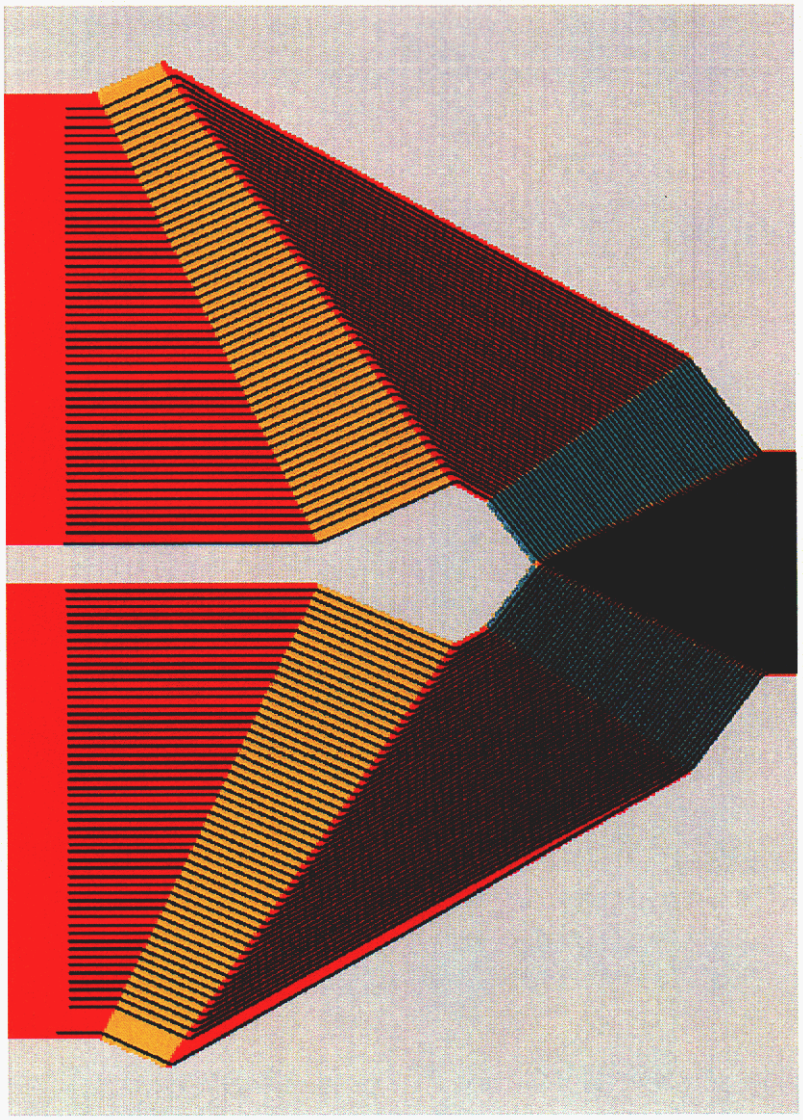

Figure 8.11: Streakline images in a skew-compensated, two-way expanding flow splitter, constructed by adding mirrored 25° turns to the two-way splitter of Fig. 8.5.

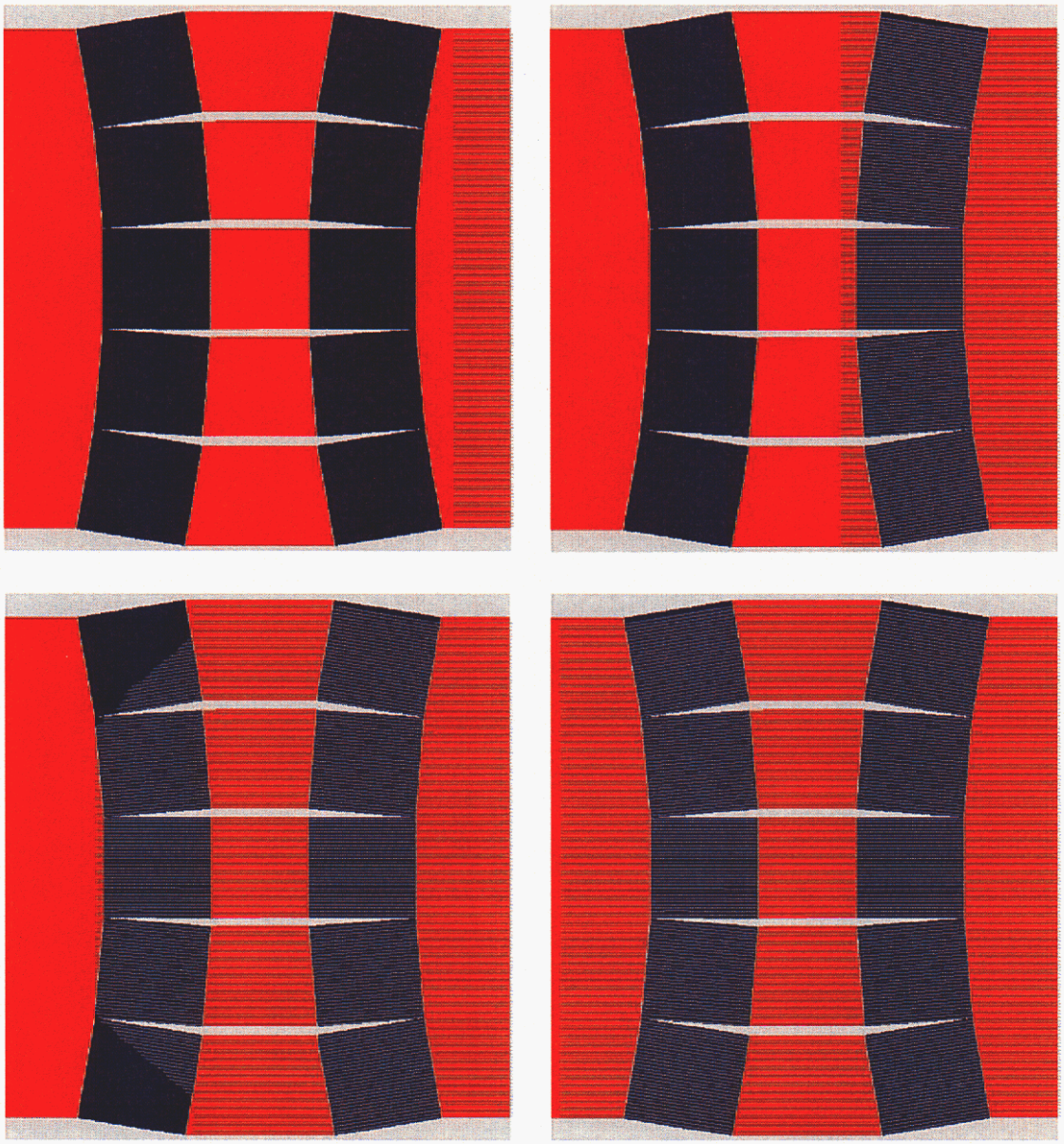

Figure 8.12: Streakline images in a skew-compensated channel with medians constructed by connecting mirrored copies of the design in Fig. 8.10.

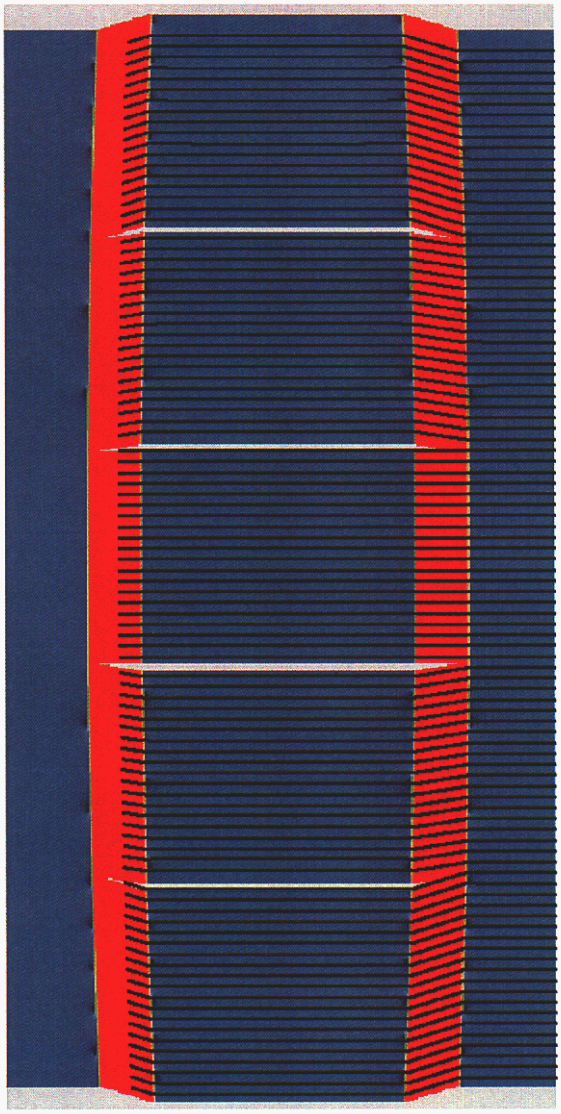

Figure 8.13: Flow splitter and combiner designed for shallow inlet and exit sections.

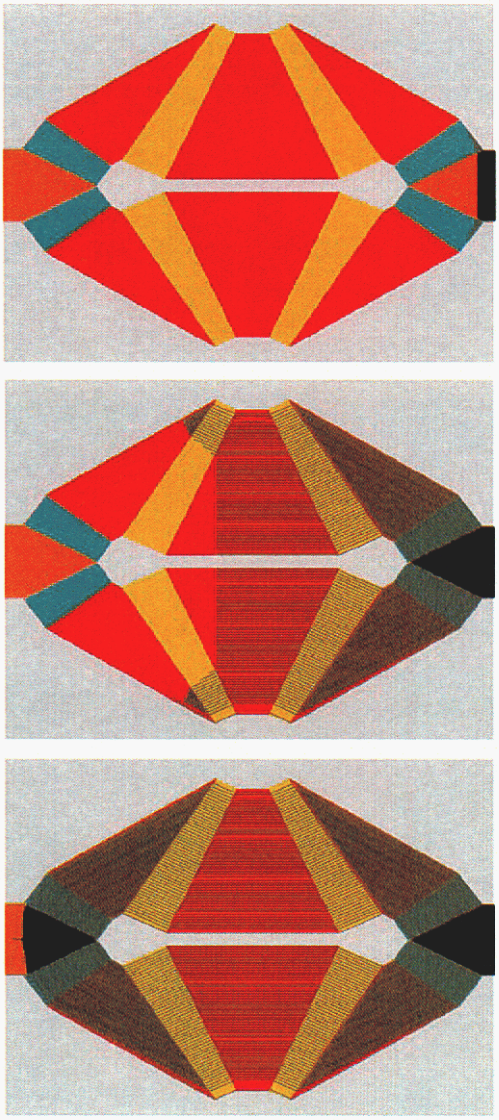

Figure 8.14: Temporal progression of streaklines superimposed over the velocity field for a 4×, two-channel, single-median flow expander constructed using 2-interface, skew compensated turns as in Fig. 8.5.

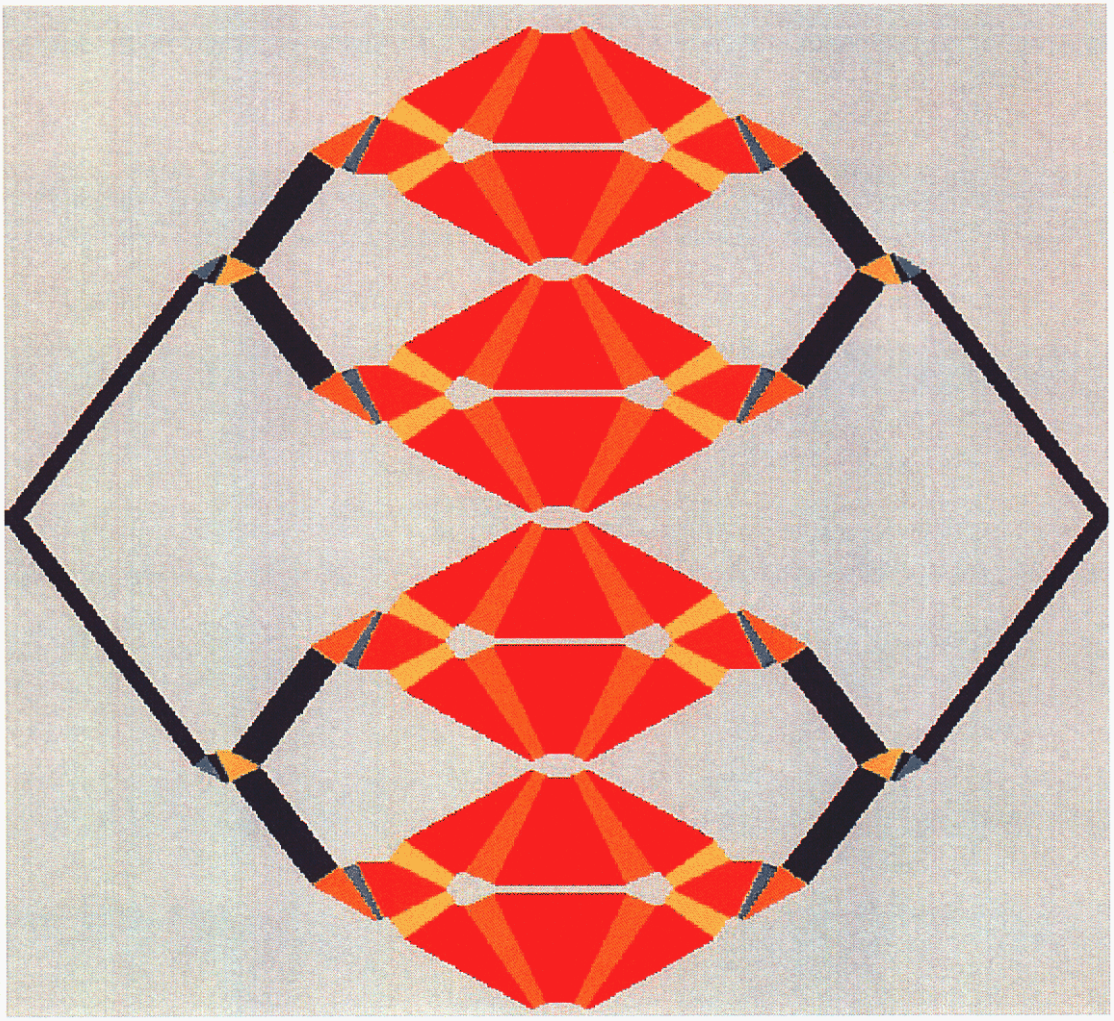

Figure 8.15: Velocity fields for an 8-channel, 7-medianed flow expander constructed using two-turn, skew-compensated expanders. The resulting overall expansion of 64× results in individual channels 8× wider than the inlet and exit channels.

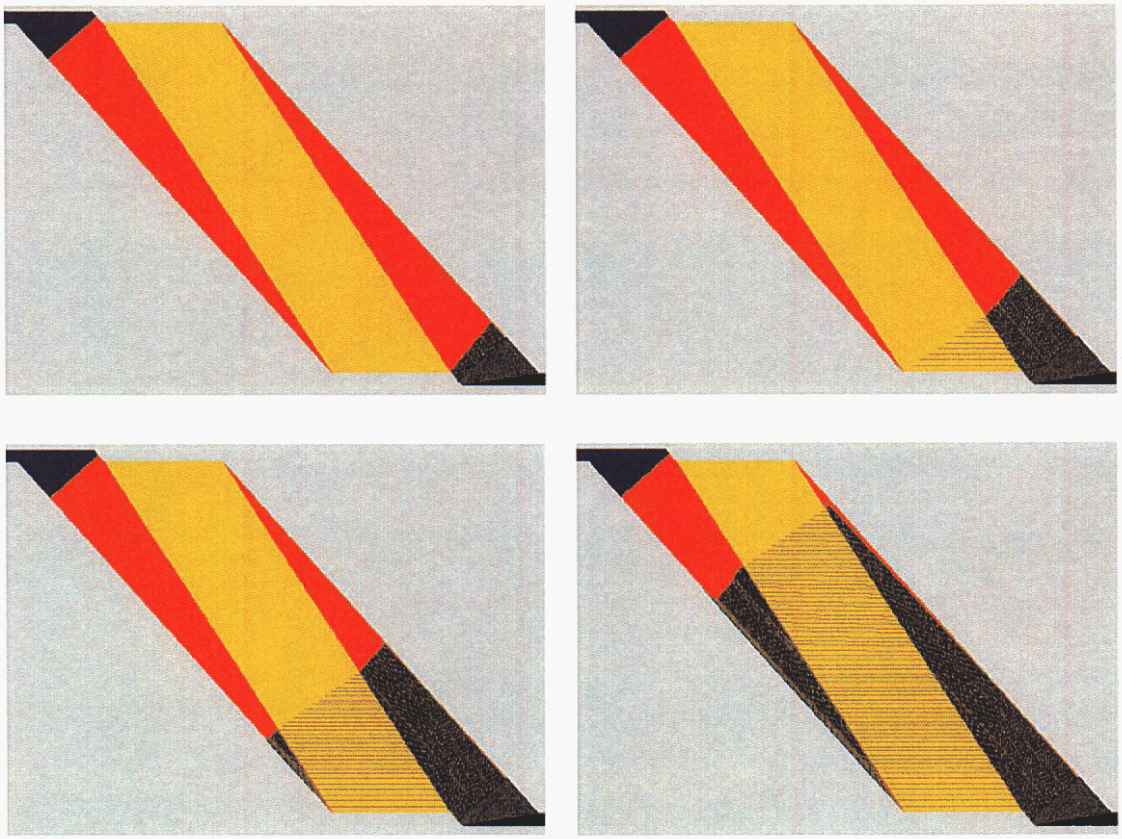

Figure 8.16: Temporal progression of streaklines superimposed over the velocity field of a three-interface, non-skew-compensated 30× expander.

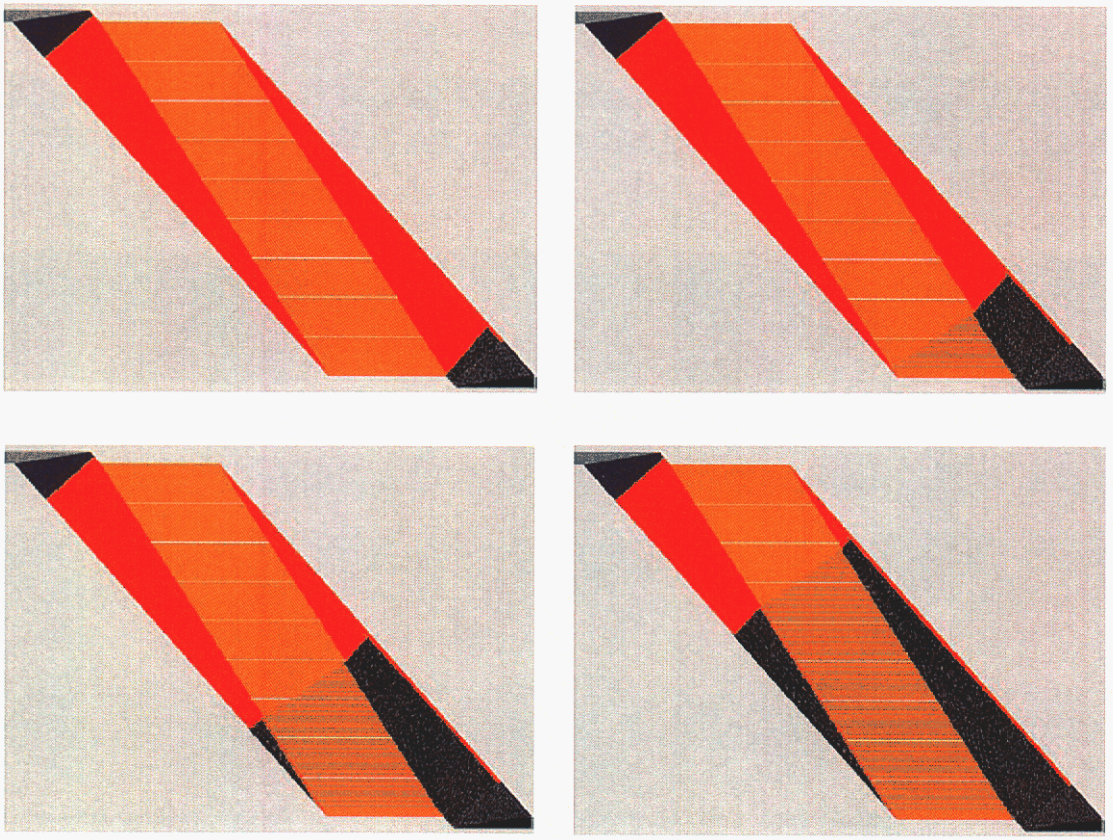

Figure 8.17: Temporal progression of streaklines superimposed over the velocity field of a three-interface, non-skew-compensated 30× expander to which 8 medians have been added to support structurally the wide, shallow central channel.

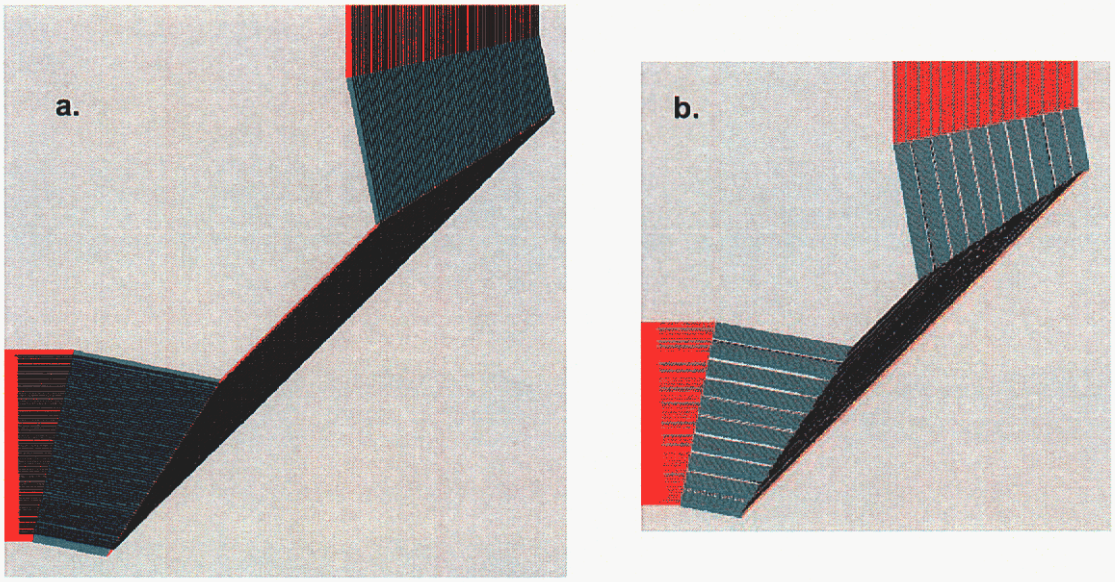

Figure 8.18: Streaklines superimposed on the velocity fields of two 90° turns, both designed using back-to-back critical 45° turns having a SPR of 11.5704. The turn shown on the left side of the figure is constructed using a two-level etch-depth ratio of 11.5704. The turn shown on the right side of the figure is constructed using a two-level etch-depth ratio of 10. Nine permeability-modifying medians are placed in the shallow regions of the turn to increase the SPR from 10 to 11.5704.

These medians increase the SPR from 10 to 11.5704, the value needed to construct critical dispersion-compensated 45° turns. Compared to the flow obtained for an open channel having an SPR of 11.5704 shown in Fig. 8.18a, there is a slight introduction of hydrodynamic dispersion as a result of the medians.

The amount of dispersion and electric field concentrations associated with the medians can be minimized by judicious design of the ends of the medians. Fig. 8.19 shows an example of medians whose ends have been patterned to reduce the (already small) amount of hydrodynamic dispersion they produce. This process is similar to "streamlining" and there is presently no rational general dispersion-minimizing design for these features. Fortunately, even without a rigorous approach, the amount of dispersion can be reduced to levels that are insignificant for all but extremely dispersion sensitive designs. Moreover, the amount of dispersion scales with the width of the medians. If the fabrication technique supports it, the dispersion can be reduced by using many thinner medians rather than a few thicker ones. In this sense, the problem of minimizing hydrodynamic dispersion is reduced to a problem of fabrication resolution.

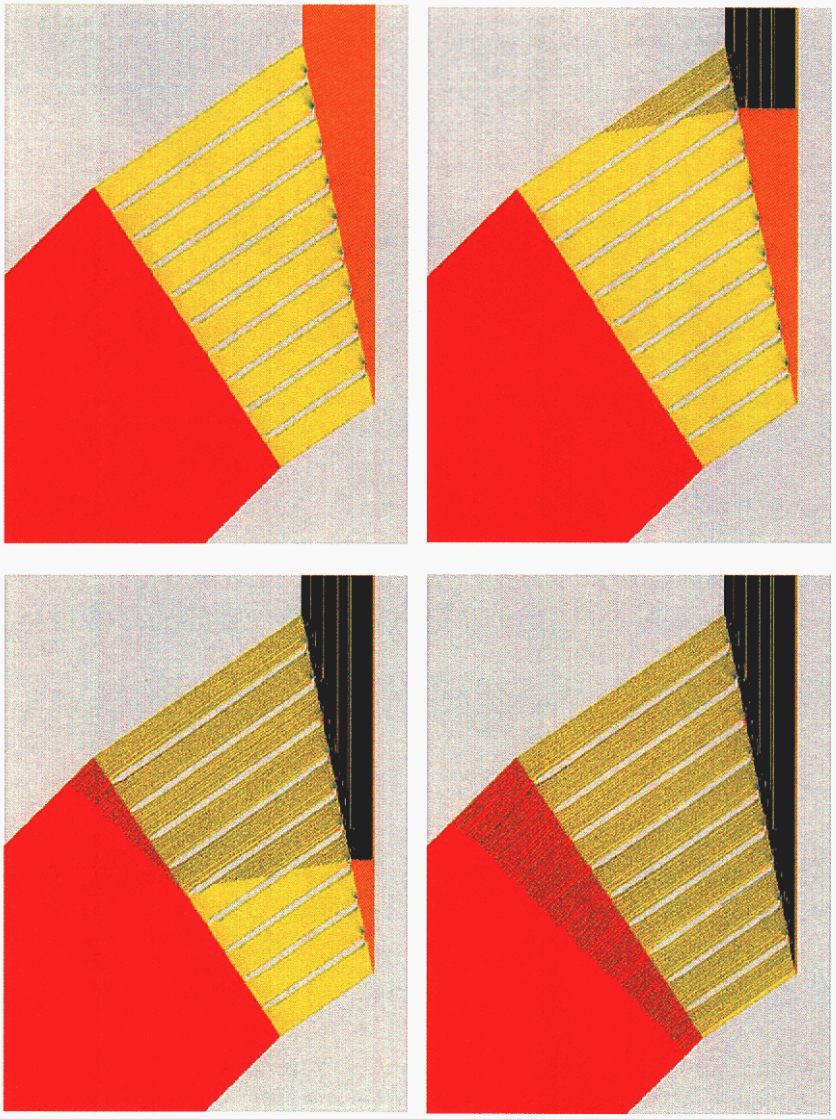

Figure 8.19: Temporal progression of streaklines superimposed over the velocity field of a 45° turn designed using permeability-modifying medians having "streamlined" ends to reduce hydrodynamic dispersion.

8.6 Enhanced line-of-sight absorption cell design

Optical absorption-based detection is disfavored in many microsystems because of the short path lengths over which absorption occurs. This design methodology allows one to stretch material lines of the fluid by orders of magnitude by flowing across one or more interfaces. The material lines remain linear so sighting an illumination source and light collector/detector directly along the stretched and generally skewed material line provides a dramatic enhancement of the absorption effect, with attendant increase in sensitivity. Because of the practical nature of on-chip waveguides, large path lengths might result in excessive light loss in launching and collecting photons. Therefore, evanescent coupling might benefit the most from this methodology, since coupling occurs in shallow channels, which can be designed such that the depth matches the penetration of photons into the channel.

8.7 Open-channel separations

Electrochromatographic (CEC) and high-pressure liquid chromatographic (HPLC) separations require analytes to approach an equilibrium partitioning between the mobile and stationary phase. The time to diffuse between these phases limits the approach to equilibrium and consequently the separation performance. Moreover, the analyte capacity of the system is a function of the surface to volume ratio. A wide, shallow, unpacked rectangular channel is an optimal configuration for such a separation system, but has not been employed in part because of the difficulty of handling injection into such a channel and detection following such a channel[12, 9, 13, 11]. The design methodology presented here provides a direct method of converting between narrow channels suitable for injection and fluorescence detection and the wide channels suitable for separation.

The simplest arrangement for this application could be a single interface pair. The first interface is operated at a large incidence angle and expands the flow directly into the separation column. Material lines are stretched and skewed, but diffusion across the channel is relatively slow, limiting the impact on separation efficiency. At the end of the separation column, the interface is repeated, rotated by 180°. This interface removes the stretch and skew and reduces the channel width to support, e.g., fluorescence detection. This arrangement has the advantage of simplicity and minimal dispersion caused by the interfaces.

An alternative arrangement could employ additional interfaces to remove the skew, increase the channel width more than is practical with a single interface, and/or reduce the sensitivity to fabrication tolerances. The cost of these extra interfaces is additional hydrodynamic dispersion at the interfaces. Figure 8.20 shows two faceted versions of the conventional "cross" type microfluidic separation column. The design in Fig. 8.20a is dispersion compensating: all material lines propagate through the long channel normal to the flow direction. The design in Fig. 8.20b is a maximum-expansion design in which material lines propagate down the channel at an incline of $\sim 45°$ with respect to the flow, causing about a factor of two increase in diffusive band broadening. This increased diffusion may be offset by the dramatically larger expansion ratios that are possible at relatively modest

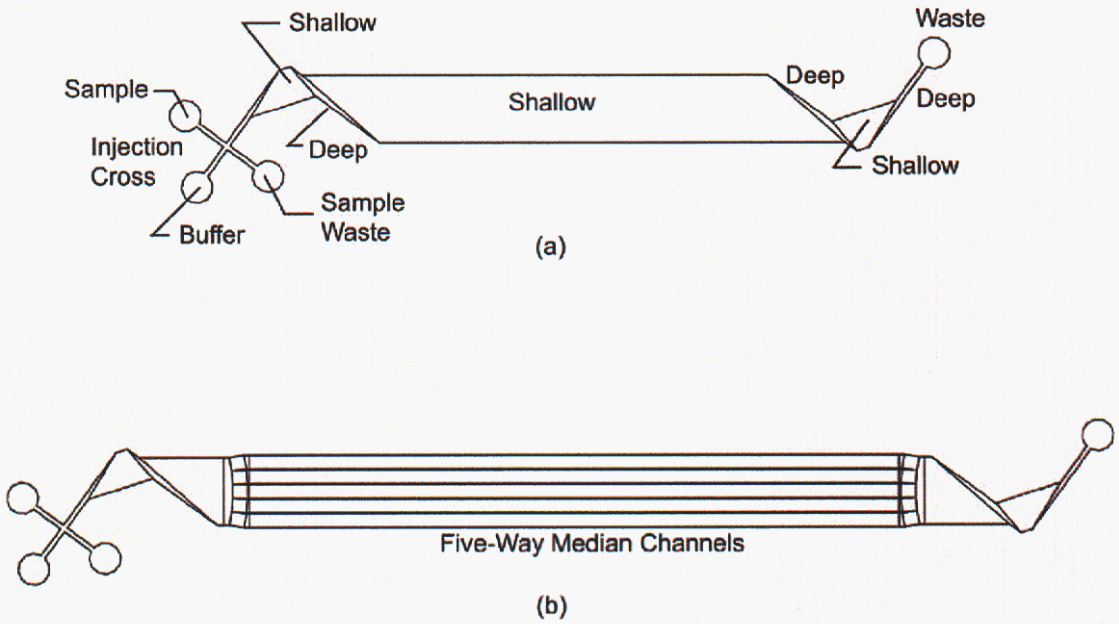

Figure 8.20: Designs of two faceted open-channel electrochromatography separation columns. a: Skew-compensated design. b: Maximum-expansion design.

angles with the uncompensated design. Because of the symmetry of the arrangement of the expansions and contractions, skew is completely compensated when the material lines reach the exit of system, facilitating fluorescence detection.

CHAPTER 9

Drafting faceted designs

9.1 Drafting an expander

The construction of skew-compensated interfaces using the methodology described in this document is surprisingly simple using popular CAD software. Figures 9.1–9.7 demonstrate one way to design the three-interface expander of Fig. 6.6a–c with a SPR of 10 and an incidence angle of 85°. In frame I of Fig. 9.1, two parallel red construction lines (labeled '1' and '2') are drawn, and in frame II a construction line (labeled '3') is drawn perpendicular to the lines of frame I. Line 3 is rotated by the incidence angle for first interface as shown in frame III.

A blue closed polyline is used to construct the first region, which is a region of specific permeability σ_1, as shown in frame IV of Fig. 9.2. Line 3 is then deleted. Lines 1 and 2 are then rotated by the turning angle for interface 1, as shown in frame V. A construction line (labeled '4') is then drawn perpendicular to lines 1 and 2, as shown in frame VI.

Line 4 is rotated by the incidence angle for the second interface, as shown in frame VII of Fig. 9.3. A blue closed polyline is then drawn to enclose this second region, as shown in frame VIII. This region of the device has a specific permeability σ_2. The labels 'i' and 'ii' annotate the distinction between this and the first drawn region. Line 4 is then deleted.

Next, lines 1 and 2 are rotated by the turning angle of the second interface, as shown in frame IX of Fig. 9.4. Construction line '5' is drawn perpendicular to lines 1 and 2, as shown in Frame X.

Line 5 is then rotated by the incidence angle to interface 3, as shown in frame XI of Fig. 9.5. The third region, (labeled 'iii') is then enclosed by a closed blue polyline, and construction line 5 is deleted, as shown in frame XII. Next lines 1 and 2 are rotated by the turning angle of interface 3. If a three-interface expansion to a shallow and wide channel is desired, then lines 1 and 2 will form the walls of the wide channel, and the design is essentially complete. Note that lines 1 and 2 follow the design through the entire drafting process.

If it is desirable to shrink the channel back to the original width of the incident conduction channel, one may select the three blue closed polylines shown in frame XIII of Fig. 9.6, copy them to a location along the wide channel formed by walls 1 and 2, and rotate

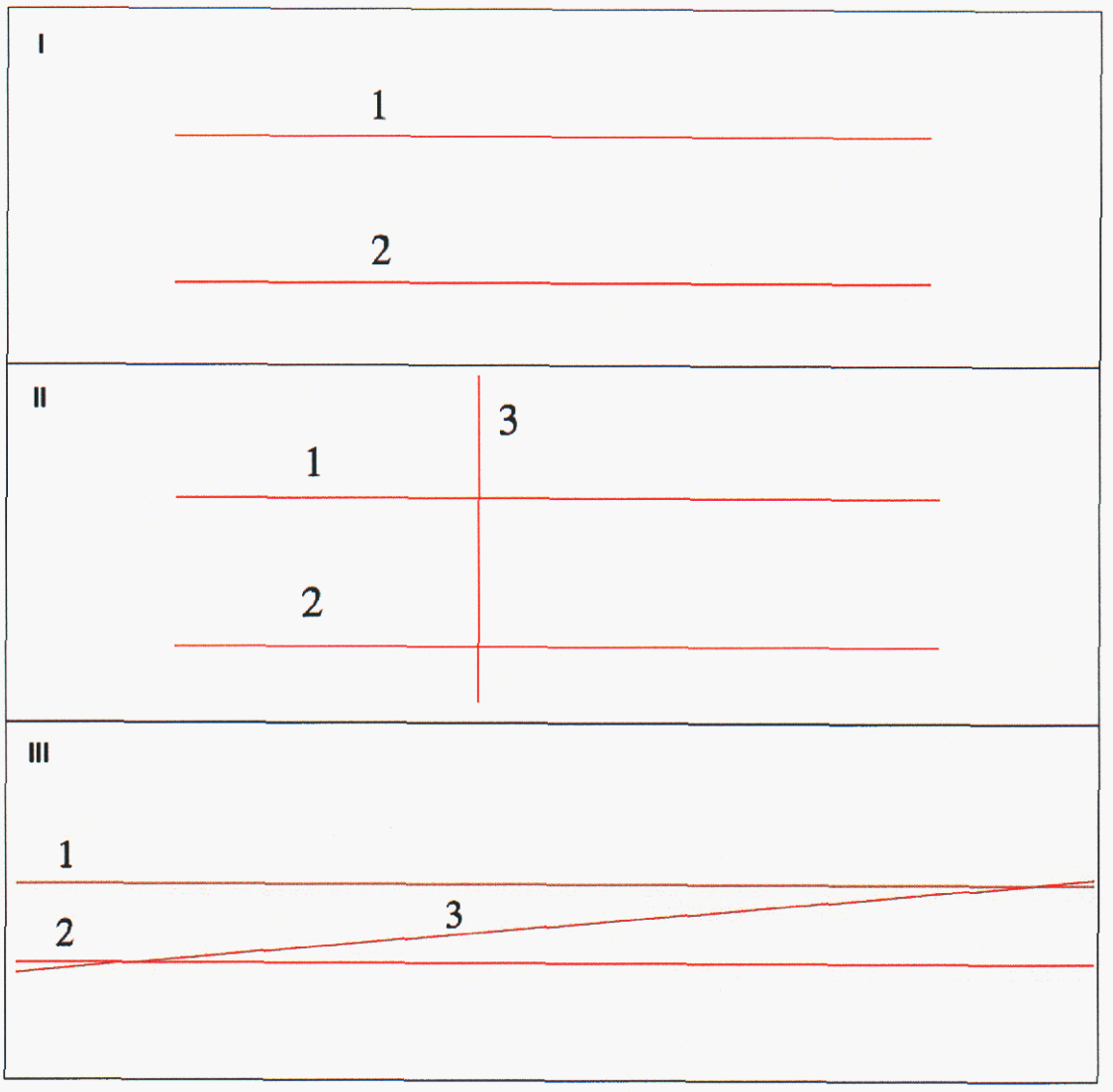

Figure 9.1: Design of a skew-compensated expander using CAD software: initial construction.

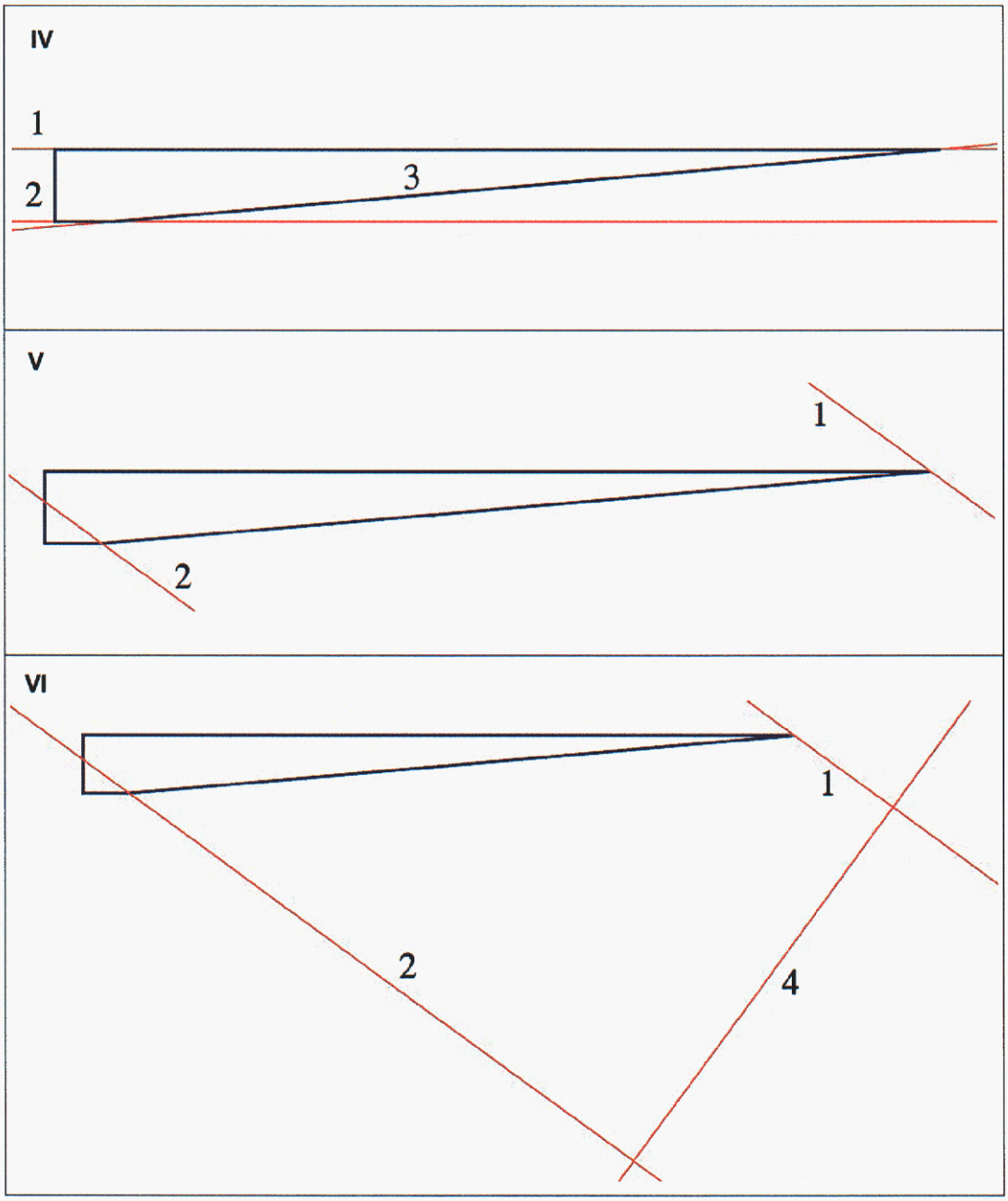

Figure 9.2: Design of a skew-compensated expander using CAD software: continued construction.

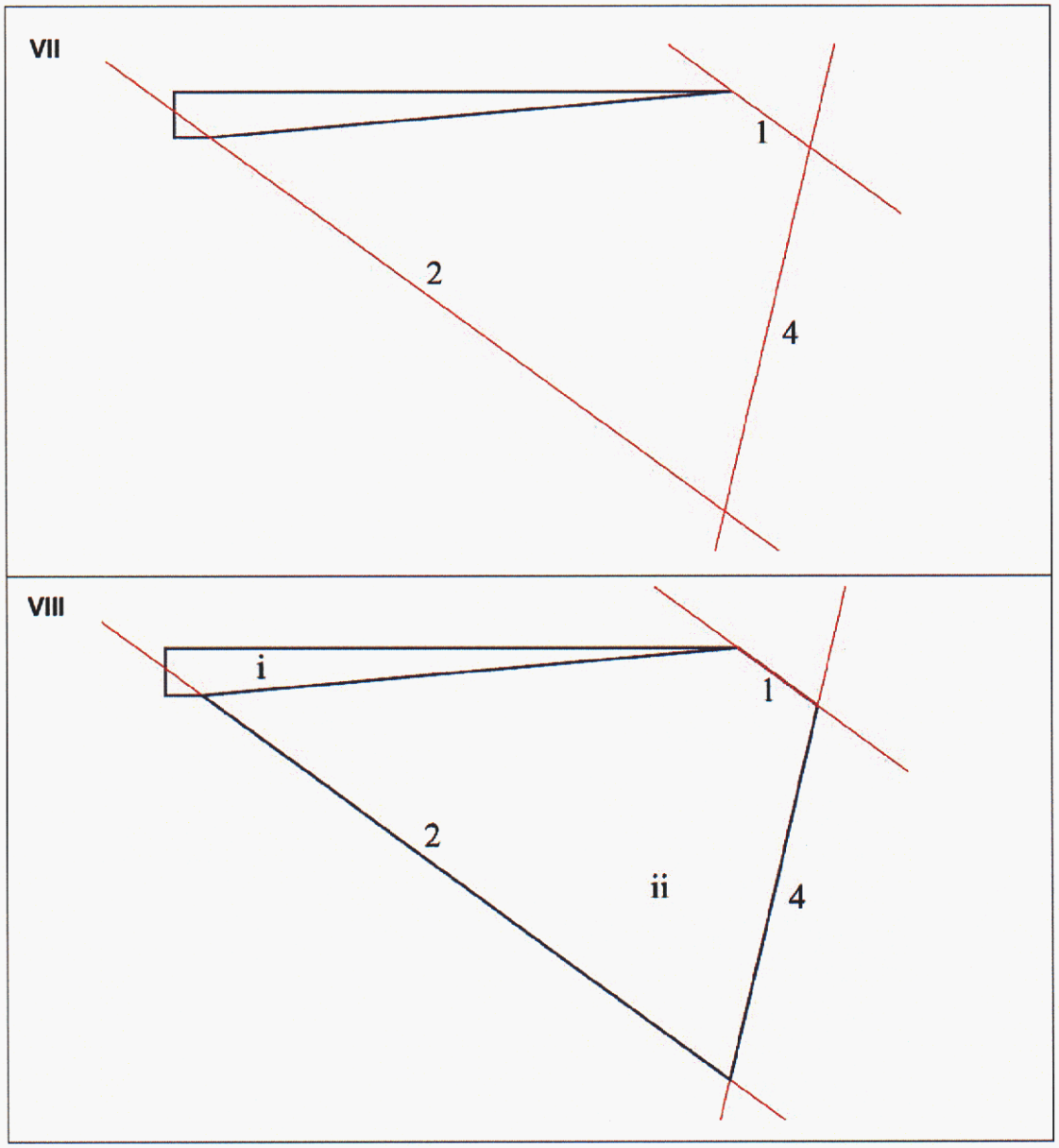

Figure 9.3: Design of a skew-compensated expander using CAD software: continued construction.

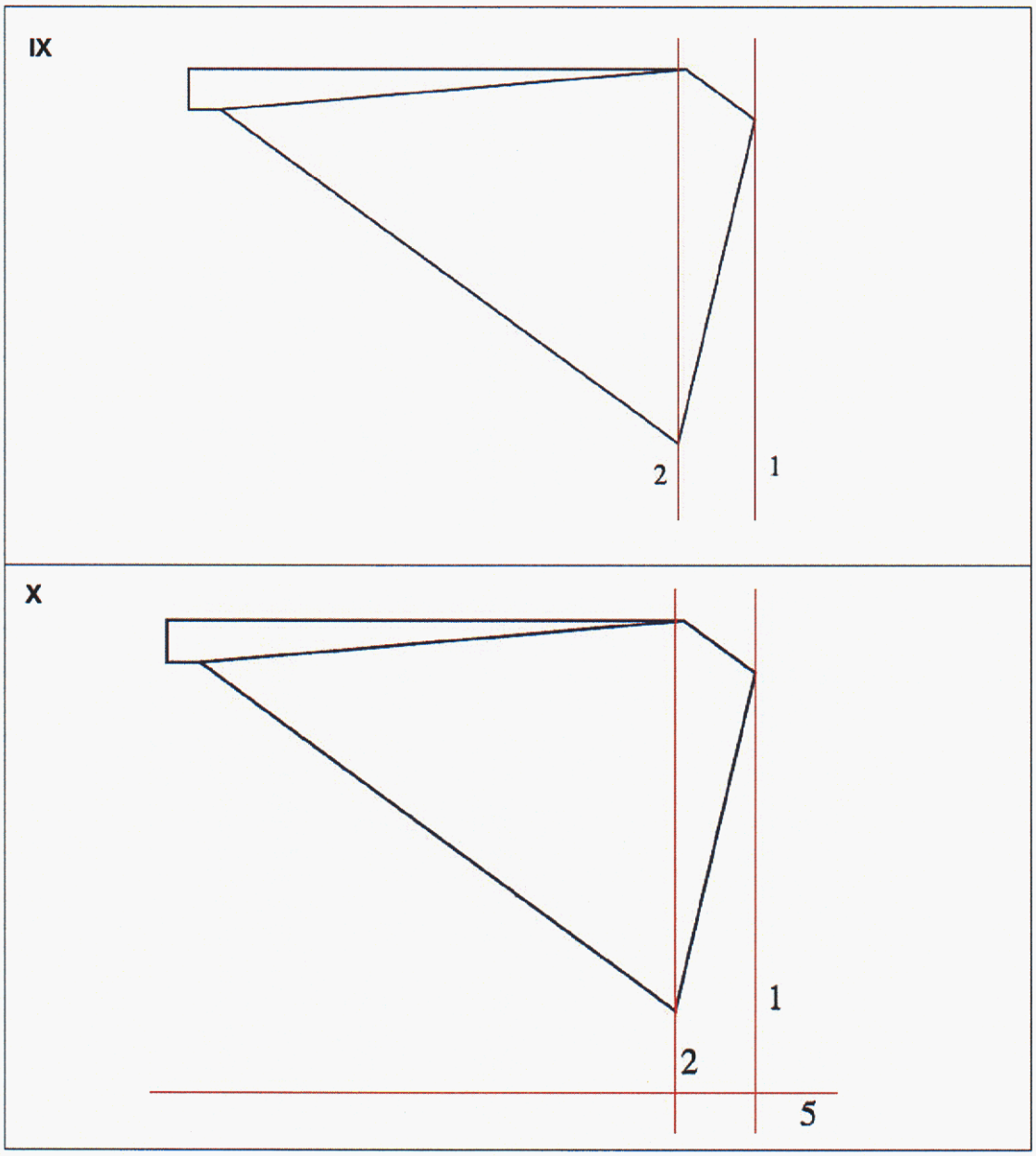

Figure 9.4: Design of a skew-compensated expander using CAD software: continued construction.

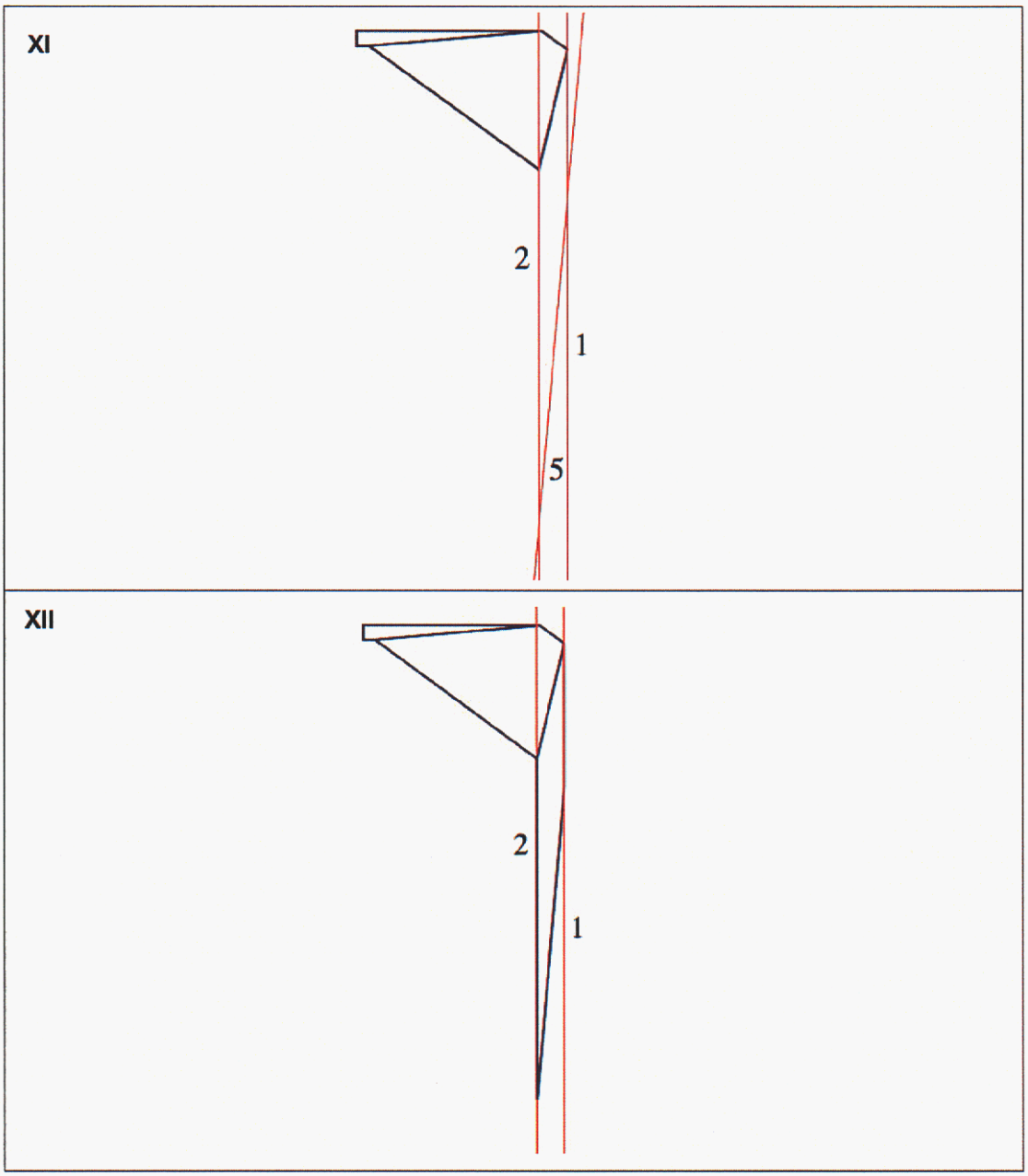

Figure 9.5: Design of a skew-compensated expander using CAD software: continued construction.

the polylines by 180°, as shown in frame XIV.

The resulting midsection is enclosed using a blue closed polyline, and lines 1 and 2 deleted producing the finished design shown in frame XV of Fig. 9.7, where regions i, iii, v, and vii are of specific permeability σ_1, and regions ii, iv, and vi are of specific permeability σ_2.

Note that the length of each region can be extended arbitrarily. For example, if region iv of Fig. 9.7 is used as an open separation column that region will likely be comparatively long. The length is adjusted by moving the interface along the walls formed by lines 1 and 2 in each respective region. Figure 9.8 demonstrates this adjustment. The upper frame of the figure is taken from frame VIII of Fig. 9.3, with the original location of the second interface represented by the green line. The upper frame shows the new interface location (line 4) shifted to shrink the second section to its minimum size, now forming a triangular section, represented by a closed blue triangle. Repeating this process for all frames of Figs. 9.1–9.7 yields the design in the lower frame of Fig. 9.8. Sections ii, iii, v and vi have each been reduced in length to their minimum relative values. Of course, reducing section iv to its minimum length actually removes it from the design. The length of section iv has been reduced substantially from that in Fig. 9.7 for illustrative purposes.

9.2 Drafting a flow splitter

Construction of flow splitters is also remarkably simple, as illustrated in Figs. 9.9–9.12 that show design steps to create both two-way and three-way splitters based on the displacer shown in frame I of Fig. 9.9. Regions i and iii represent regions of specific permeability σ_1; region ii represents a region of specific permeability σ_2. In frame II of Fig. 9.9, the displacer is copied, pasted, and then mirrored vertically (also called "flipped" in some common drawing software). The original and mirrored displacers are aligned as shown. The two regions labeled 'iii' are merged within an single closed polyline as demonstrated in frame III of Fig. 9.9. This is the final design of the two-way splitter shown and simulated in Fig. 8.4b.

To obtain a three-way flow splitter, the design of frame III is copied and pasted as shown in frame IV of Fig. 9.10, resulting in two neighboring central regions labeled 'i.'

These regions are enclosed in a single blue closed polyline, as demonstrated in frame V of Fig. 9.11. The splitter of frame III is again copied, and then pasted as shown in frame VI of Fig. 9.11. Unfortunately, the relative proportions of the splitter do not match the proportions of the object in frame V, requiring some modification of the splitter.

As shown, the two exit regions of the splitter (labeled 'i') are aligned with the two regions labeled 'iii' on the object of frame V, as shown in frame VII of Fig. 9.12. The two regions labeled by the red 'ii' on the splitter are, consequently, too large and overlaps region iii of the splitter. These must be scaled to fit, resulting in the object of frame VIII. Next, the neighboring regions iii and i are combined using blue closed polylines, resulting in the splitter of frame IX of Fig. 9.12. This design is the three-way splitter shown and simulated in Fig. 8.9. The same "copy-and-rescale" procedure can be used to obtain the five-way splitter of Fig. 8.10 starting with the design of frame IX of Fig. 9.12.

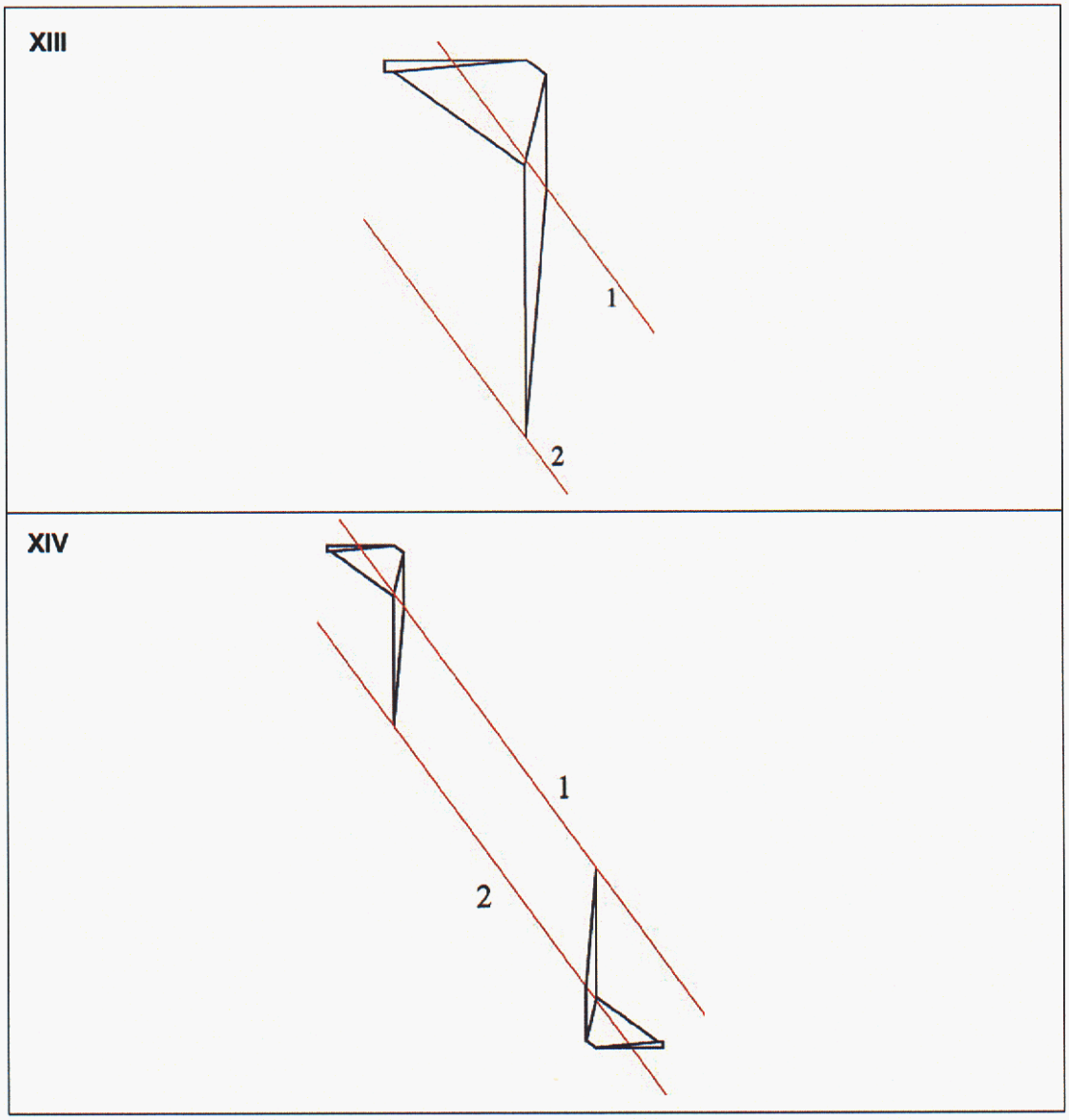

Figure 9.6: Design of a skew-compensated expander using CAD software: continued construction.

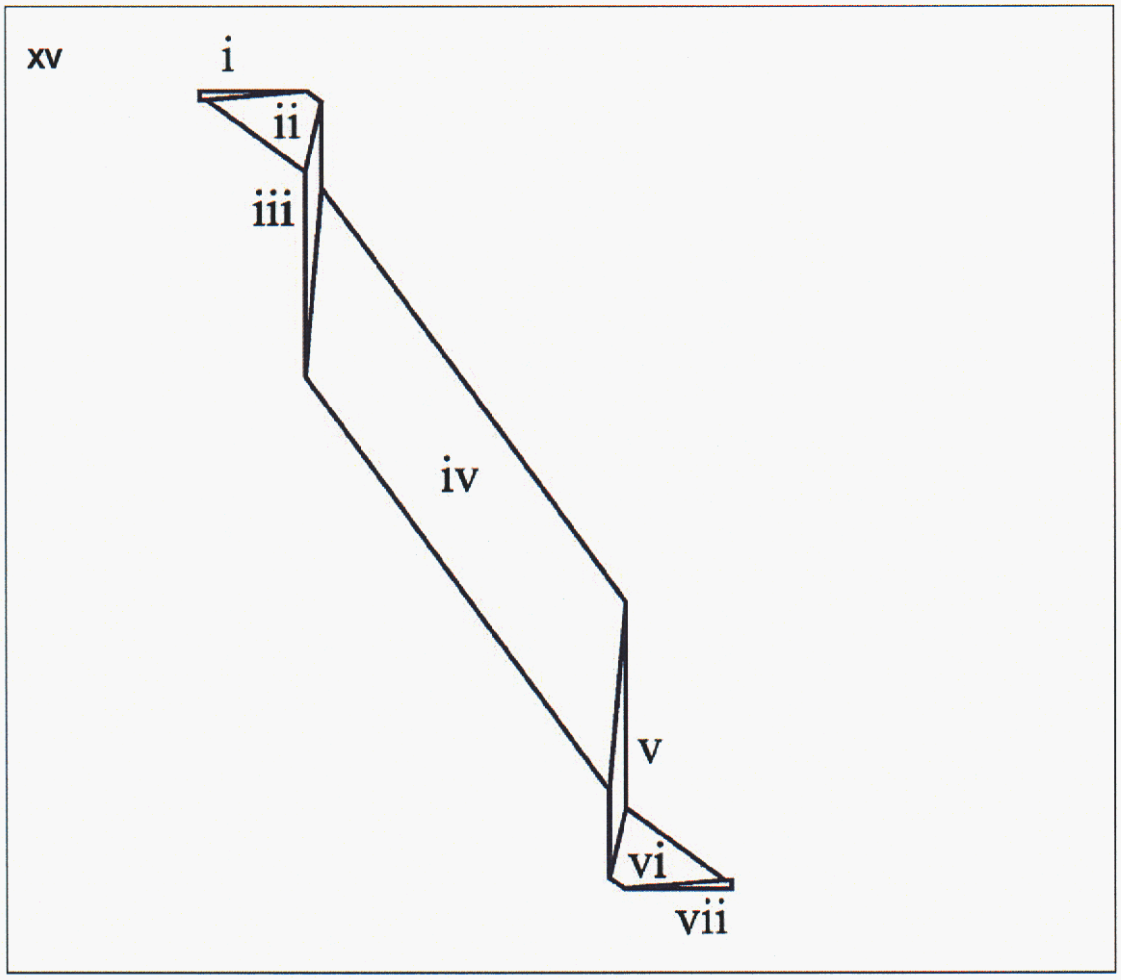

Figure 9.7: Design of a skew-compensated expander using CAD software: continued construction.

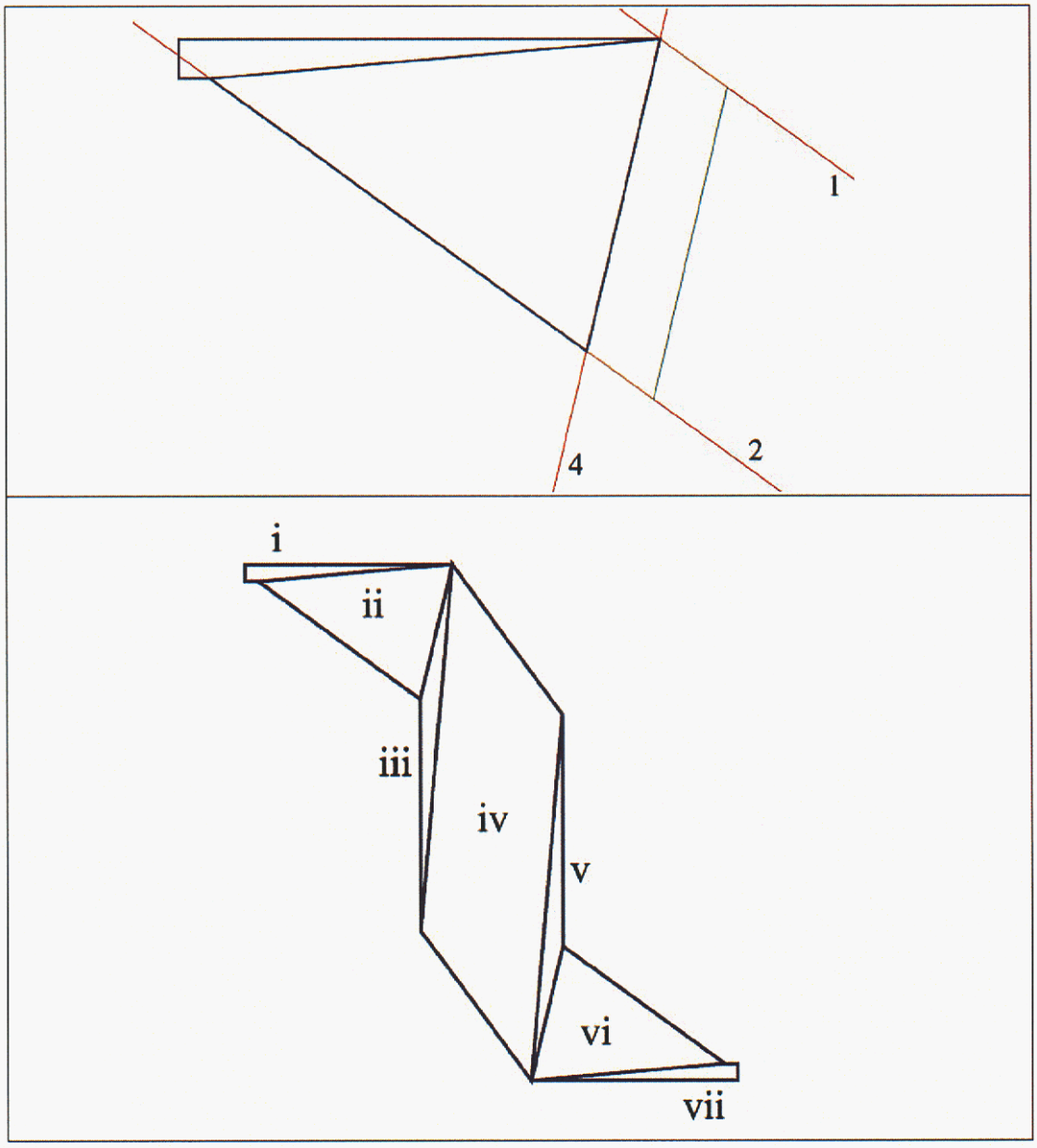

Figure 9.8: Procedure used to change the length of various regions of Fig. 9.7.

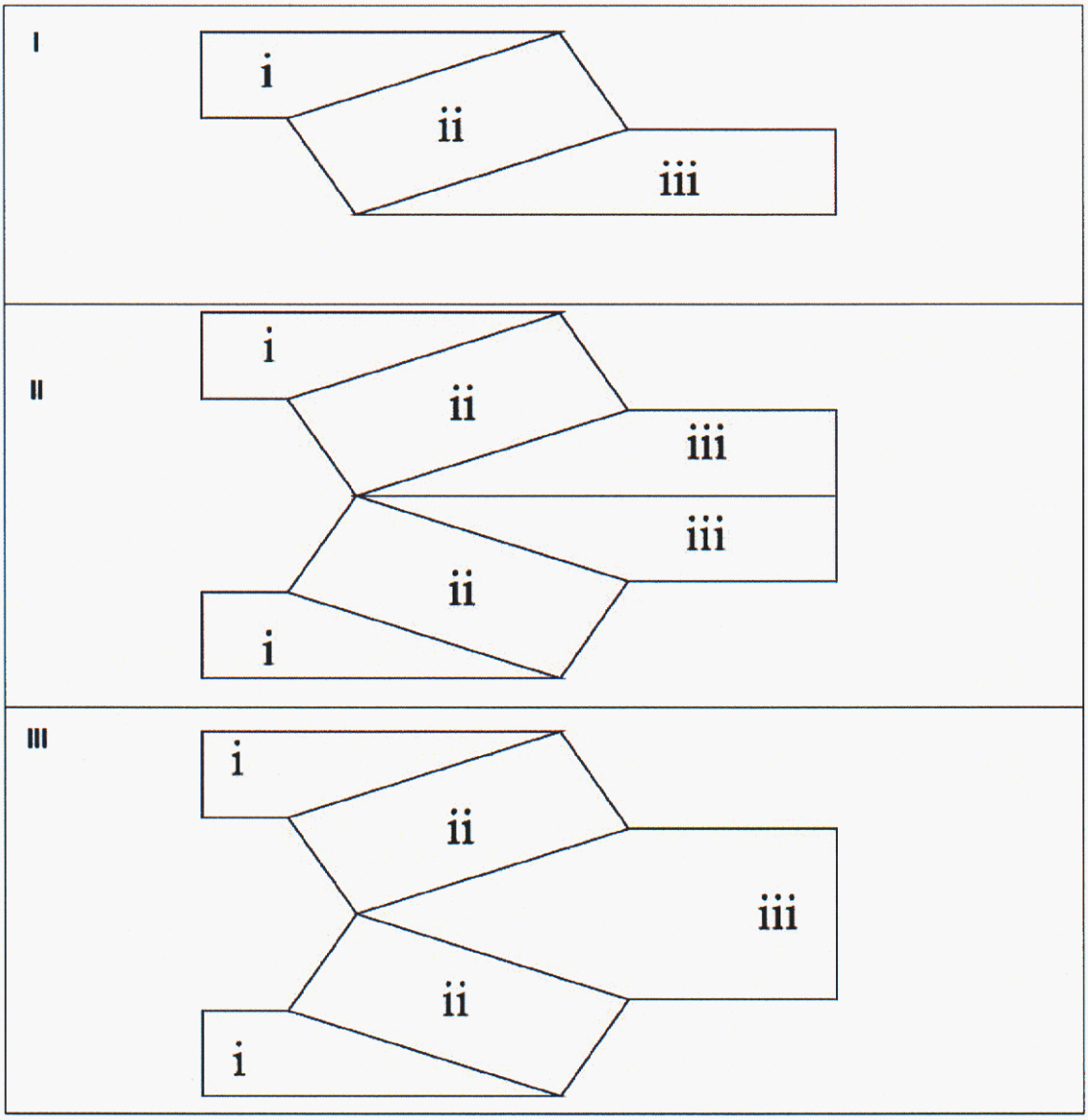

Figure 9.9: Design of a skew-compensated flow splitter using CAD software.

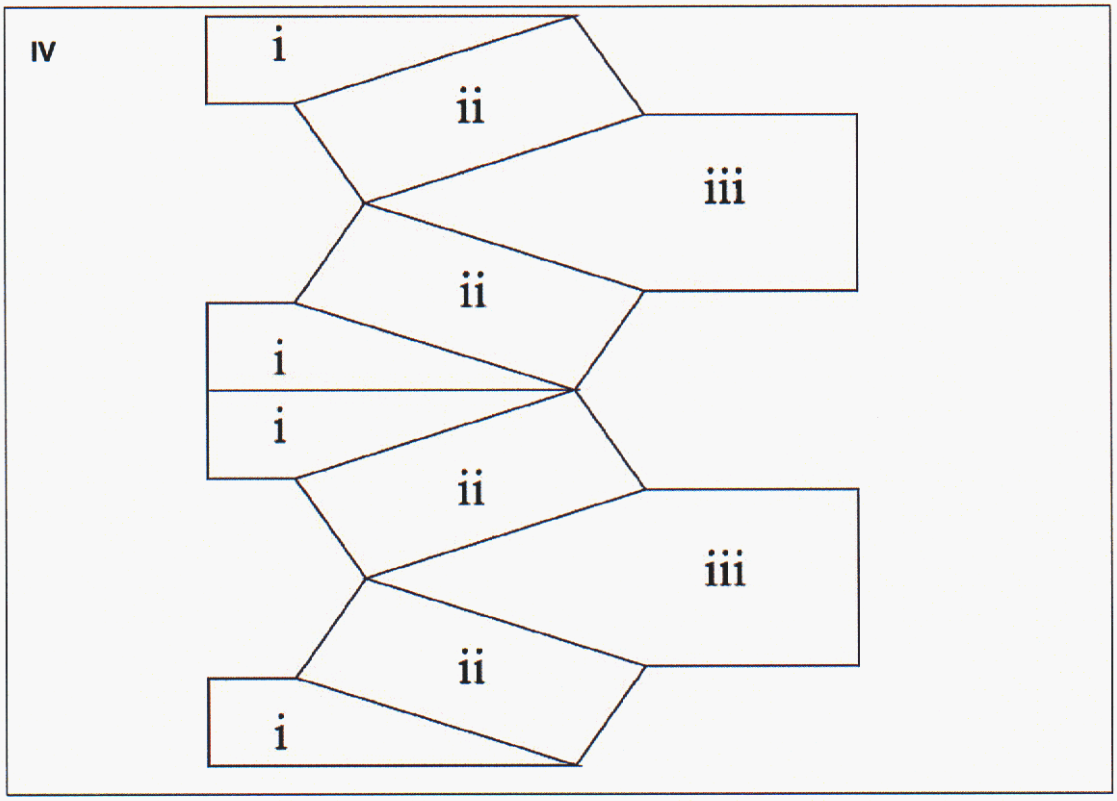

Figure 9.10: Design of a skew-compensated flow splitter using CAD software: continued construction.

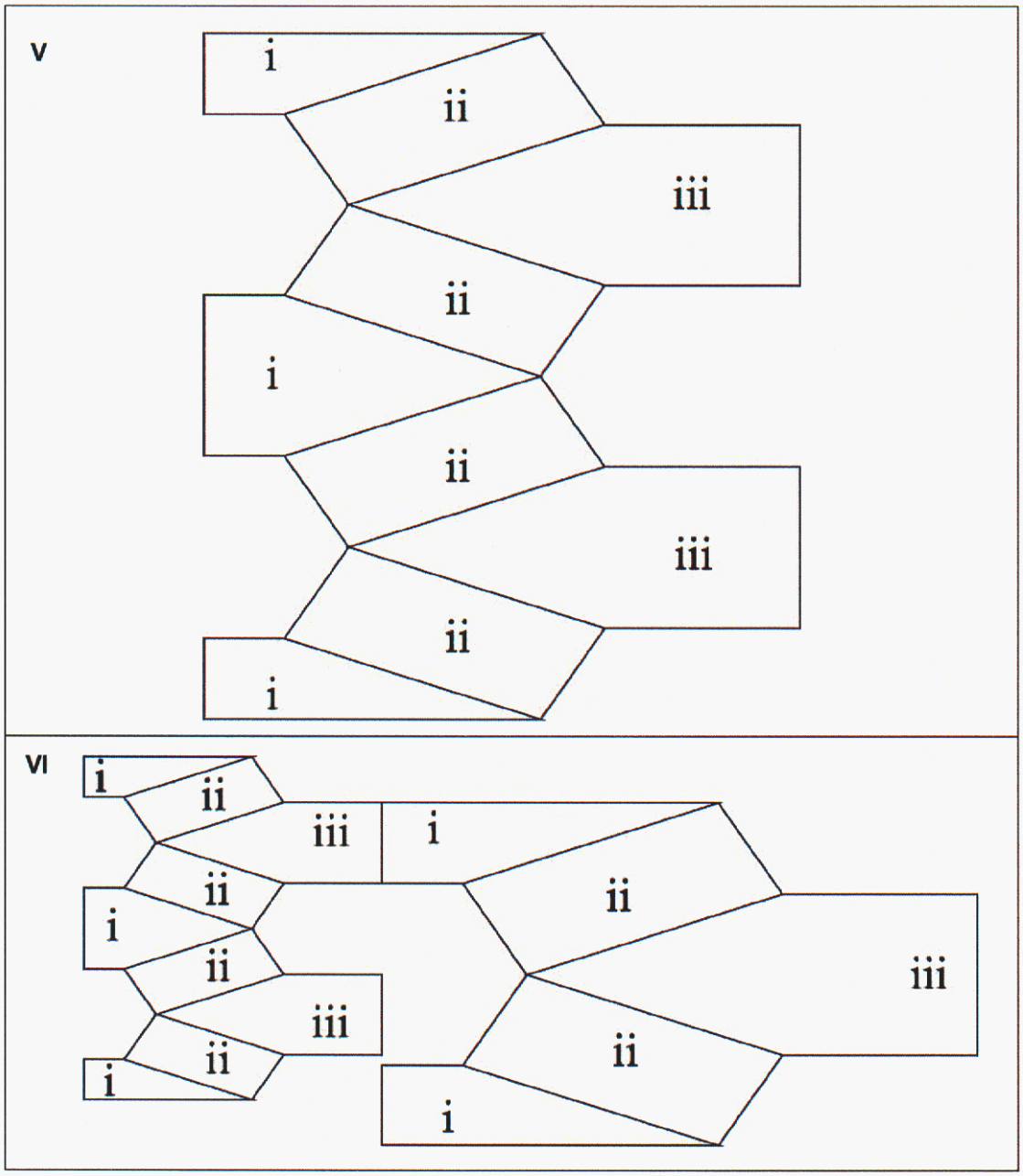

Figure 9.11: Design of a skew-compensated flow splitter using CAD software: continued construction.

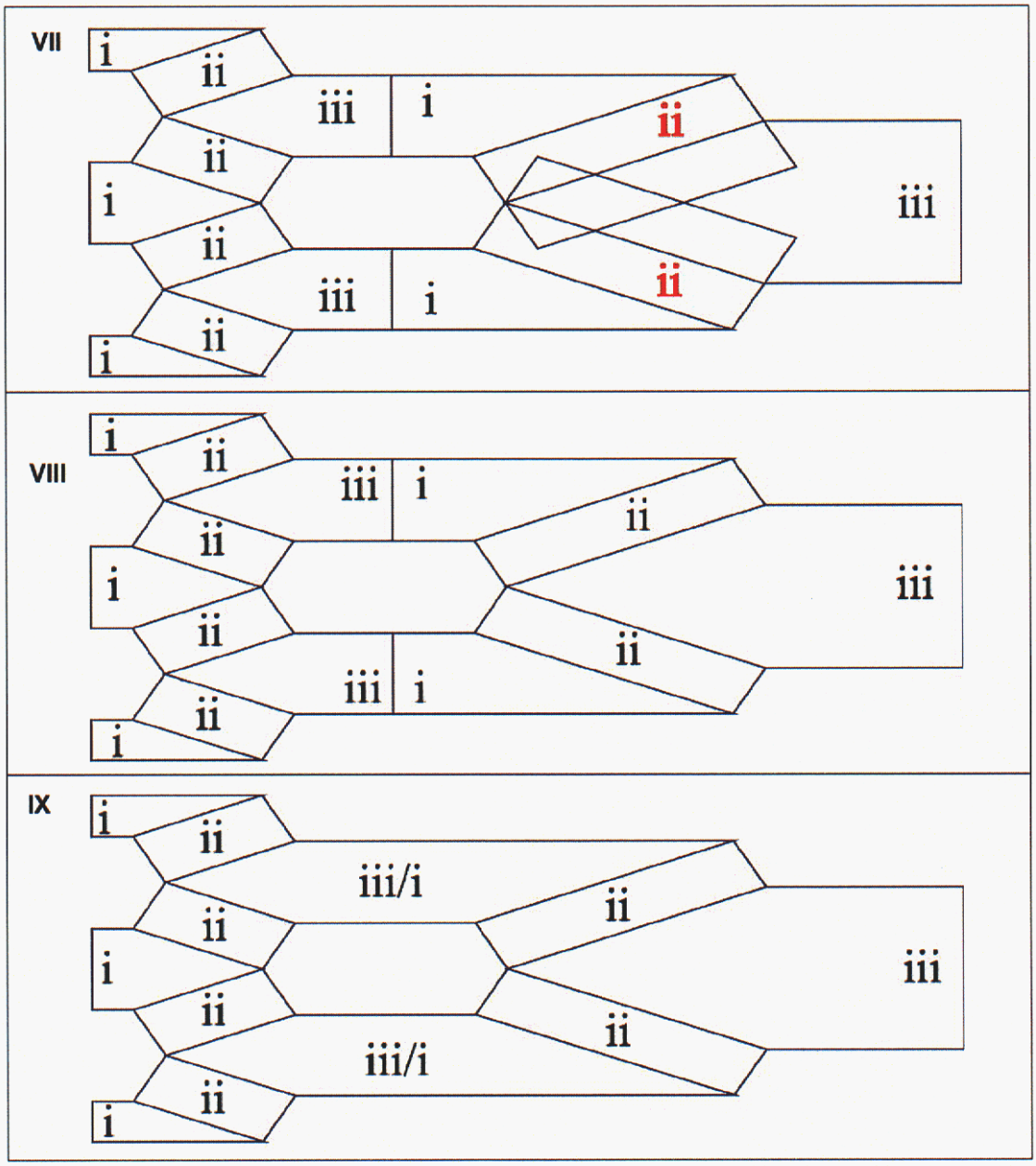

Figure 9.12: Design of a skew-compensated flow splitter using CAD software: continued construction.

CHAPTER 10

Conclusions

A novel design methodology has been developed for flows that satisfy or approximately satisfy the Laplace equation and can therefore be viewed mathematically like conduction. Most of the emphasis in this discussion is oriented toward microfluidic design, particularly for electrokinetic systems. For example, the emphasis on compensating for skew of material lines is intended to extend the utility of the methodology to systems that must transport analytes with minimal hydrodynamic dispersion. The same methodology can be used for electrical and thermal conductor and Darcy's-law flow system design.

The methodology permits one to design these devices using a calculator, rather than a simulation code. Moreover, the designs are completely uncoupled: the interfaces are immune to the details of what passes before or after, so long as their compatibility conditions are locally satisfied. This allows complex systems to be plumbed together from simpler subsystems, e.g., a 256:1 low-dispersion channel expander can be pieced together simply once a 4:1 low-dispersion prism is designed.

This methodology is a step toward rational engineering design of microfluidic systems. The relative simplicity of the flow fields allow simple exact forms for optimal device geometries. The ability to tailor the skew of material lines simply and accurately in this methodology is unique in all of fluid mechanics and is bound to have considerable applications outside of the comparatively narrow scope of this study.

As stated in the introduction, the discovery of this methodology is owed entirely to quite serendipitous observations during experiments and modeling. Even with this discovery, it is unlikely that the methodology would have been fully developed had it not been for a circumspect knowledge of scientific needs, fabrication issues, and engineering considerations that comes from working in a multidisciplinary environment like Sandia National Laboratories.

This page intentionally contains only this sentence.

APPENDIX A

Useful geometric constructions

To obtain the result of Eq. 2.12, consider the geometry given in Fig. A.1, which is similar to the diagram of Fig. 2.5. The channel walls are drawn using blue lines. The red lines in the figure denote construction lines, which are drawn parallel to each channel wall, and both parallel and perpendicular to the interface. The parallel and perpendicular interface construction lines form a cross, which is rotated by both θ_1 and θ_2 with respect to the interface. The resulting rotated constructions lines are used to form the black triangles shown in the upper figure. These triangles are expanded in the lower figure to show the length of the interface, h, the widths of the channels, w_i, and the angles θ_i. Since both triangles share the interface of length h as their hypotenuse, the formula of Eq. 2.12 follows directly.

The geometry of Fig. A.2 is useful in the derivation of the expression of Eq. 5.1. Here, the channel walls are again shown as blue lines. The green dashed lines represent the material lines, which have a steeper angle in the second region, corresponding to a region of lower specific permeability, σ_2, with respect to that of the inlet region, σ_1. The material angles, ψ, are given as the angle between the normal to the material line and the walls. The two triangles in the lower half of Fig. A.2 are obtained by tracking a material line as it travels a distance Z_1 before the interface and a distance Z_2 after the interface. Since the triangles share the channel interface as a common side, it follows that

$$\alpha_1 = \psi_1 + \theta_1 \tag{A.1}$$

and

$$\alpha_2 = \psi_2 + \theta_2, \tag{A.2}$$

leading after some manipulation to the result Eq. 5.1.

The concept of the overall flow-turning angle for a two-interface turn is illustrated in Fig. A.3. The walls and interfaces are shown by blue lines in the upper half of the figure. Red construction lines are drawn parallel to the upper channel walls for each of the three sections. The turning angle for an interface is defined as the angle from the extension of a channel to the wall of the following channel, denoted by θ_{T1} for the turning angle of the interface between sections 1 and 2 and θ_{T2} for the turning angle of the interface between sections 2 and 3. The overall turning angle $\theta_T = \theta_{T1} + \theta_{T2}$ can be defined as the angle

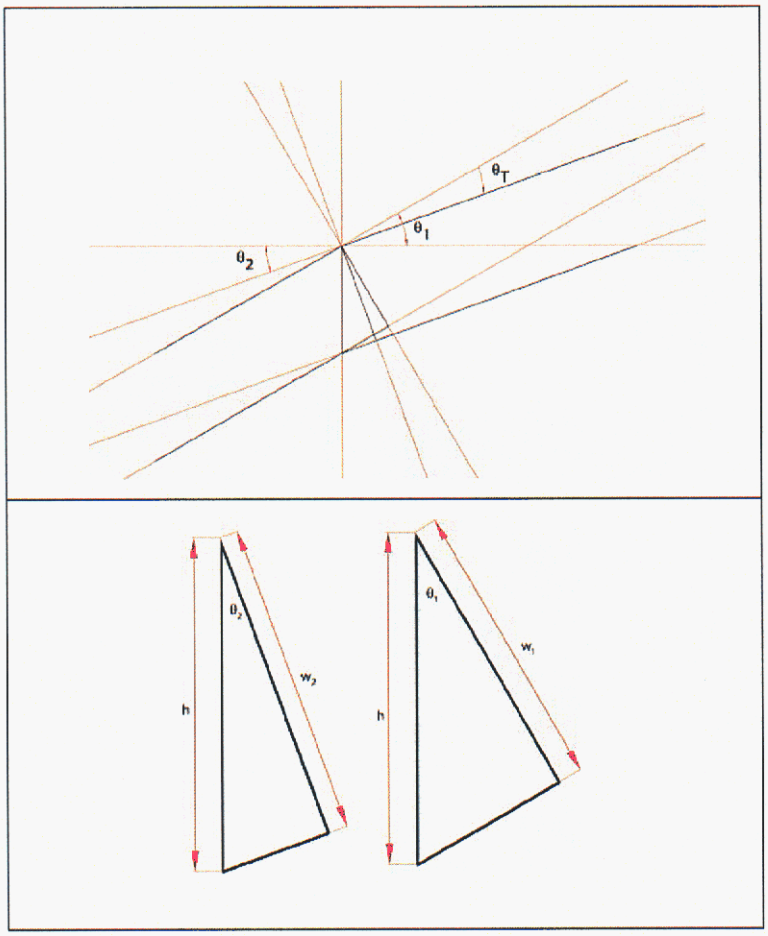

Figure A.1: Geometric diagram used to derive Eq. 2.12. The upper diagram represents the channels of Fig. 2.5 with blue channel walls and red construction lines. The lower right triangles that share hypotenuse h (formed by the interface) correspond to the black triangles in the upper diagram, and are created by clockwise rotation of the interfacial construction line and its 90° complement through angles θ_1 and θ_2 and then bisecting the rotated construction line with the extension of the walls of channel 1 and the walls of channel 2, respectively.

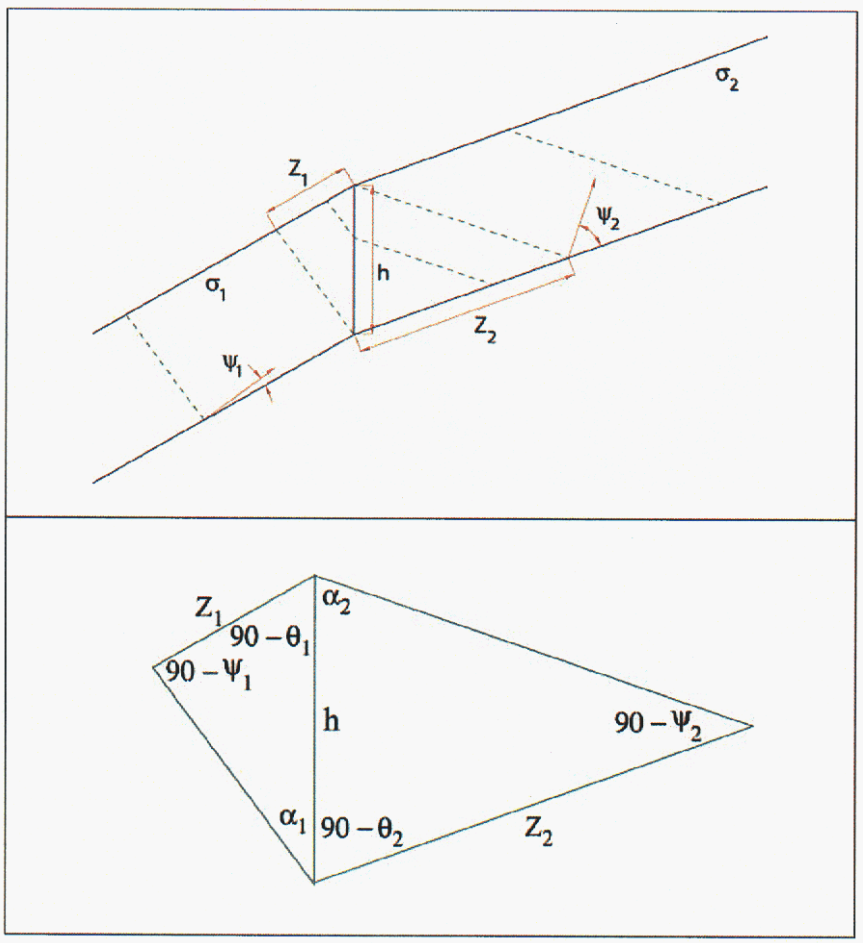

Figure A.2: Geometric diagram used to derive Eq. 5.1. The upper diagram represents the channels of Fig. 2.5 with blue channel walls. Green dashed lines represent material lines. The right triangles that share hypotenuse h (formed by the interface) in the lower figure are obtained from the geometric construction in the upper figure.

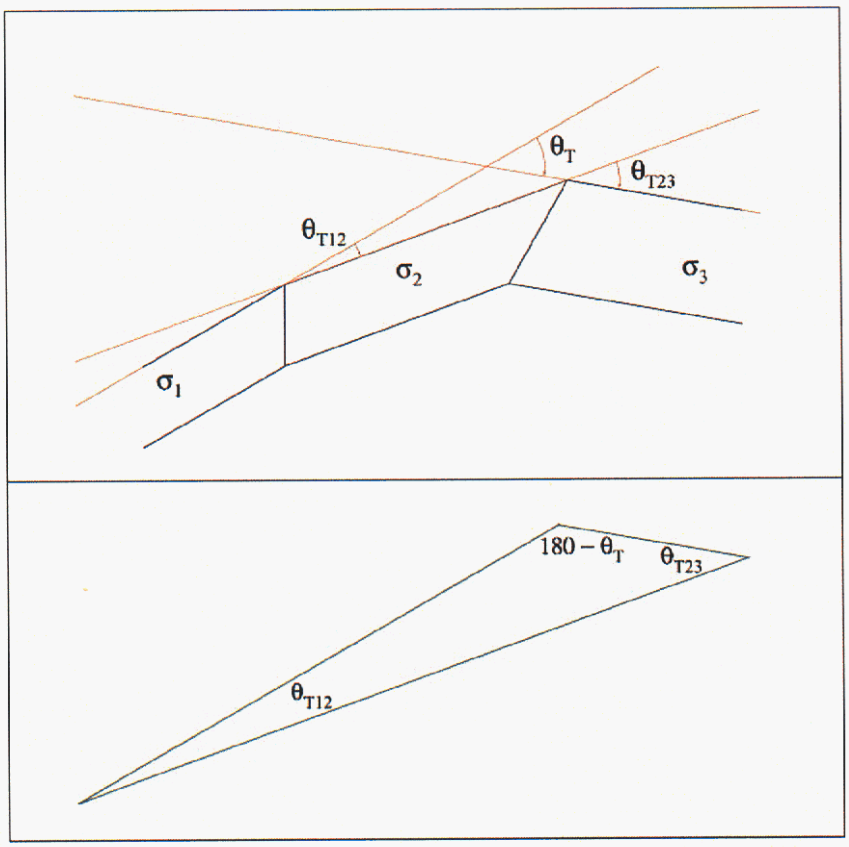

Figure A.3: Geometric diagram used to derive Eq. 5.3. The upper diagram represents the channels of Fig. 2.5 with blue channel walls. The red construction lines—formed parallel to the upper channel walls—intersect to form a triangle, which is shown in green in the lower figure.

from the extension of the first section wall to the extension of the section after the second interface. This definition can be generalized for a system having and arbitrary number N of interfaces,

$$\theta_T = \sum_i^N \theta_{Ti}, \tag{A.3}$$

where θ_{Ti} is the turning angle of the ith interface.

The green triangle shown in the lower half of Fig. A.3 is formed by the intersection of the three red construction lines in the upper half of the figure. Simple trigonometry on this construction leads to Eq. 5.3.

Bibliography

[1] C. H. Chen, H. Lin, S. K. Lele, and J. G. Santiago. Convective and absolute electrokinetic instability with conductivity gradients. *Submitted to J. Fluid Mech.*

[2] E. B. Cummings. Applied electrokinetic and pressure-driven microfluidics. Technical Report SD99-8228, Sandia National Laboratories, Livermore, CA, 1999.

[3] E. B. Cummings. Streaming dielectrophoresis for continuous-flow microfluidic devices. *IEEE Eng. in Med. and Bio.*, page in press, January, 2004.

[4] E. B. Cummings, G. J. Fiechtner, A. K. Singh, B. A. Simmons, Y. Fintschenko, and B. Lapizco-Encinas. Continuous streaming dielectrophoretic particle filter/concentrators. In M. A. Northrup, K. F. Jensen, and D. J. Harrison, editors, *μTAS 2003: Proceedings of the Seventh International Conference on Miniaturized Chemical and Biochemical Analysis Systems*, pages 41–44. Transducers Research Foundation, Cleveland Heights, OH, 2003.

[5] E. B. Cummings, S. K. Griffiths, and R. H. Nilson. Applied microfluidic physics, ldrd final report. Technical Report SAND2002-8018, Sandia National Laboratories, Livermore, CA, 2002.

[6] E. B. Cummings, S. K. Griffiths, R. H. Nilson, and P. H. Paul. Conditions for similitude between the fluid velocity and electric field in electroosmotic flow. *Anal. Chem.*, 72:2526–2532, 2000.

[7] E. B. Cummings and A. K. Singh. Dielectrophoretic trapping without embedded electrodes. *Proc. of SPIE Conference on Micromachining and Microfabrication, September 17–20, Santa Clara, CA*, 4177:164–173, 2000.

[8] E. B. Cummings and A. K. Singh. Dielectrophoresis in microchips containing arrays of insulating posts: theoretical and experimental results. *Anal. Chem.*, 75:4724–4731, 2003.

[9] Z. H. Fan and D. J. Harrison. *Anal. Chem.*, 66:177–184, 1994.

[10] G. J. Fiechtner and E. B. Cummings. Faceted design of channels for low-dispersion electrokinetic flows in microfluidic systems. *Anal. Chem.*, 75:4747–4755, 2003.

[11] L. M. Fu, R. J. Yang, G. B. Lee, and H. H. Liu. *Anal. Chem.*, 74:5084–5091, 2002.

[12] S. C. Jacobsen, R. Hergenroder, L. B. Koutny, R. J. Warmack, and J. M. Ramsey. *Anal. Chem.*, 66:1107–1113, 1994.

[13] E. Verpoorte. *Electrophoresis*, 23:677–712, 2002.

[14] J. A. A. West, T. W. Lane, J. F. Stamps, I. R. Shokair, and J. A. Fruetel. Detection and identification of viral agents by protein fingerprinting using the hand-portable μChemlab. In M. A. Northrup, K. F. Jensen, and D. J. Harrison, editors, *μTAS 2003: Proceedings of the Seventh International Conference on Miniaturized Chemical and Biochemical Analysis Systems*, pages 143–146. Transducers Research Foundation, Cleveland Heights, OH, 2003.

Distribution

1		Tom Sobota, APRI 1925 McKinley Drive, Suite B LaVerne, CA 91750	
1	9052	Mark Allendorf	8367
1	9055	Sarah Allendorf	8353
1	9054	Robert Carling	8350
10	9951	Eric Cummings	8358
10	9951	Greg Fiechtner	8358
1	9951	Julie Freutel	8358
1	9042	Stewart Griffiths	8750
1	9054	Don Hardesty	8360
1	9953	Brent Haroldsen	8118
1	0825	Wahid Hermina	9110
1	9403	Jill Hruby	8700
1	9056	Wen Hsu	8368
1	9001	Miriam John	8000
1	9409	Wendell Kawahara	8754
1	9401	Glenn Kubiak	8750
1	9056	Tom Kulp	8368
1	9953	Jane Ann Lamph	8111
1	9951	Duane Lindner	8101
1	9051	Andy McIlroy	8351
1	9054	Bill McLean	8300
1	1413	Terry Michalske	1040
1	9042	Robert Nilson	8752
1	9951	Arthur Pontau	8358
1	9051	Larry Rahn	8350
1	0151	Arthur Ratzel	9750
1	9052	Allen Salmi	8367
1	9951	Joe Schoeniger	8130
1	9951	Anup Singh	8130
1	9004	Rick Stulen	8100
1	9103	Karl Wally	8111
3	9018	Central Technical Files	8945-1
1	0899	Technical Library	9616
1	9021	Classification Office, 8511 for Technical Library, MS0899	9616
1		DOE/OSTI via URL	
1	0323	Donna Chavez, LDRD Office	1011

This page intentionally contains only this sentence.